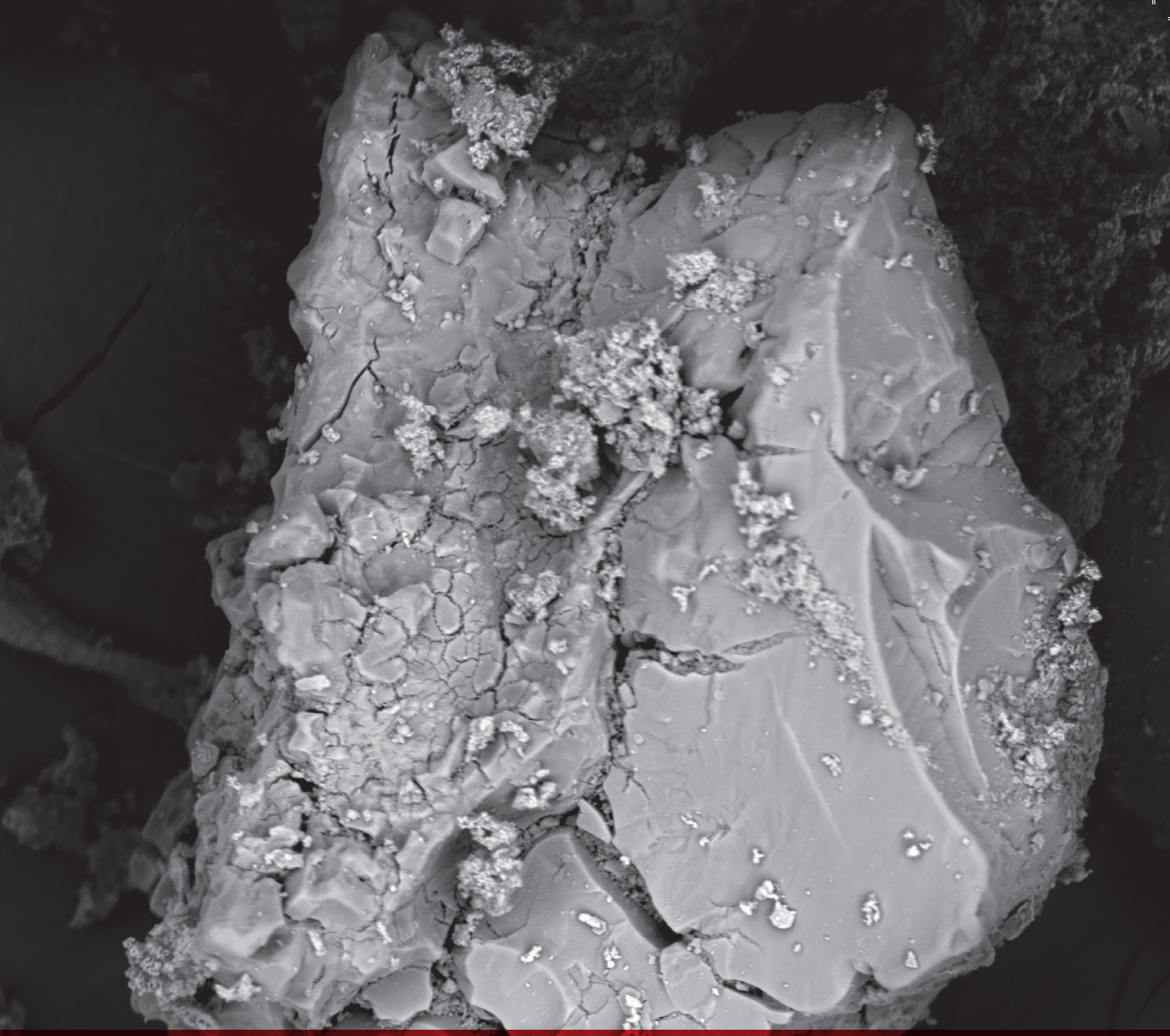

Municipal Solid Waste Incineration residues:

ANALYSIS, TREATMENT, AND APPLICATION

Ekaterina Loginova

Bouwstenen 339

Municipal Solid Waste Incineration residues:

Analysis, treatment, and application

PROEFSCHRIFT

ter verkrijging van de graad van doctor
aan de Technische Universiteit Eindhoven,
op gezag van de rector magnificus prof.dr.ir. F.P.T. Baaijens,
voor een commissie aangewezen door het College voor Promoties,
in het openbaar te verdedigen
op 17 november 2022 om 16:00 uur.

door

Ekaterina Vadimovna Loginova

geboren te Penza-19, Soviet-Unie

Dit proefschrift is goedgekeurd door de promoten en de samenstelling van de promotiecomissie is als volgt:

Voorzitter: prof.dr.ir T.A.M. Salet

1e promotor: prof.dr.ir. H.J.H. Brouwers

2de promotor: prof.dr. M.A. Proskurnin (Lomonosov Moscow State University)

Co-promotor: dr. Katrin Schollbach

Leden: prof.dr. C. Cheeseman (Imperial College London)

prof.dr. H. Justnes (Norway University of Science and Technology)

prof.dr. M. Illikainen (University of Oulu)

prof.dr.ir. D.M.J. Smeulders

Het onderzoek dat in dit proefschrift wordt beschreven is uitgevoerd in overeenstemming met de TU/e Gedragscode Wetenschapsbeoefening

Municipal Solid Waste Incineration residues:

Analysis, treatment, and application

E. Loginova

Eindhoven University of Technology

November 2022

This work is part of the research programme "Development of eco-concretes by using industrial by-products" with project number 13318, which is (partly) financed by the Netherlands Organisation for Scientific Research (NWO)

CIP-DATA LIBRARY TECHNISCHE UNIVERSITEIT EINDHOVEN

Municipal Solid Waste Incineration residues: Analysis, treatment, and application / by Ekaterina Loginova

A catalogue record is available from the Eindhoven University of Technology Library

ISBN: 978-90-386-5603-8

Bouwstenen 339

NUR 955

PhD Thesis, Eindhoven University of Technology, the Netherlands

Cover design: Photograph © Ekaterina Loginova

Printed by: ADC-Dereumaux

Простую дорожку ты всегда успеешь выбрать, так что,
начинай с более сложной.

Папа

You can always choose the easy path, so, start with the hard one.

In loving memory of my father

(1964 – 2015)

Preface

The work presented in this thesis is part of a NWO project titled “Development of eco-concretes by using industrial by-products”. I joined this project on 16 March 2016, as a Ph.D. student in the Building Materials group at the Eindhoven University of Technology under the leadership of prof.dr.ir H.J.H. Brouwers.

Firstly, I would like to express my sincere thanks to my supervisor and promotor prof.dr.ir. H.J.H. Brouwers, who provided me this opportunity. During the last six years, you assisted me in every possible way for the successful completion of the project. I am grateful to you for placing your trust in my abilities. This thesis would not be possible without your guidance and contribution.

I am also thankful to my 2nd promotor, Co-promotor, and daily supervisors, prof.dr.chem M.A. Proskurnin, dr.dipl.-min K. Schollbach, and dr.dipl.-eng M.V.A. Florea for their scientific input, patience, assistance, support, and last but not least, freedom in the determining the research direction on my own, which they provided during the last six years. I am grateful that at every step of this journey I could always count on your support in answering my questions and helping me with the practical part in the lab. Especially, I am thankful to prof.dr.chem M.A. Proskurnin and his current and my former colleague dr.chem D.S. Volkov for providing me a possibility to perform a substantial part of the chemical analysis in their lab with more than generous practical assistance from both of them.

I am grateful to the members of the promotion committee, prof.dr. C. Cheeseman from the Imperial College London, prof.dr. H. Justnes from the Norway University of Science and Technology, prof.dr.ir. D.M.J. Smeulders from the Eindhoven University of Technology, and prof.dr. M. Illikainen from the University of Oulu for reading my work and providing valuable suggestions for its improvement.

I want to thank industrial partners and user committee for their contributions toward this project. The user committee includes Mr. A. Dekker (v.d. Bosch Beton), dr. A. Keulen (Mineralz), Mr. M. Bruin (HeidelbergCement), Mr. M. Brito van Zijl (Mineralz), Mr. M. van Kempen (Blue Phoenix Group), dr. G. Hüsken (BAM Bundesanstalt für Materialforschung und -prüfung), Mr. R. Bleijerveld (Mineralz), Mr. A. Cakir (Attero), dr. S. Grünewald (CRH Europe Sustainable Concrete Centre & Struyk Verwo Infra), dr. M.L.J. van Leeuwen (CRH Europe Sustainable Concrete Centre). Especially, I am thankful to Mineralz and HeidelbergCement for providing materials for the research.

Behind every successful thesis, there is a tremendous amount of hard work from the laboratory technicians and supporting staff. Therefore, I would like to express my gratitude to our lab technicians, especially A.C.A. Delsing, and H.L.W. Smulders for providing valuable suggestions and input for the experimental work in the lab. Special regards to our wonderful staff of the secretariat, including Léontine, Ginny, Moniek, Nathaly, and Manon who were always there to take care of the bureaucratic matters and providing us with the lovely and organized work environment.

I have met many amazing people in the Building Materials group. I had great pleasure to enjoy their company and support during my thesis. I would especially like to mention Perry, Veronica, Chris, and Qadeer, with whom I shared many unforgettable moments. I will always cherish our relationships! We have had innumerable conversations about research and beyond, had lots of fun during conferences, and with some of you even shared accommodations for a while. Especially I would like to send loving regards to my partner and former colleague Perry, without your support and enormous help of all kinds, this thesis would not have happened. Also, I enjoyed working with all the members of our group and we did many activities together, including game nights, dinners, and conferences. For all pleasant time we spent together, I would like to thank: Tao, Jawad, Kinga, Alberto, Guillaume, Yuri, Florent, Pei, Azee, Yangyueye, Yuxuan, Qingliang, Sieger, Xu, Anna, Hoss, Katka, Peipeng, Gang, Zhengyao, Winnie, XiaoXiao, Bo, Iris and Jonathan. It was a great pleasure working with you! Part of this thesis was performed with the assistance of the master student Jeroen Hoevers. Thank you for your help. I wish you the best of luck with your future career and life.

My journey to this doctoral thesis began in Moscow, Russia, where I spent almost eight years prior to moving to the Netherlands. During my studies at the Lomonosov Moscow State University I acquired many friends and long-lasting connections, some of which were of a great emotional support and encouragement during this thesis. I would especially like to thank dr. Stepan S. Denisov for pitching the idea of the immigration, and dr. M. Polynsky for being there for me through the darkest period of my life.

During this thesis a lot of personal and global things have happened: a heart attack of my husband, giving birth to our child Austin, the COVID-19 pandemic, and even the war. Sometimes it felt as “a tiny bit” too much; however, I am eternally grateful for all the mental resources and love that my parents (Vadim and Svetlana) gave me, which always helped me to go on. Of course, I would like to mention my brother Alexander, who I can always count on, and for gloomily cheering me up when necessary. The last special thank you goes to dr. A.I. Kulikov, who provided a lot of emotional and intellectual support over the last two years.

Ekaterina Loginova

October 2022

Table of Contents

CHAPTER 1

Introduction

1.1 Research relevance

Due to the annual growth of the population, the amount of Municipal Solid Waste (MSW) produced is also increasing[1]. Abundant waste amounts together with the lack of landfill space in small countries, such as the Netherlands, lead to an acute challenge of waste disposal[2]. The first step of dealing with it in most countries is Municipal Solid Waste Incineration (MSWI)[3]. Even though the MSWI process reduces the waste amount by 80–90% w/w[4], the residual amount accounts for approx. 2–4 thousand tons per day of MSWI residues (in the Netherlands[5], the population is approx. 17 million people), particularly Bottom Ash (BA), Fly Ash (FA), and Air Pollution Control residue (APCr)[6].

Subsequently, the next issue approaches: unprocessed MSWI residues (without purification treatment) cannot be disposed of at a common landfill or used for applications[7]. MSWI FA and APCr are classified as hazardous waste, while the BA is more contaminated than the environmental requirements allow for[8]. Additionally, according to the Dutch Green Deal B-076, from 2020 all the residues from waste-to-energy plants in the Netherlands should neither be used in a non-sealed environment nor landfilled[9]. All the materials that were previously discarded will have to be treated and reused. The use in protective applications will also be eliminated[10].

Thus, the urgency of this research lies in finding solutions for treatments and applications of the MSWI residues to make them suitable for reuse. One of the most promising areas is application in the construction industry[11]. This is possible due to similarity of the chemical composition and physicochemical properties of BA and FA and concrete ingredients (cement and aggregates)[12]. The convergence of these two industries (waste handling and building materials) is attractive from several points of view, namely:

(1) waste residue disposal and reuse.

(2) replacement of natural materials used in the construction industry, availability of which is also decreasing, (natural aggregates, sand, clay, limestone, etc.).

(3) reduced carbon footprint due to the use of less cement.

Additionally, reuse and recycle of waste contribute to the goal of a circular economy[13].

BA can be divided into at least two fractions: fine (below 3–4 mm), and large (above 3-4 mm). Today, the large fraction (> 3-4 mm) of the BA is successfully used as a natural aggregate replacement[14,15]. However, application of the fine BA fraction is hindered but rather important to be developed because the share of the

fine fraction is about 50% w/w[16]. At the same time, it is also valuable to investigate the large fractions further for their potential to be used as cement replacement.

Challenges on the way from unprocessed MSWI residues to the cement/aggregate-product are:

1. Even BA is quite contaminated and cannot be used as a substitute for concrete ingredients unless it meets the environmental requirements[8]. However, considering that BA is the least contaminated of all residues, it is worth investigating from the perspective of its potential reuse.

2. Fine particle size fractions of BA (< 3 mm) have several disadvantages (high porosity and metallic aluminum, both causing bubbles and cracks in cement-containing products, a high contamination level[10]), which prevents their use as aggregate or cement substitutes due to the possible significant deterioration of the final concrete product[17].

3. FA is a potentially promising by-product for the substitution of cement[18–21]. However, extremely high concentrations of chloride, sulfate, lead, zinc, copper, etc. require a special purifying treatment before this material will be even considered for any options but landfilling[22–24].

Thus, the objectives of this thesis include a detailed study of the chemical, physical, mineralogical, structural, and environmental properties of MSWI residues (BA and FA) to develop treatments improving the quality of these residues, so they would become suitable for the use in concrete applications.

An additional objective of the study was to identify weaknesses in the waste and MSWI residues handling steps that contribute to the worsening of those materials.

1.2 History of Waste Management in the Netherlands

In the Netherlands, the era of modernization of waste management began in the 1970s. As in several European countries, the focus back then was on substituting or completing waste elimination[25]. A new environmental policy on waste prevention, recycling, and reuse as secondary materials was introduced in the Netherlands in 1988. First results of this approach led to an increase of the share of reusable waste, and emergence of the household waste separation into several categories: green waste, paper, glass, chemical waste, textile, and the remaining part (1993[26]). This residual part was submitted to the MSW Incineration (I) process, producing BA, FA, and APCr (see further Figure 1.2).

In 1997, 90% w/w of BA was allowed to be used in road base applications and embankment if the material was isolated. FA was utilized as a filler in asphalt applications, and APCr were landfilled under special conditions due to high

water-soluble salt contents. Since 1998, FA has not been allowed to be used without treatment reducing the leaching of the material[27]. To be able to figure out if certain MSWI residues can be utilized or landfilled, the leaching test approach was implemented, as it was considered that the total element content characterization often did not provide truthful information regarding the ability of the material to contaminate soils and ground waters[28].

The waste management objectives between 1998 and 2001 were focused on[25]:

1) not to increase amounts of packaging produced.
2) not to landfill combustible waste.
3) to recycle (up to 60% w/w) packaging waste.

The waste management policy of those times is depicted in Figure 1.1.

Figure 1.1 Waste management policy in the Netherlands in the end of 1990s.

Eventually, the goals for packaging were reached by 2005[26].

Several vital steps according to the new waste management policy had been mastered by 2010, namely:

1) Waste sorting and collection of various categories (up to 20) had become organized by the municipality.
2) Separate collection of plastic waste was started in 2009[26].

By 2010, the level of waste recycling has reached 51% w/w, and the material recovery rate has risen by 83% w/w (in comparison with 1985), while the share of landfilled waste decreased from 35% to 4%, w/w[26].

Even though, the recovery and recycling were quite successful, the annual analysis of the residual part of MSW showed that it still consisted of 30–40% w/w

of waste streams which should have undergone segregation (e.g., valuable materials, organic materials, or paper). Moreover, a detailed analysis of an average waste bin suggested that it only held around 2–8% w/w of residual waste which cannot fit into any category of separately collectable materials[26]. In 2011, different tariffs for residual, organic, and plastic waste collection were introduced to entice the residents to separate waste more thoroughly[26].

Several trial strategies were evaluated to stimulate waste separation among the residents of the Eindhoven region. The most efficient inventions were decreasing fees for green-waste container collection and increasing fees for residual waste; organizing collection points for the residual waste (no curbside collection); and paying citizens money for bringing recyclable waste to the special collection point (shops)[26]. These pilot projects took place in 2010–2011.

These days, different regions of the Netherlands use most of the inventions of those pilot projects depending on the region. Municipalities decide the exact way how they deal with the waste collection (curbside or collecting points). In most places, up to twenty waste categories are available for sorting.

1.3 Municipal Solid Waste Incineration and further processing

Currently, the most accepted way to process residual waste is through the waste-to-energy MSWI process (Figure 1.2). The residual part of waste, after being separated from streams, suitable for reuse and recycle, undergoes the incineration. During combustion, several fractions of incinerated residues are produced: coarse fraction at the bottom (BA), the fraction of small particles and dust, one of which is combined with the BA, and another one, FA, goes through the additional incineration treatment to considerably reduce the amounts of furans and dioxins[4]. At the last step, the residual part (after BA and FA discharge) goes through the capture of heavy metals (mercury and cadmium), and acid neutralizing treatment with the injection of lime and sodium hydroxide, producing gypsum, which creates the APCr[4]. The heat created during the incineration is delivered to steam turbines to produce electricity.

Further, the BA is quenched (sprinkled with water or placed in water tanks) to cool down, while FA is mostly landfilled[27].

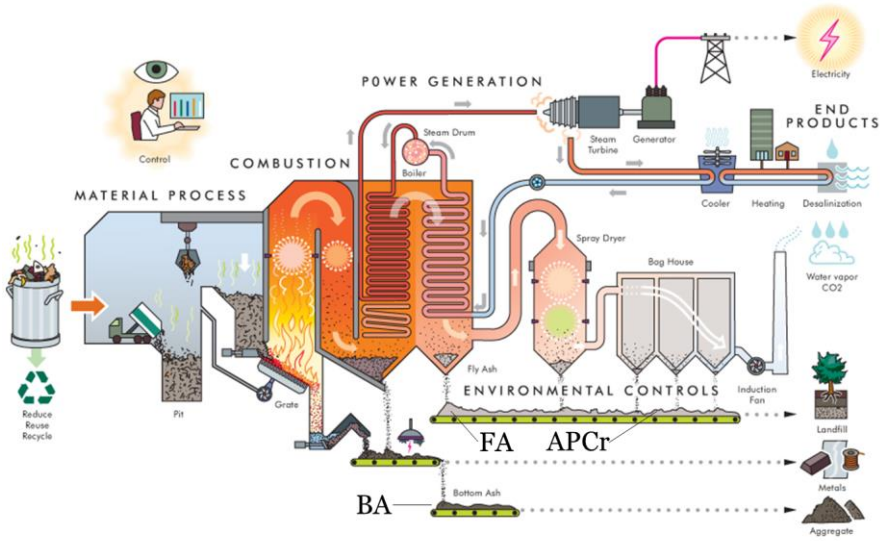

Figure 1.2 Schematic representation of a waste-to-energy plant in the Netherlands[29]. Note: the separate or combined collection of FA and APCr varies per plant, and per country.

1.4 MSWI residue

Among these solid waste residues, BA is predominant (80% w/w)[4]. The size of BA particles varies widely, from 0.01 to 100 mm. The primary BA constituents are noncombustible materials (rocks, slag, glass, etc.), unburnt organic matter (threads, films, etc.), and metal scraps[30].

Figure 1.3 MSWI bottom ash used in the study: fine fraction (< 63 μm) (left) and large fraction (22.4 mm) (right) (Mineralz, the Netherlands).

FA (15% w/w) and APCr (5% w/w) are severely contaminated with salts and Potentially Toxic Elements (PTEs)[24], and thus require expensive purifying treatment before they can pass the environmental legislation standards[8]. High

concentrations of chloride, sulfate, lead, zinc, copper, etc., turn MSWI FA into a "hazardous waste"[22–24]. The photos of FA can be found in Chapter 4.

These by-products might be of value as potential secondary building materials due to their chemical and mineralogical composition, as well as physical properties[31]. Most research is focused on BA as it is much cleaner.

According to regulations in the European Union, BA can be reused in construction materials if the quantities of PTEs and salts that can leach into ground waters are below a certain threshold[8]. The prevalent amounts of these contaminants are concentrated in FA and APCr with particle sizes below 1 mm, which are not widely processed and thoroughly analyzed to date due to the laborious and expensive treatment needed for these fractions to match legislation requirements[15].

1.5 Construction and building materials

One of the most promising courses for the application of BA is the construction industry[11]. For decades by now, these residues were successfully used in low-grade applications such as road bases, pavements, water barriers, etc. However, the depletion in natural resources for concrete components (aggregates, limestone, and clay), and the environmental impact (CO_2 emission) associated with cement production stimulate the development of alternative materials allowing to pursue at least two goals: (i) preserving nature and (ii) using valuable waste residues. This led to a successful application of the coarse fraction (above 3–4 mm) of BA in the last decade as a secondary building material (as a substitute for natural aggregates). The fine fraction (below 3 mm) has mostly been landfilled due to a high level of contamination[32]. However, should this fraction undergo a treatment with a purpose of purification, and procedures allowing to overcome the disadvantages of porosity and metal presence mentioned above, there are several possibilities to apply this material in concrete (discussed in the Introduction Section 1.7).

1.6 Concrete ingredients

To understand the potential of the BA to be used in building materials, it is necessary to look over the components of concrete, and their roles in it. "Basic" concrete consists of three ingredients: a binder (cement), aggregates (e.g., common rocks, sand), and water. Fine artificial aggregates can substitute natural sand, while large aggregates are used to replace gravel[33].

If a material such as BA or FA is of the appropriate size to be able to substitute cement (finely dispersed material by itself or milled), it can also be used if all other requirements are met[34].

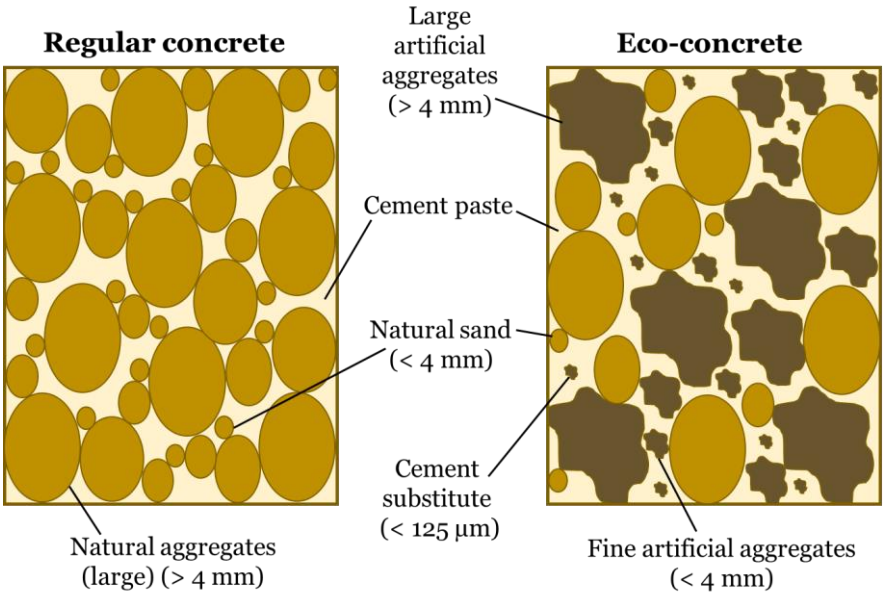

Figure 1.4 A schematic comparison of the components of regular concrete (left), and eco-concrete (where some components are substituted by treated by-products such as BA) (right).

Thus, the possibilities for BA to become a substitute are the binder, the filler part of the binder, and aggregates, e.g., it can be used as a replacement for both cement and aggregates. However, chemical properties (lower than the standard for pozzolanic materials total content of Si, Al, and Fe oxides[35]) prohibit the fine fraction of BA to become a binder, at least without various forms of the activation, such as mechanical or chemical. It was shown that BA, activated through melting to obtain reactive pozzolanic slag, demonstrated the results for compressive strength (90 days, 10–20% replacement, w/w) very close to pure Portland cement[36,37]. Another study showed that the activation of the BA with calcium chloride (40 °C-curing) led to the compressive strength even higher than for pure Portland Cement (PC) (10 and 20 days)[38]. In another study of the pozzolanic activity of BA, it was found that mortars with ground BA (0 - 1 and 0 - 4 mm) 20% w/w replacement showed severe deterioration, exhibiting the compressive strength at 28 days from 38 to 77% w/w from the reference for the fraction below

4 mm, and from 63 to 73% w/w for the fraction below 1 mm; the difference is due to variations in the water/binder ratio[35].

The use of fine aggregates derived from BA also does not appear promising due to crucial obstacles mentioned in the previous section and discussed further.

To sum up: to overcome the disadvantages of the BA fine fraction, it preferably requires milling before being used as a substitute of any kind. At the same time, a relatively high (> 10% w/w) replacement level (for cement) provides a significant (disproportionate) loss[35] in the compressive strength, which is not desired. Therefore, the most promising area for the application should coincide with both parameters: fine particles (or milled) and the replacement level below 10% w/w.

According to regulations, it is possible to use Minor Additional Constituents (MACs) in cement, which cannot exceed 5% w/w and must be below 125 μm in size[39]. The use of MACs reduces the costs related to the cement production (accompanied with the reduction of the carbon footprint) while consuming the waste material. Low replacement levels are less likely to have a noticeable detrimental effect. The Netherlands alone produces more than 1.4 million ton of cement per year[1]. Using BA fines as a 5% w/w MAC replacement would make it possible to make use of around 70 thousand tons (more than 10% w/w) of the BA fines produced yearly. However, the studies on such a low-range (less than 10% w/w) replacement level are almost absent[40,41].

1.7 Main challenges for transforming waste into secondary building materials

As previously described, while BA might have a certain value as a source for secondary building materials, there are obstacles as well. Contamination with PTEs and salts[42,43], undesirable physical properties (high water demand and porosity[17,44]), components, adversely affecting the quality of cement products (metallic aluminum[10,45], organic matter[46]), all of it should be taken into consideration to propose the treatment which would grant to rid the material from these disadvantages.

Contamination

Unprocessed (unwashed) BA and FA are relatively contaminated[47]. The level of pollution of the BA is significantly lower than of FA, which only passes the environmental legislation for the “hazardous waste” category[8]. For BA the main challenge is the leaching of chloride and sulfate, Sb, Cu, and Zn[32,48]. However, it is worth mentioning that the main hazard is coming from the fraction below 1 mm, while the leaching of large BA fractions approaches the “safe” level[49]. Unlike

BA, FA is highly contaminated, especially with chloride, Zn, and Pb[50]. Before any of these by-products could be used, they must be treated to avoid contamination of the ground waters[51].

High water demand and porosity

The BA has a relatively high porosity in comparison with the materials it can substitute. Its use "as is" leads to increased water demand[52], concrete structures with reduced density[53], and, therefore, deterioration of the mechanical performance[52]. From the practical perspective, during the preparation of the mixtures with the replacements by BA, a higher water demand would require more water added to the mixture. If done, this might lead to a decrease in strength due to the increase in the water/binder ratio[52]. At the same time, if the material porosity and, thus, the water demand is too high, not adjusting the amount of water may also cause a decrease in strength because too much water will be absorbed by the BA leaving too little for the cement hydration. Eventually, depending on the severity of the porosity, a decent share of the cement in the mixture will not be contributing to the hydration process, therefore, reducing the strength.

Metallic Aluminum

This challenge is relevant for both materials (BA and FA)[54,55]. When metallic Al is in contact with the alkaline environment, it would form hydrogen gas, which leads to the formation of gas bubbles in the cement mixture:

$$2Al + 2OH^- + 6H_2O \rightarrow 2[Al(OH)_4]^- + 3H_2 \uparrow \qquad (1.1)$$

While hardening, if the bubbles are entrapped into the cement matrix, the pores will be formed[56]. However, even though the presence of the metallic aluminum particles (in forms of shavings, bids, flakes, and chunks, depending on the particle size) is a well-known problem, the detrimental effect from it differs depending on the particle size fraction[57]. Large chunks of aluminum being in the alkaline environment (provided by cement) would cause large, poorly distributed in the volume pores[56], severely influencing the structure of the cement product, and, therefore, the strength. At the same time, if the share of Al does not exceed 0.1% w/w[39], and the particle size of the bids is quite small, this can provide a relatively even distribution of small pores in the concrete structure, which will lower the density, but the effect on strength will be less noticeable[58].

1.8 Research strategy

To be able to transform MSWI residues into a valuable secondary material, it is necessary to get an understanding of the full profile of physicochemical

properties of the material before it undergoes any treatments. The more properties are included in the consideration before planning regarding treatment developing, the more effective and cost efficient it is going to be. The same goes for a fractionation of the material because it is well known[59] that the fine and coarse fractions differ significantly, especially from the viewpoint of the contaminants[32]. A great deal of literature has been focused mostly on studying the leaching behavior of the whole BA (not differentiating between coarse and fine fractions)[60] or developing treatments to minimize the adverse effect of by-products used as secondary building materials[61]. Most treatments aimed to reduce the PTE leaching are washing[62], carbonation[63], and heating treatments[10]. Another share of treatments includes separation[64], milling[65], and solidification[66].

In the Netherlands, BA, FA, and APCr are handled separately, and now, it is not considered to be beneficial to use APCr as a potential substitute for building materials. Therefore, APCr was not included in the study.

The first-part goals of this research were (1) to characterize various properties of two by-products (BA and FA) sufficiently to study both the distribution of the contaminants throughout the fractions and inside of the material itself, and (2) to study and compare the properties of multiple BA fractions to assess, which parts of these by-products are suitable as secondary building materials, and which are not. The second part of goals were (3) to select a fraction of most interest and (4) develop a treatment to use it as a cement component. Further, (5) to develop a treatment, which includes all the steps needed to considerably improve properties of BA, and (6) to test recipes with differently treated BA, with several types of cement.

Subsequently, (7) to evaluate cement-containing products (pastes and mortars) for various properties to determine the effect of added BA. The final part of the thesis originated from the data from the first part, and observations obtained at the final steps. It resulted into (8) composing a semi-empirical leaching model, which may be useful for predictions on the environmental impact of BA fractions, and as a demonstration of the detrimental effect of the quenching procedure.

1.9 Outline of the thesis

To transform MSWI residues into valuable secondary building materials, at least two vital steps are needed. First, to develop a treatment that simultaneously creates material assets needed for its successful application as a substitute for concrete components (e.g., free from the contaminants and reduced particle size), and combats the disadvantages of the original residue (Al, porosity, and organic

matter). Second, to launch a thorough preliminary study of the properties of the residues allowing not only selecting the most appropriate treatment, but also segregating the most and least promising fractions for applications, as well as developing tailored treatments for fractions with different properties. The last part includes developing the leaching model to estimate or predict the contamination level of a particular particle size fraction inside the whole range using the information from the most and least contaminated fractions of the BA.

This thesis is organized as described below. Figure 1.5 depicts all parts of the study and connections between them.

The methods and procedures used in the study are listed in Chapter 2.

Chapter 3 provides the analysis of 14 particle-size fractions of BA to determine the total elemental composition and leaching capacity, mineralogical composition, and shape variety of fine particles to assess the applicability of all the fractions. The division of fractions based on the mineralogical composition and contamination level is proposed.

To complete the first overview of both types of the residues, the next chapter is devoted to FA. Due to a remarkably high contamination level of this residue, the study includes both characterization and treatment as it is of particular interest to study this material before and after a chemical treatment.

Chapter 4 shows the efficiency of a new three-step combined treatment with two complexing agents (ethylenediaminetetraacetate and gluconate) to increase the toxic-element elution from FA in contrast to conventional water-only treatments. The compositions of raw and differently treated (reagent-combined and water-only treatments) FA are compared by macro- and microelement, mineralogical, and microstructure analysis, in addition to the standard leaching test. The relevancy for such comprehensive analysis of FA prior and after treatments to minimize the environmental risks is shown.

Based on the data on material's potential, further study is focused on the BA fine fractions, as FA is severely contaminated and before applied as building materials, it must undergo an extensive purifying treatment that does not seem an economically feasible choice at that moment. The coarse fraction of the BA by that point of the research have already been successfully studied and applied as a natural aggregate substitute.

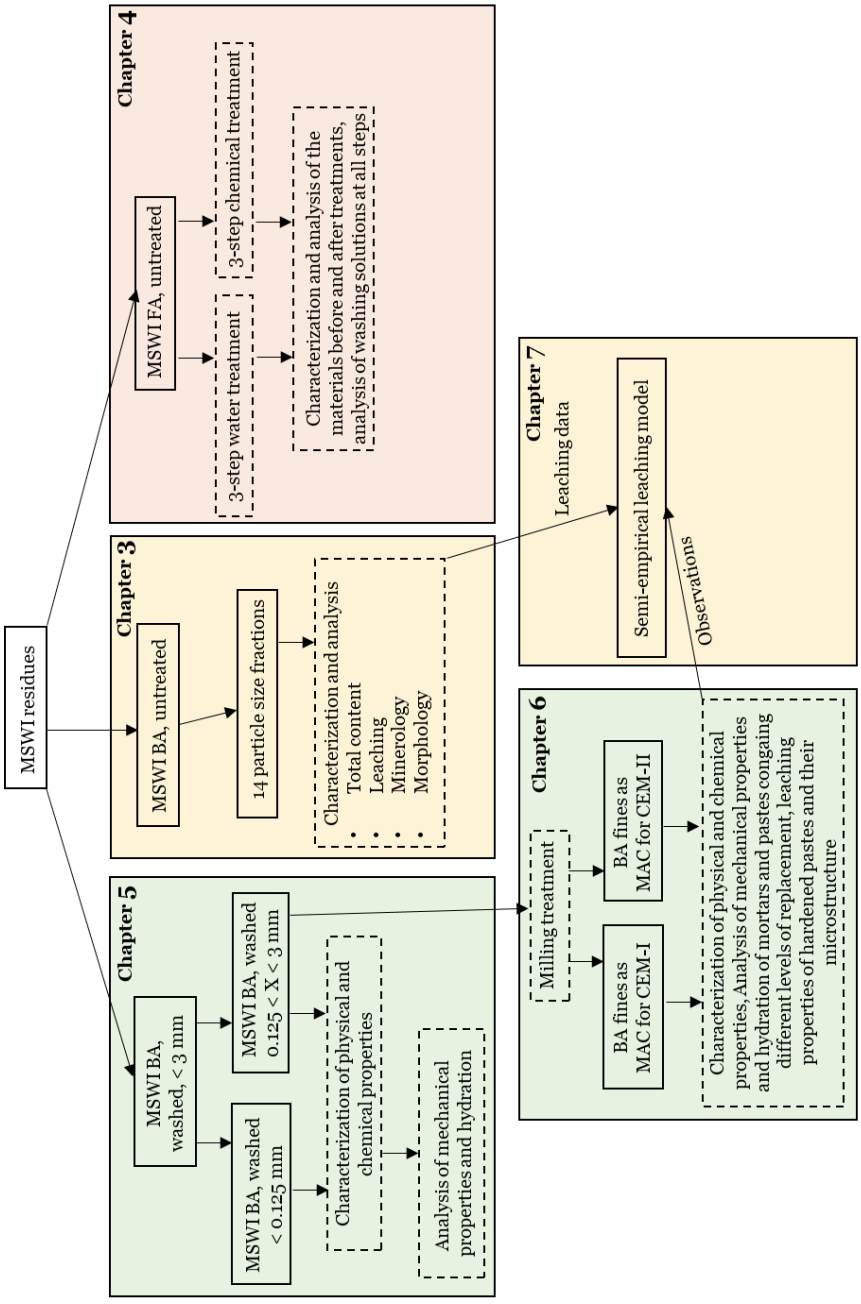

Figure 1.5 Scheme of the thesis outline.

Chapters 5 and 6 are devoted to the investigation of milled fines produced out of BA fines (0.125–3 mm) to match the size distribution of CEM I 52.5 R and CEM I 42.5 N. Treated fines are also compared to the untreated fines (< 0.125 mm) from the same BA. The influence of milling on the fines is investigated by SEM (morphological analysis) and the leaching test to assess the potential environmental impact. The effect of the designed fines on cement hydration studied by isothermal calorimetry. The mechanical performance of mortars containing designed fines as a MAC is assessed.

The final part of the thesis contains the semi-empirical leaching model presented in Chapter 7. The mathematical (stereometric) model is based on the leaching data from the entire range of particle size fractions and the idea of the influence of the quenching layer on the leaching.

Chapter 8 covers the main conclusions of the research and provides recommendations for further studies.

CHAPTER 2

Materials and methods

2.1 Introduction

In this chapter, all the materials, methods, and procedures used in this study are presented. Three types of the material are used in this thesis: two types of the MSWI BA (untreated, and washed), and untreated MSWI FA. The general descriptions of the methods and procedures which were used for most parts of the work are summarized here, and more detailed versions or specific procedures which were used singularly can be found in the relevant chapters.

2.2 Materials

2.2.1 MSWI bottom ash (untreated)

BA was supplied by the municipal solid waste-to-energy incinerator plant of Mineralz (Duiven, the Netherlands), where it underwent the standard washing and ferrous and non-ferrous metal removal process. The material had been stored for 3 months after the production, prior to analyses. For all types of analyses, the material was oven-dried (105 °C) to a constant mass. The material is used in Chapters 3 and 7.

2.2.2 MSWI bottom ash (treated)

BA fines (< 3 mm) were supplied by the municipal solid waste-to-energy incinerator plant of Mineralz (The Netherlands), where they underwent the standard washing and ferrous and non-ferrous metal removal process. Prior to each step fines were oven-dried (105 °C) to a constant mass. The material is used in Chapters 5 and 6.

2.2.3 MSWI fly ash (untreated)

FA was supplied by the municipal solid waste-to-energy incinerator plant of Mineralz (Duiven, the Netherlands). The material was oven-dried at 105°C to a constant mass. The material is used in Chapter 4.

2.2.4 Cement production, composition, and hydration

The production of PC requires significant amounts of natural resources. Commonly, limestone and clay are heated to a high temperature (circa 1500 °C) in a kiln, where they react into calcium silicates. In this process, substantial amounts of carbon dioxide are emitted[33].

When cement reacts with water, it forms several hydration products. Each of the cement components contributes to the hydration process and strength of hydration products as they have different reaction rates: from slow for belite (mostly C_2S (dicalcium silicate)) to fast for C_3A (tricalcium aluminate) + $C\hat{S}H_2$

(gypsum), and respective amounts of liberated heat, and different effect on strength (high for alite (mostly C_3S, tricalcium silicate), first low, then high for C_2S, and low for other components)[33]. Components such as gypsum play their role as retardants of the early hydration reaction.

For main cement components, the hydration reactions are[33]:

$$2C_3S + 11H \rightarrow C_3S_2H_8 + 3CH \quad (2.1)$$

$$2C_2S + 9H \rightarrow C_3S_2H_8 + CH \quad (2.2)$$

$$C_3A + 3C\bar{S}H_2 + 26H \rightarrow C_6A\bar{S}_3H_{32} \quad (2.3)$$

where H is water, $C_3S_2H_8$ is calcium silicate hydrate, CH is calcium hydroxide, and $C_6A\hat{S}_3H_{32}$ is ettringite.

The hydration process is best followed by isothermal calorimetry, where any changes and effects on the heat release by components added to the cement can be observed as the heat flow is proportional to the reaction rate. The early hydration involves five stages: (1) initial hydrolysis (circa 15 min), (2) dormant period (ends within 2–4 h from the reaction start), (3) acceleration (early hardening, 4–8 h), (4) deceleration (8–18 h), and (5) steady state (18–36 h)[33].

2.3 Methods and procedures

2.3.1 Standard leaching test

Every studied sample (Section 3.2.1) was subjected to the leaching test according to EN 12457-4. Upon completion (24 h of shaking, L/S 10), all the leachates were filtered (0.2 μm) to prepare them for later analyses by IC (Section 2.3.7) and ICP–AES (Section 2.3.2).

2.3.2 Inductively coupled plasma atomic emission spectrometry

ICP–AES was selected as it provides a rapid and highly sensitive multielemental analysis of BA and FA with a high level of precision and accuracy[67,68]. An axial ICP Atomic Emission Spectroscopy (AES) 720-ES spectrometer with an SPS3 autosampler and ICP Expert software 2.0.5 (Agilent Technologies) with a low flow axial quartz torch with a 2.4 mm i.d. injector tube (Glass Expansion), a double-pass glass cyclonic spray chamber, a glass pneumatic nebulizer (Agilent Technologies), and a Trident Internal Standard Kit (Glass Expansion) was used. All emission lines were measured simultaneously. An internal standard solution was added online.

Deionized water (specific resistance, 18.2 MΩ×cm) from a Milli-Q Academic system (Millipore) and HNO_3 (69% w/w, ACS-ISO grade, Panreac) were used for

all the operations with ICP–AES (the preparation of calibration solutions and washing).

All standard solutions were from High Purity Standards. A mixture of standard solutions ICP-AM-6 (100 mg/L of Al, Sb, B, Ba, Be, Cd, Ca, Co, Cr, Cu, Fe, Li, Mg, Mn, Mo, Ni, K, Na, Si, Pb, Tl, Sr, V, Zn) and ICP-MS-68B (100 mg/L of Sb, Ge, Hf, Mo, Nb, Si, Ag, Ta, Te, Sn, Ti, W, Zr) from High-Purity Standards was used for the calibration in the range 0.01–10 mg/L. A mixture of an ICP-AM-15 standard solution (10000 mg/L of Na, K, Ca, Mg), P (10000 mg/L) and S (10000 mg/L) was used for the calibration in the range 1–100 mg/L. An internal-standard solution of Sc (20 mg/L) was prepared from a standard solution (Inorganic Ventures, 1000 mg/L).

Data Treatment (ICP-AES)

The measurement results are presented in accordance with the requirements of ISO/IEC 17025:2005. Limits Of Detection (LODs) and Limits Of Quantification (LOQs) were calculated as the ratios of three and ten times standard deviation of twenty blank readings to the calibration-curve slopes. Concentration detection limits by ICP–AES were recalculated to BA quantities.

2.3.3 Fused bead preparation

To prepare fused beads, the following procedure was used: 0.95 g of BA was mixed with 9.5 g of a flux (67.00% $Li_2B_4O_7$ – 33.00% $LiBO_2$, w/w, Claisse), and 0.1 g of LiBr (Claisse) as a non-wetting agent. Mixtures were put individually into borate fusion ovens for 24 min at 1065 °C. The procedure was made for 3 replicates for each studied sample.

The borate-fusion technique allows rapid and easy sample preparation to conduct a subsequent multielement analysis using ICP–AES. Compared to microwave digestion, which frequently causes difficulties with a factually complete sample dissolution[68,69], a sample is completely dissolved. A blend of lithium metaborate and tetraborate was selected as a mixture of basic and acidic fluxes, which provides a complete and reproducible sample preparation of industrial waste BA including different incinerator types[70], various types of slag (blast furnace, steel)[71], and BA[72] as all these residues contain both types of oxides.

2.3.4 Sample preparation for ICP (fused beads)

Fused beads were ground for 2 min in a planetary ball mill, and 1-g weighed portions were dissolved in 50.00 mL of 5% w/w HNO_3 (p.a. grade) in an ultrasonic bath for 1 h and subjected to ICP–AES. The estimated average concentrations of designated elements (µg/mL) were recalculated to mg per 1 kg of the raw material.

2.3.5 X-ray fluorescence spectroscopy

A PANalytical Epsilon 3 (The Netherlands) energy-dispersive X-ray fluorimeter (EDXRF) with a 9 W / 50 kV rhodium X-ray tube, and a silicon drift detector and standardless Omnian software 1.0.E was used to analyze the composition of BA and FA samples and cement.

2.3.6 X-ray Diffraction analysis

The BA mineralogical composition was determined by XRD using a Bruker D2 PHASER (a Co tube, 1.79026 [Å]) with a LYNXEYE 1-D detector and fixed divergence slits. XRD measurements were performed on pre-dried powdered samples. Phase identification was performed using X'Pert HighScore Plus 2.2 and the PDF-2 database.

2.3.7 Ion chromatography

IC was used as a standard method for chloride and sulfate determination in leachates[73]. A Thermo Scientific Dionex 1100 ion chromatograph was used: 2×250 mm AS9-HS ion-exchange columns, isocratic flow (0.25 mL/min). Ion detection was carried out by measuring a suppressed conductivity with an electrolytically regenerated suppressor (Thermo Scientific Dionex AERS 500 2 mm). A solution of Na_2CO_3 (9 mM) was used as eluent.

2.3.8 Brunauer–Emmett–Teller (BET)

The Specific Surface Area (SSA) of 4 types of BA fines and cement was assessed by a Micromeritics Tristar II 3020 analyzer (software, TriStar V1.03) using a single-point BET technique by volumetric nitrogen adsorption at 77.35 K.

2.3.9 Scanning Electron Microscopy

Scanning Electron Microscopy (Phenom ProX, PhenomWorld) with a backscattering electron (BSE) detector with a spot size of 4.0 and a voltage of 15.0 kV was used. The samples prior to analysis were covered with a 14 nm gold layer by means of a SOP K575X Dual Turbo sputter coater.

2.3.10 Flameless atomic-absorption spectrometry coupled with pyrolysis

An RA-915+ Mercury Analyzer (Ohio Lumex Co.), a portable multifunctional AAS instrument with Zeeman high-frequency modulation of polarization for background correction, with a RP-91C pyrolysis attachment (Lumex) was used for mercury determination in FA.

2.3.11 Standard procedure for microwave digestion

The M-MVI 80-2008 standard method of microwave-assisted acid digestion for performing measurements of mass fractions of elements in samples of soils and bottom sediments using AES and AAS was used. The digestion procedure was adapted specifically for these samples. The volumes of 9 mL of conc. HCl, 3 mL of conc. HNO_3, and 0.5 mL of conc. HF (ISO-grade, AppliChem Panreac, Spain) were added to the samples (150–200 mg), the mixtures were placed in high-pressure vessels, and were heated for 1 h in a microwave oven.

2.3.12 Mortar and paste preparation

Mortars with cement-fines mixtures were prepared according to EN-196-1. A reference batch was made from 450 g of cement, 225 g of water, and 1350 g of sand. The batches containing 5% w/w of the cement replacement had 22.5 g of fines (MCF, BF, SOF-52, and SOF-42) and 427.5 g of cement: the rest of the recipe was the same. The mortars were prepared in Styrofoam molds and cured in water. All mixtures were premixed and homogenized with a vortex mixer prior to adding them to water.

2.3.13 Flexural and compressive strength

Prepared mortars (4×4×16 cm) were submitted to compressive and flexural-strength testing (Zwick Z020). Samples were tested after 2, 7, 14, 28, and 91 days of curing.

2.3.14 Auxiliary Equipment

A lab-scale jaw crusher (Retsch BB 100) fitted with waved manganese steel jaws set to an opening of 8 mm, a planetary ball mill (Fritsch PULVERISETTE 5) fitted with zirconium oxide grinding bowls, and 20 and 10-mm mill balls were employed successfully for the sample size reduction. A chamber furnace (Thermo Scientific Heraeus K 114) was used for Loss On Ignition (LOI) (550 °C). A fusion instrument (Claisse leNEO) was used. Riffle boxes (sample splitters), 15-D0438 and 15-D0438/F (Controls Group), were used to obtain randomly divided samples. An SM-30 shaking table (Edmund Bühler GmbH) was used to perform the leashing test. Automatic Eppendorf Research pipettes (Eppendorf International) were used for the preparation of calibration solutions. A-class polypropylene volumetric flasks (Vitlab) with volumes (50.00 ± 0.12) mL and (100.00 ± 0.20) mL and polypropylene test tubes (Axygen) were used for the preparation of calibration and test solutions. An analytical balance (Mettler Toledo XP 504), a floor scale (Mettler Toledo ID5 Multirange), and a UF 260 drying oven (Memmert) were used for sample preparation. Bulk densities of BA

samples were measured by a common pycnometer. The specific density of materials was measured using a He pycnometer (Micrometrics AccuPyc 1340). The Punkte test was used to examine the water demand of BA powders[74]. Particle size distributions (PSD) of all powders were measured by laser diffraction (Mastersizer 2000, Malvern). The hydration process was studied by isothermal calorimetry (a TAM Air calorimeter).

CHAPTER 3

Detailed characterization of particle size fractions of MSWI BA

This chapter has been published as:

E. Loginova, D.S. Volkov, P.M.F. van de Wouw, M.V.A. Florea, H.J.H. Brouwers, 2019. Detailed characterization of particle size fractions of municipal solid waste incineration bottom ash. Journal of Cleaner Production. 207, p. 866-874. doi: 10.1016/j.jclepro.2018.10.022.

3.1 Introduction

The previous research on BA properties was mainly focused on the mineralogical characterization, and in particular, the composition of phases bearing heavy metals[75]. In another study, BA was analyzed by SEM/EDX with an emphasis on the potentialities of the methods for microstructures of mineral phases and nanophases embedded into vitreous structures[76]. Using such an approach, XRD, and chemical speciation, the sources of chlorine and heavy metals in BA as the main factors of potential environmental risks were studied revealing the possible sources of these hazardous components in the ash[77].

SEM/EDX microstructure analysis followed by the characterization of the leaching behavior of BA added to concrete and asphalt mixtures revealed metals that can be retained by these construction materials either physically or through chemisorption; the potential hazard was shown for European and Asian BA[78]. A combination of several methods (element mapping and PARC, SEM/EDX, and leachate analysis) was used to study the composition and contaminants effect of a 0–4 mm BA fraction on the cement hydration[79].

The composition of calcium- and silicon-containing phases of alkali-activated BA was characterized using XRD and FTIR spectroscopy; the comparison of cement-like structures in BA with Portland cement showed similarities and differences of these materials[80]. However, the literature providing comprehensive information about the whole BA fraction range is rather limited.

Among the most relevant to this topic are studies devoted to the use of different grain sizes of treated BA mineral fractions in designing concrete recipes[31]; however, mineralogy and morphology of the treated material is not discussed. Different particle-size fractions of BA were investigated, but the fractionation was not very detailed (6 fractions), and fines were studied as a single 0–2-mm fraction[81]. Previously, it was suggested that BA fines, while processing, can be divided into two groups: 0–50 μm and 50 μm – 2 mm; however, the reasoning was not presented[73]. In general, in the literature related to the fractionation of BA and its properties, the main shortage is in the number of fractions, leaving the properties and behavior patterns within those undivided fractions uninvestigated.

Obtaining a full picture about BA fractions would make it possible to justify its fractional division for further use instead of unifying fractions presumably similar in properties without supporting it with reliable data. This is especially relevant for fine fractions of BA which might be used in production of small-grain size

lightweight artificial aggregates because treated fines can still be used as fillers[82] or in the production of blended cement[52].

Regarding the environmental impact from hazardous components of BA, it is primarily important to evaluate their leaching capability[51]; for this reason, almost every legislation is based on leaching. However, to fully understand latent properties of BA, it might be beneficial to study not only the leaching properties but the total elemental and mineralogical composition as well.

The literature shows that the knowledge gap is laying in a detailed characterization from two viewpoints: a full material 'portfolio' requires a combination of properties (leaching, elemental, and mineralogical) rather than some of them individually; and many BA size fractions should be analyzed to prove or disprove the necessity to divide them in a certain way for further analysis, treatment, and utilization.

A complete picture of BA properties might allow the most adequate assessment of not only which treatment methods to use for a particular fraction, but also to understand whether it should be done at all, and how to utilize all fractions most efficiently (sorbents, metal extraction, building materials, etc.). This can make it possible to use BA more efficiently as a secondary building material. This can help to analyze, process, and reuse more efficiently materials of this type, reducing the landfilled amount and diminishing the proportion of natural materials used in construction. Possessing a wider picture of BA fractions would help to effectively reduce its environmental impact by removing toxic substances. In this study, the aim is to assess the vital properties for a detailed set (14 narrow size ranges) of BA fractions, such as leaching capacity, total elemental, mineralogical compositions, and morphology of fine particles, which, to the best of our knowledge, was not implemented previously.

3.2 Materials and methods

The general materials and methods are discussed in Chapter 2. Here, specific details and/or unique for the chapter procedures are presented.

BA was supplied by the municipal solid waste-to-energy incinerator plant of Mineralz (Duiven, the Netherlands). The material had been stored for 3 months after the production, prior to analyses.

3.2.1 Sample preparation

Due to high heterogeneity of BA, three samples (the fraction below 31.5 mm, 15 kg each) were used as replicate samples. Prior to analysis, samples were crushed to break agglomerated or cemented materials, then ferrous and

nonferrous metals were extracted. Further, the material was dried in an oven at 105 °C to a constant mass. Next, to obtain the entire range of fractions, each sample was sieved into 19 size fractions according to EN 933-1 (2012) and EN 933-2 (1995) with the addition of sieves with the following mesh sizes: 22.4 mm, 11.2 mm, 5.6 mm, 2.8 mm, 1.4 mm, 710 μm, 355 μm, 180 μm, and 90 μm to provide more fractionation of coarse fractions and to render the initial detailed set of similarly distributed fractions for coarse, medium, and fine fractions. Then, some of these sieved fractions were unified if they had insufficient mass to be analyzed. Table 3.1 presents the fractional distribution of the investigated BA.

Table 3.1 Mass distribution among the BA particle size fractions

Fraction	Share (w/w)	Fraction	Share (w/w)
< 63 μm	1%	0.71 – 1 mm	5%
63 – 90 μm	1%	1 – 2 mm	14%
90 – 125 μm	1%	2 – 2.8 mm	8%
125 – 180 μm	2%	2.8 – 4 mm	9%
180 – 250 μm	2%	4 – 11.2 mm	13%
250 – 355 μm	2%	11.2 – 22.4 mm	22%
355 – 710 μm	8%	> 22.4 mm	12%

This resulted in the set of 14 fractions: < 63 μm, 63 – 90 μm, 90 – 125 μm, 125 – 180 μm, 180 – 250 μm, 250 – 355 μm, 355 – 710 μm and 0.71 – 1 mm, 1 – 2 mm, 2 – 2.8 mm, 2.8 – 4 mm, 4 – 11.2 mm, 11.2 – 22.4 mm, and > 22.4 mm. Each fraction of replicates was divided with sample splitters: the first half was saved for later use for total quantitative analysis by ICP–AES; the second half was used for a leaching test. Next, the particle size was reduced using a crusher and a planetary ball mill to prepare samples for borate fusion (required particle size less than 500 μm). Fractions with a particle size > 4 mm were both crushed and milled. Fractions with a particle size from 500 μm to 4 mm were milled without crushing. Each fraction was milled at 200 rpm for 1 h and 40 min with a 5 min break every 10 min. After milling, fractions larger than 500 μm were sieved through a 500-μm sieve to remove unmilled matter (generally, flattened metal particles, threads, rope pieces, etc.). The largest content of these components in the studied fractions was in the range of 1% w/w.

3.3 Results and discussion

3.3.1 SEM of fine BA fractions

A SEM analysis was conducted to discover differences in the shape and structure of BA particles among the fine fractions up to 500 μm. Among the literature on the topic, no SEM research on different particle size fractions of this material was made previously. Among the newest studies, the outlook[83] and photos of BA particles ground below 45 μm[84] can be found. Figure 3.1a illustrates the shape of particles from the finest fraction. Particles of this fraction, which have a very small size (about 20 μm) and a large surface, are predominant. There are only a few large particles, and their surface appears to be similar to the one of the smallest BA particles. For the fraction 63–90 μm (Figure 3.1b), despite the obvious predominance of fairly large particles with large surfaces, tiny particles about the same size of 10–20 μm and even smaller are also present, Figure 3.1a.

Figure 3.1 (c and d) illustrates the appearance of 125–180 and 180–250 μm fractions at the same scale as the previous ones. They have the same very large surface, and there are also very small particles nearby, but much less. Figure 3.1 (e and f) shows the remaining fractions from the fine-size range with a larger scale. The shape of the particle surface does not differ from 125–250 μm. Particles of at least 500 μm are significantly different from those of larger fractions (which resemble very small pieces of rock, glass, etc.), and the morphology does not differ among fine fractions. These particles, called quench products, are formed during water spraying on hot BA after the incineration[59]. They have amorphous and microcrystalline structures mainly consisting of calcium silicate hydrate with the particle size below 0.4 mm[85]. These quench products adhere to larger particles, forming a fragile surface layer. It was shown that the quenching phase of BA processing highly affects the leaching of PTEs[86]. The large surface of these particles, serving as a high-capacity absorbent, might be a source of their significant release during their subsequent use in building materials[43,87].

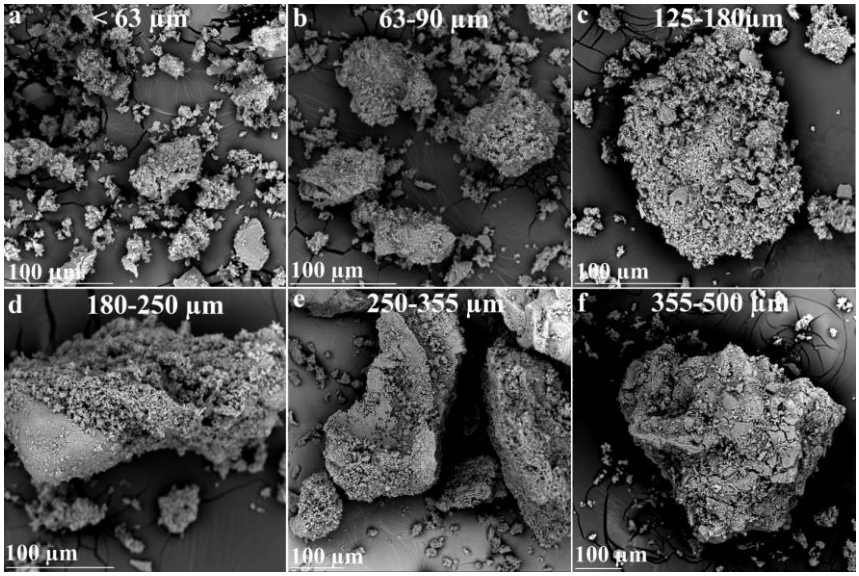

Figure 3.1 SEM images of BA fine particle size fractions. The fraction size is given at the top of each part of the figure.

3.3.2 Mineralogical composition of BA fractions

The 14 original BA fractions, mineralogically, can be divided into six combined groups, Table 3.2. The minor fractions are virtually the same in composition, so in Table 3.2 and in Figure 3.2, groups of fractions are presented to avoid the duplication of information.

Table 3.2 Main mineral phases in the composition of 6 combined particle size fractions of BA.

Mineral	< 180	180-500	0.5-1	1-4	4-22	> 22
	µm		mm			
Quartz	+	+	+	+	+	+
Feldspar	+	+	+	+	+	+
$MgFe_2O_4$	+	+	+	+	+	+
Melilite	–	+	+	+	+	+
Spinel	–	+	+	+	+	+
Pyroxene	–	+	+	+	+	+
Sylvite	+	+	+	+	+	–
Zeolite	+	+	+	+	–	+
Calcite	+	+	+	+	–	–
Anhydrite	+	+	–	–	–	–
Halite	+	–	–	–	–	–
Mica	–	–	–	–	–	+

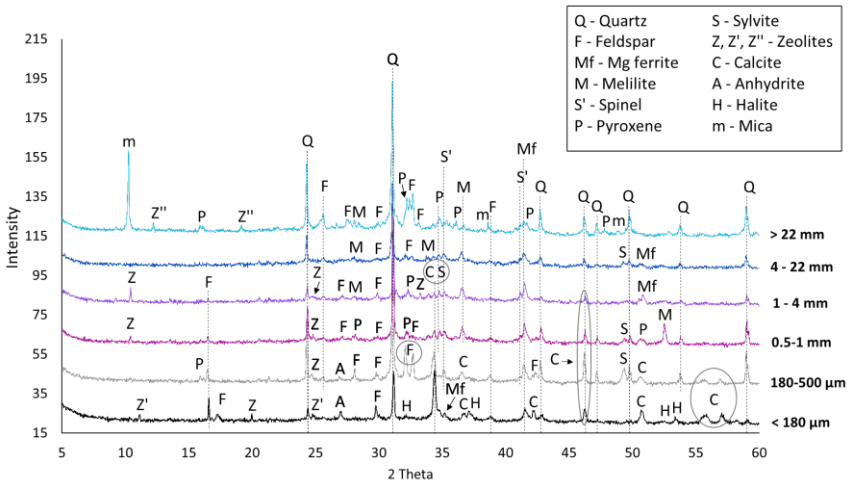

Figure 3.2 Diffractograms (Co radiation) of 6 combined BA fractions; for the sake of convenience, the plots are shifted relative to each other; the intensity scale is given in square roots of original values.

Quartz is prevalent in all the fractions. This is in line with literature as the main mineral in fine fractions below 2 mm[88] and coarse fractions, 2 – 50 mm[89]. Due to a mechanical resistance, the amount of quartz in the fractions increases with the particle size (Figure 3.2). Two other components, which are also present in all fractions but in slightly different amounts, are feldspar and magnesium ferrite, which were also found previously[45].

The next group of minerals — melilite, spinel, and pyroxene — are present in all fractions except <180 µm[90]. Sylvite, as well as its modifications (all denoted as S) containing different amounts of K and Na, is present in all fractions except the largest one (> 22 mm), which agrees with the leaching test results for these fractions (Section 3.3.4). In fractions below 4 mm and in the largest fraction, traces of zeolites of various composition were found. Their absence in 4–22 mm fractions can be explained by the fact that zeolites have a domestic source represented by sufficiently fine particles, e.g., washing powders[91], adsorbents[92], which, in the incineration process, are more likely to end up in BA fine fractions. The presence of zeolites in the largest fraction can be explained by attached fine particles[59]. Calcite and anhydrite are commonly found in BA phases[45]. Calcite can be seen in all fractions below 4 mm. Anhydrite is present in fractions below 500 µm, which agrees with the leaching test results for sulfate, a steep decline in sulfate leaching after the 500 µm fraction (Figure 3.6).

Halite is detected in fractions below 180 μm only. The last mineral that distinguishes the largest fraction from all the others is mica. This could be explained by the fact that micas are widely used in the glass manufacture, from decorative to optical[93], and the glass share in the largest fraction is (visually) larger compared to fractions below 22 mm.

The predominant phases in the investigated BA are quartz and various aluminosilicates, which makes it possible to consider all the fractions as secondary building materials. The results agree with the literature[75].

3.3.3 Total elemental composition of BA fractions

The major elements found in BA fractions were Si, Ca, Fe, Na, S, and Mg, which is in accordance with mineralogical data (Section 3.3.2) and literature[94]. Figure 3.3 demonstrates that concentrations of Ca, Fe, and S decrease as the particle size increases. The trend for Si is the opposite. The contents of Na, Al, and Mg vary insignificantly among fractions, but there is no decreasing trend.

Figure 3.4 illustrates the particle-size dependence of the content for elements present in medium concentrations in the BA, including PTEs; there is no full set of data for these fractions and elements in the literature. In all cases, there is a gradual decrease in the concentrations of all the elements for fines below 355 μm (the larger the fraction, the lower the content). This agrees with SEM data on the same particle shape for these fractions and is caused by the SSA of these particles and quench-product particles. A significant increase in concentrations for larger-size fractions is observed, which is due to a change in the mineralogical composition of particles; this effect is strongest for Cu (1 – 2.8 mm) and Zn (2 – 4 mm). To the best of our knowledge, this is observed for the first time. The Ti content varies insignificantly among fractions above 355 μm (3200 – 4000 mg/kg). Similarly, Ba and Mn contents remain approximately at the same level with insignificant fluctuations among fractions above 355 μm. The contents of Cr, Pb, Ni, and Sb decrease smoothly and with fluctuations with an increase in the particle size.

The Relative Standard Deviation (RSD) values for all investigated particle size fractions of BA for all the elements in this study presented in Appendix A, Table A.1). The results for 3 replicates show negligible differences for most elements and fractions. Higher RSDs for Cd, Sb, and Sn for some fractions might be explained by the trace level of concentrations (Cd max. 14 mg/kg, Sb max. 170 mg/kg, and Sn max. 350 mg/kg) for these elements. As during the preparation, samples were significantly diluted (Section 3.2.1), this might be considered as one of the limitations of this method to investigate the total content of trace elements.

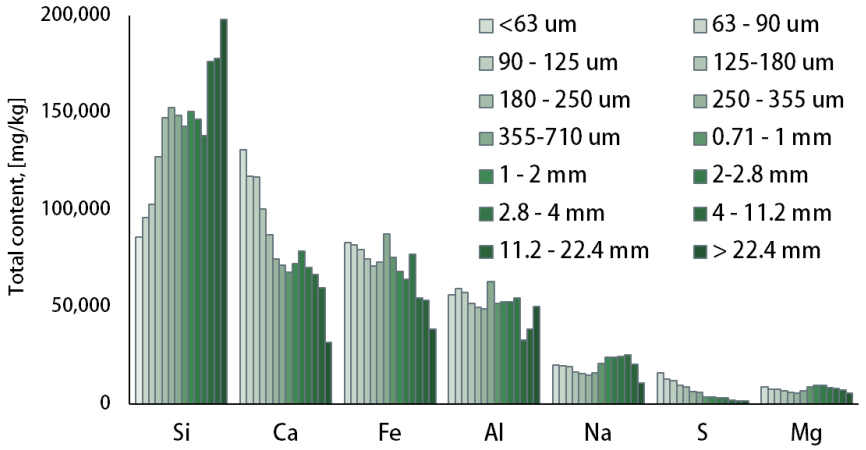

Figure 3.3 Total content of major elements in 14 particle size fractions of BA.

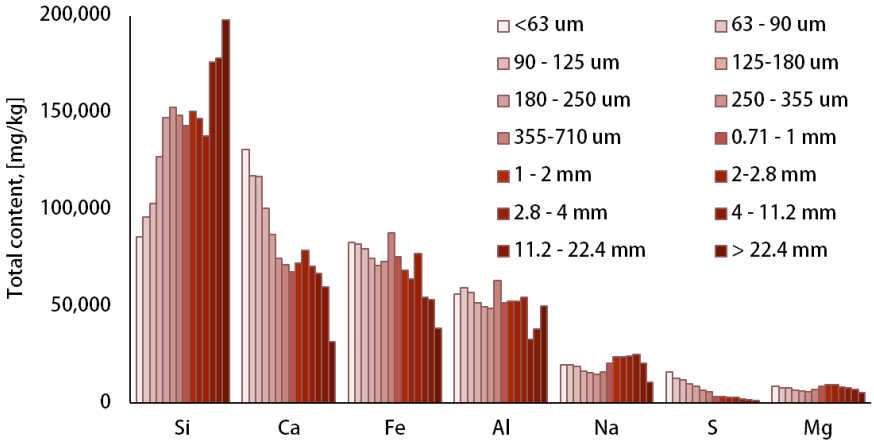

Figure 3.4 Total content of PTEs and medium concentrated elements in 14 particle size fractions of BA.

3.3.4 Leaching test and its fraction dependences

For total analysis, the elements forming major basic (Na, Mg, Ca, Ba) and acidic (Si, P, S) oxides in BA, and medium-concentration (Al, Cu, Zn, Ti, Cr, Mn, Fe, Co, Ni) and trace (V, Sr, Zr, Sn, Sb, Pb) elements[43] were selected; out of these, only a few exceed the environmental Legislation Limits (LL) in BA, which are shown in Table 3.3.

Table 3.3 Maximum allowable leaching (LL) for non-shaped building materials according to The Soil Quality Decree[8].

Element	Cd	Cr	Cu	Ni	Sb	Zn
LL (mg/kg)	0.04	0.63	0.9	0.44	0.32	4.5

Major cations and anions

Table 3.4 shows the pH over the range of fractions. It varies between 8.8 and 9.2, and does not account for differences between the leaching behavior of the samples.

Table 3.4 pH of 14 particle size fractions of BA.

No.	µm	pH	No.	mm	pH
1	< 63	8.9	**8**	0.71 – 1	8.9
2	63 – 90	8.9	**9**	1 – 2	9.1
3	90 – 125	8.8	**10**	2 – 2.8	9.0
4	125 – 180	8.8	**11**	2.8 – 4	9.2
5	180 – 250	8.8	**12**	4 – 11.2	9.1
6	250 – 355	8.8	**13**	11.2 – 22.4	9.1
7	355 – 710	8.9	**14**	> 22.4	9.2

The shapes of the concentration dependences in BA fraction leachates on the particle size of the corresponding fraction for the main cations (Ca, Na, and K) are quite similar to each other (Figure 3.5). For fines, a rather steep decrease after 125 µm is observed for all cations, and after 0.71 – 1 mm fraction, the concentration level does not change significantly, generally decreases and reaches a plateau. The shapes of these curves are very similar as well to the curve shapes for sulfate and chloride (Figure 3.6). This might be an indication of a similar mechanism of dissolution of components which consist of major cations and anions. Such data can be attributed to the overall increase in the particle SSA with the decrease in its size together with changes in the matrix and the particle shape. It is changing from round packed (stones, pieces of glass, etc.) to less dense particles (Figure *3.1*) with a substantially higher SSA and agrees with the literature[95].

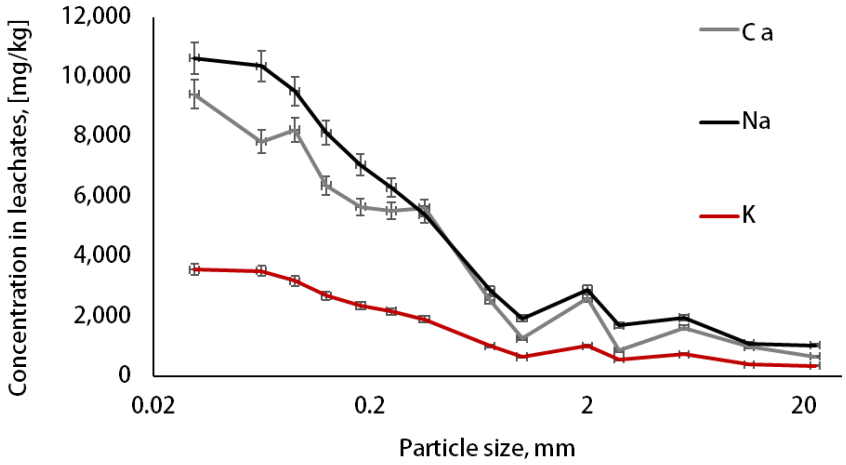

Figure 3.5 Leaching of major cations (Ca, Na, and K) related to the BA particle size. X-axis values are shown on a logarithmic scale.

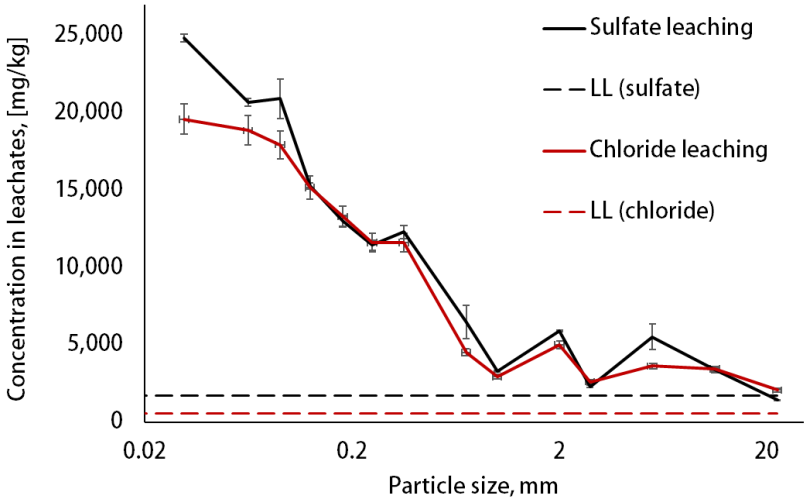

Figure 3.6 Chloride and sulfate leaching related to the BA particle size. X-axis values are shown on a logarithmic scale.

Major cations and chloride and sulfate may affect the leaching behavior of medium-concentration and minor cations[96]. The leached amounts of sulfate and chloride among fractions show a similar pattern (Figure 3.6).

PTEs

The leachability dependence on particle size is shown in Figure 3.7 for PTEs which are present in the studied BA and if their level is higher than the LL (Ni, Cu, Zn, and Sb). For Co, Cr, Mo, Pb, Sn, Cd, and V concentrations in leachates are below LOQs (< 0.05 mg/kg recalculated to the sample mass).

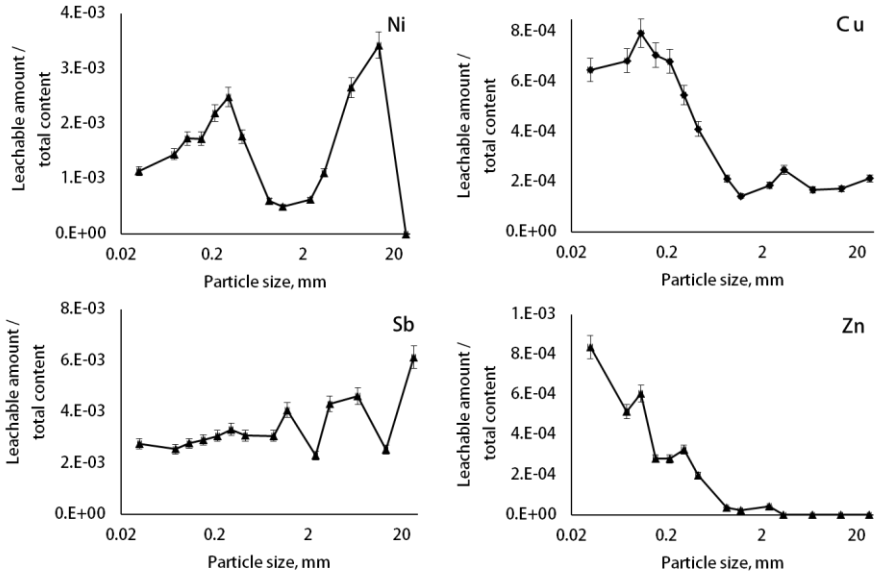

Figure 3.7 Leaching capacity (percentage of the total) vs. fraction size for Ni, Cu, Zn, and Sb. X-axis values are shown on a logarithmic scale.

Copper

A high level of copper leaching is a common challenge in BA processing[97] due to the ability of Cu to transform into stable inorganic compounds[98], e.g., $Cu(OH)_2$[0], $Cu_4(OH)_6SO_4 \cdot 1.3H_2O$ and to form stable and readily soluble complexes with organic ligands[99]. These copper compounds are readily distributed in many materials and living organisms[100]. Concentrations above the LL were found for all fractions of 500 μm and lower and for some coarse ones (Figure 3.8a).

As exceeding the limit of leachable copper content in these fractions is not too high (32 and 77 percent above the limit) in comparison with finer fractions (up to 6-fold higher than the limit); it can be concluded that its source is also the attached fine-particle layer (Section 3.3.1). The difference between the leaching levels of different metals in the coarse fractions attributed to this reason might be explained by the difference in content/leaching of corresponding metals in fines.

If the metal leaching in the finest fraction exceeds the LL by several times it might be enough to contaminate the whole fraction. If the leaching of a certain metal in the most contaminated fraction merely exceeds that limit, then due to a low share of fines in a coarse fraction, the overall leaching of this coarse fraction can be still low. Though the amount of copper in the leachates of fines exceeds the LL, the leaching capacity of copper is not very high (Figure 3.7). Among fine factions, it decreases from 0.08% to 0.01% w/w and then remains at this level.

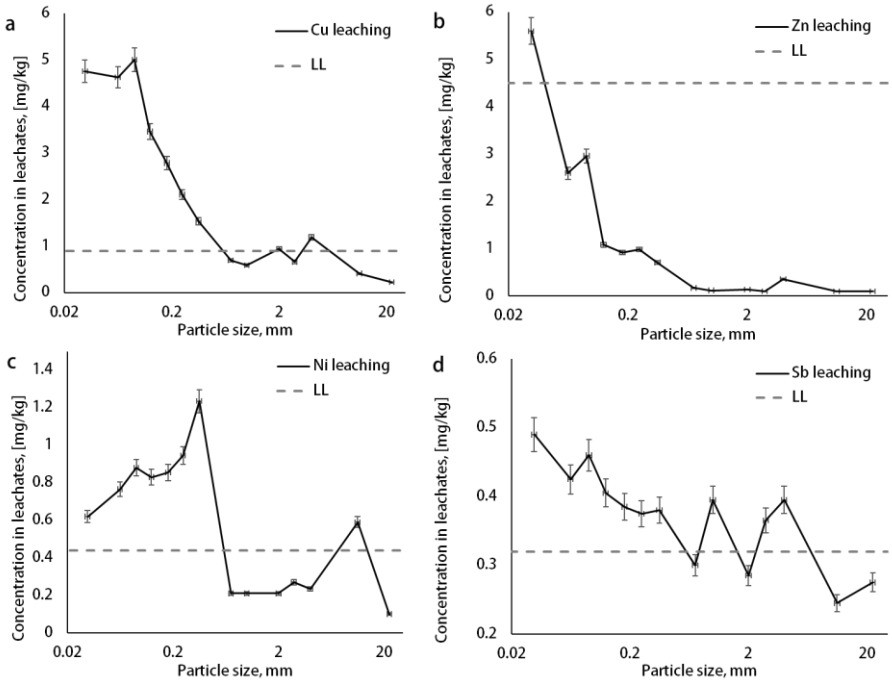

Figure 3.8 Leaching of Cu (a), Zn (b), Ni (c), Sb (d) related to the BA particle size. X-axis values are shown on a logarithmic scale.

Zinc

Despite the relatively significant zinc content in the BA (Figure 3.7), exceeding the LL is only observed in the finest fractions (Figure 3.8b). Together with a linear decrease in Zn total content down to 710 µm (Figure 3.9), the zinc concentration in leachates decreases in the same manner as Cu. Then it reaches a plateau, even though Zn total content varies significantly (Figure 3.9).

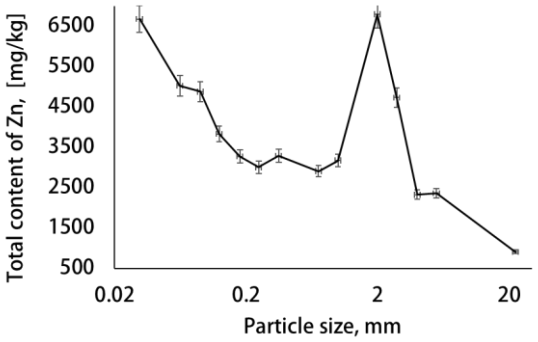

Figure 3.9 Zn total content related to the BA particle size. X-axis values are shown on a logarithmic scale.

Nickel

Leaching concentrations above the limit were found in all fine fractions 500 μm and lower (Figure 3.8c). Also, the leachate concentration was slightly above the limit in the 4–11.2-mm fraction, which, as in almost all cases in this study, is most likely due to attached fine particles (Section 3.3.1).

The Ni leaching capacity is still quite low compared with the prevailing ions (chloride, Na, Mg, and K); in the most contaminated fractions, only 0.35% w/w of Ni total content transfers into a leachate (Figure 3.7). In fractions with no LL exceeding, less than 0.13% w/w of total Ni migrates into the leachate. Unlike most other elements, the leaching capacity of Ni has no distinct trend among fines, with the leached amount dropping but then increasing steeply with a peak for 4–11.2-mm fraction (Figure 3.7). A correlation between the total content of Ni in the BA and its leaching capacity is not observed.

Antimony

The Sb leaching from BA is a well-known problem[101]; the literature on antimony leaching is mainly focused on the influence of pH, carbonation, and weathering of BA[102] or mineral additives and organic acids[103], but not on leaching dependence on particle size. Sb values exceeding or very close (for two fractions 0.30 and 0.29 mg/kg) to the LL (Table 3.3) are found in all fractions below 4 mm (Figure 3.8d). In contrast to other PTEs, the antimony content in the leachates of fines does not vary significantly (Figure 3.7), and its leaching capacity is in the range of 0.2–0.5% w/w, regardless of the particle size.

The leaching of other elements that might pose an environmental risk (Table 3.5) might have not been observed for two main reasons: firstly, they are present

in BA samples in low or trace amounts; secondly, these elements leach very low (see Table 3.4) or not at all at such pH conditions[104].

Table 3.5 Total content of PTEs present in BA samples (the range over 14 particle-size fractions, 0–22.4 mm).

Element	Total content (mg/kg)
Cd	0 - 14
Co	100 - 250
Cr	100 - 1400
Pb	200 - 1000
Sb	50 - 350
V	0 - 40

The leaching test and total analysis show that a linear correlation between the total amount of an element and its leaching capacity is not observed for any of the test elements. However, some leaching curves (major cations, anions, Cu, and Zn) have similar shapes with higher leaching in the region of fines (up to 125 μm) with a steep decrease for fractions above 0.5 mm and a plateau for coarse fractions 1 mm and larger (Figure 3.5-Figure 3.6, and Figure 3.8(a, b)).

3.3.5 Division of BA for decontaminating treatments

Based on the leaching data, total elemental composition, and mineralogical analysis, the studied BA is suitable for use in building materials, with the condition that a pretreatment adequate to the level of contaminants is performed. Because BA fines (< 125 μm) are the most contaminated and leach significantly more than coarser fractions and show morphology and mineralogy different from larger fractions, it is advised to separate them from the rest of the material for the following washing treatment, to not contaminate the fraction above 125 μm. Mineralogically, morphologically, and even total element content-wise all three fractions below 125 μm are virtually the same.

Fractions from 125 μm to 1 mm are far less contaminated and yet demanding a treatment against both anions (Cl^- and SO_4^{2-}) and cations. Mineralogically, they do not differ significantly as well, so they can be combined in a single medium fraction from the viewpoint of treatment and use.

The coarsest fraction (> 1 mm) is just slightly contaminated with anions and mostly free from large amounts of leachable PTEs; this part of the material needs just a slight washing with water, after which it can be divided for further

applications based on the total content of elements and mineralogical composition.

Hereby, for purifying BA from PTEs, Cl^-, and SO_4^{2-} a size division into three groups is suggested: fine (< 125 μm), medium (125 μm – 1 mm), and coarse fractions (over 1 mm). Table 3.6 shows the ranges of concentrations of PTEs and anions in combined groups of fractions, which have different concentration levels of all these components.

Table 3.6 Ranges of concentrations of PTEs and anions in 3 combined (for further treatment) fractions of BA.

Component	< 125 μm	125 μm – 1 mm	over 1 mm
	mg/kg		
Total PTE leaching (Cu, Ni, Sb, Zn)	8 – 12	4.5 – 6.5	0.65 – 2.5
Chloride	18,000 – 20,000	12,000 – 15,000	2,000 – 4,500
Sulfate	20,000 – 25,000	6,000 – 15,000	1500 – 3500

3.4 Conclusions

Based on the leaching data, total elemental composition, and mineralogical analysis, dividing BA into groups is suggested for different purposes according to their properties. Hereby, it is suggested to consider various properties of a fraction potentially applied for a certain use (building materials, adsorbents, metal extractions, etc.), to justify the suitability of the selected way of reuse/recycling.

From the point of view of the mineralogical composition, 6 particle size fractions (<180 μm, 180–500 μm, 0.5–1 mm, 1–4 mm, 4–22 mm, > 22 mm) can be distinguished, because the smaller fractions form groups with similar compositions. The morphology in small-size fractions (up to 500 μm) also does not differ. It is worth mentioning that the leaching shows that the large surface of these particles provides not only efficient absorption of PTEs, water, etc., but also their release in case of their further use. The total analysis of BA fractions

confirms a possibility for using it in building materials after a suitable pretreatment. It is vital to consider the limitations such as chemical properties, mineral composition and the particle structure features. The main insight that can be derived is that it would be beneficial, and, perhaps, easier in some cases to eliminate sources of PTEs in waste rather than deal with these contaminants afterwards.

To decontaminate BA from PTEs, the final size division into three groups is suggested: fine (<125 μm), medium (125 μm – 1 mm), and coarse fractions (over 1 mm). This is most beneficial from the economical point of view because the treatments which these three fractions should undergo would vary significantly in cost. In the case of washing coarsest fractions, with the help of the division process, they will not be contaminated with fines which are responsible for a fair share of the leaching. Such information on the BA properties, including the leaching dependences vs. the total element composition, mineralogical composition, and morphology of fines, will allow faster and more efficient analysis of waste materials such as BA. Based on these data, appropriate treatments can be applied to successfully use them in building materials.

This study was carried out only on one BA material (one country, one plant), and we consider the result as a primary empirical generalization. It seems possible to develop empirical models of PTE leaching to predict the expected range of concentrations in leachates of different BA fractions without conducting the leaching analysis. To reach this goal, it seems necessary to obtain similar BA datasets for different plants, countries, and seasons. On top of that, it would be expedient to study the behavior of different fractions and the fractionation effect on the properties of building materials in which BA can be used. Further studies should also include the development of a BA treatment procedures which are appropriate for the contamination level and BA chemical properties, which would ensure matching the environmental legislation.

CHAPTER 4

MSWI FA composition analysis: a case study of combined chelatant-based treatment efficiency

This chapter has been published as:

E. Loginova, M. Proskurnin, H.J.H. Brouwers, 2019. Municipal solid waste incineration (MSWI) fly ash composition analysis: a case study of combined chelatant-based washing treatment efficiency. Journal of Environmental Management. 235, p. 480-488. doi: 10.1016/j.jenvman.2019.01.096.

4.1 Introduction

The utilization of waste residues challenge has been dealt with for over 25 years[105]. During the incineration process of MSW, ash residues are approximately 80% w/w bottom ash and 20% w/w fly ash[4]. High concentrations of chloride, sulfate, lead, zinc, copper, etc. turn waste FA into a "hazardous waste"[22–24]. Due to the landfill space reduction along with environmental regulations concerning potential leaching of various pollutants into ground waters[106], these residues should be treated. To convert FA into a safe material suitable for landfilling or reuse, it is necessary to reduce the leaching of PTEs.

Main ways to achieve this goal have been water washing in combination with solidification[18,107,108], stabilization using various chemicals[109,110], adding silica fume to hydrated FA pastes[111], carbonation[112,113], and thermal treatments[114,115]. However, recently, metal extraction from FA[116,117] to retrieve valuable metals has become comparably attractive[118,119]. As metal concentrations in FA are considerable, research has been focused on making this extraction as efficient as possible[55,120]. However, currently these methods are not being aimed to reduce the FA contamination level.

Among other applications, the FA is considered as a promising cement substituent in the production of concrete[18–21] or lightweight artificial aggregates[121]. FA is conventionally water-treated[30], and the subsequent leaching test estimates its suitability for reuse. However, the washing procedure is not very economically feasible, reported L/S are high (above 10)[122] or the procedure is not optimized, and the leaching test is not performed on the final product (containing FA) to test the treatment efficiency[21]. Moreover, unlike coal-combustion fly ash (CCFA) mostly consisting of spherical particles[123], FA particles are not studied well. They presumably consist of an inert glassy core surrounded by a porous, partially dissolvable mineral matrix layer (Al, Si, and Ca are the main components) covered with easily soluble alkali-metal chlorides[124]. Thus, washing FA may decompose the matrix, which would lead to a PTE release. Hence, if the potentially soluble part of FA does not dissolve entirely, FA can be hazardous if washed again or incorporated in cement.

Thus, water-only treatments proved to be effective for readily soluble salts but not all PTEs. Several assisting agents (separately) for heavy-metal recovery (Zn, Pb, Cu, Mn, and Cd) from FA were studied due to their high complexation constants[125], and it was reported that disodium ethylenediaminetetraacetate (EDTA) and sodium gluconate are especially efficient for Zn and Pb[107]. However, a detailed study on the effectiveness of these complexing agents and their combined use for FA purification was not performed.

Therefore, the goal of this chapter is to study the effectiveness of the combined use of chelatants (EDTA and gluconate) to improve PTE extraction from FA while using lower water volumes. Apart from complexation constants, the agents were selected due to their ability to make water-soluble complexes with most metals in FA and, thus, simulate the matrix decomposition of FA particles, a process that might have occurred outdoors with assistance of environmental agents like humic compounds or other natural substances[126].

The study involved the comparison of untreated and treated FA by the standard leaching test and macro- and microelemental, mineralogical, and microstructure analyses, and the analysis of individual hazardous elements in the leachates and remaining FA material.

4.2 Materials and methods

The general materials and methods are discussed in Chapter 2. Here, specific details and/or unique for the chapter procedures are presented.

FA was supplied by the municipal solid waste-to-energy incinerator plant of Mineralz (Duiven, the Netherlands).

Two chelatants used in this chapter are sodium gluconate (Merck, 99%) and disodium ethylenediaminetetraacetate (Sigma Aldrich, 99-101%).

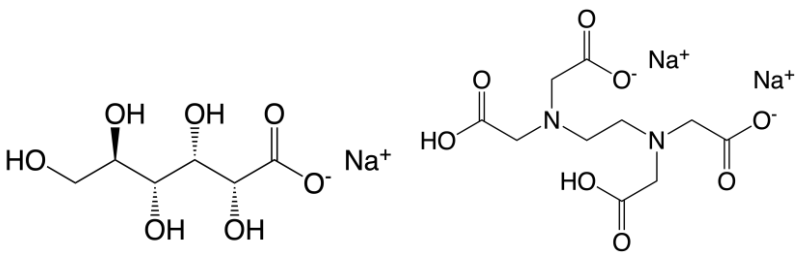

Figure 4.1 Sodium gluconate (left), and EDTA (right).

4.2.1 Sample preparation

Fresh FA samples were used for analyses and treatments. The material was oven-dried at 105°C to a constant mass. Next, the FA fraction above 500 μm was sieved out (3.8% w/w), because it contained significant amounts of unburned carbon. LOI at 550°C of the fraction above 500 μm is 16.84. Next, the material was randomly divided with a sample splitter: the first half was saved for treatments; the second half was used for the standard leaching test and microwave-assisted acid digestion. Subsequently, treated samples were collected and subjected to the standard leaching test, ICP–AES, mercury by flameless AAS,

and XRD analysis again to assess the treatment efficiency and examine its impact on FA composition.

4.2.2 Standard leaching test

The standard leaching test[127] was performed on untreated FA, the fraction below 500 μm (5 replicates of 40 g each) to evaluate the level of PTEs, chloride, and sulfate. This test was also used to evaluate the combined (COMBY) and water-only (WATER-3) treatments (Section 4.3.4 below). After the standard leaching test (24 h shaking, L/S 10, 200 rpm), the samples were filtered through 17–30 and 0.2-μm filters to prepare leachates for IC and ICP–AES/AAS.

4.2.3 COMBY and WATER-3 treatment procedures

To test the efficiency of complexing agents, individual solutions of EDTA and sodium gluconate (Na-Gl) were used. A FA sample (40 g) was added to 200 mL of 0.05M EDTA and shaken for 20 min (200 rpm). The mixture was filtered (17–30 and 0.2-μm filters), and the washing water was collected for further analysis. The same procedure was repeated for another FA portion, but Na-Gl instead of EDTA was used.

Figure 4.2 illustrates the scheme for both treatments consisting of three steps. WATER-3 serves as a reference, it follows all steps from COMBY, but instead of the additive solutions deionized water was used. Due to the dissolution of soluble components, in all cases L/S was taken with respect to the initial sample mass.

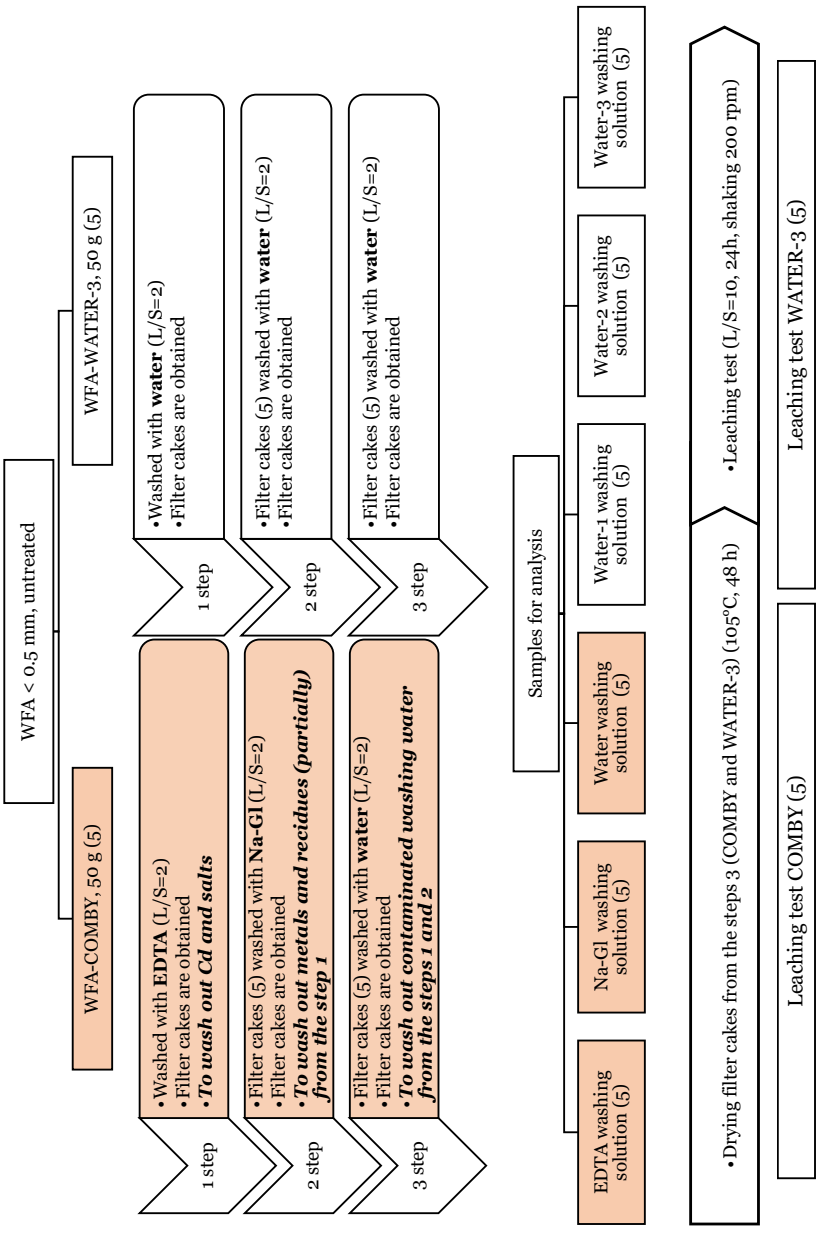

Figure 4.2 Scheme of WATER-3 and COMBY treatments and analysis (figures in parentheses denote the number of replicates for each stage).

4.3 Results and discussion

4.3.1 Untreated FA properties

Comparison of leaching vs. bulk element composition

The results for bulk FA element contents (Table 4.1) show that the samples are highly contaminated and pose a potential hazard. Such high PTE contents in FA allowed us to test the efficiency of complexant-based treatments.

The standard leaching test results (L/S 10) on the untreated FA show that Cr, Pb, Cd, Mo, and Zn concentrations exceed the LL significantly (leachate pH was 13). However, they are only a small fraction of the total PTEs present in FA, and despite a significant content of Sb, Cd, Cu, their leaching is below the quantification limits. These elements are probably embedded in FA particles rather than are at its dissolvable surface layer.

Table 4.1 PTEs in the FA: their total content, leaching, and legislation limits (LL), $n = 5$, $P = 0.95$.

Element	Total content	Leaching	LL [128]	Times over LL
	mg/kg	mg/kg	mg/kg	(for leaching)
Sb	1500 ± 100	< 0.02	0.32	–
As	60 ± 1	< 0.1	0.9	–
Ba	1500 ± 100	2.9 ± 0.3	22	–
Cd	300 ± 10	0.10 ± 0.01	0.04	2.5
Co	22 ± 1	< 0.1	0.54	–
Cr	290 ± 10	1.9 ± 0.2	0.63	3
Cu	1500 ± 100	0.10 ± 0.01	0.9	–
Hg	< 0.001	< 0.001	0.02	–
Mo	30 ± 1	6.7 ± 0.7	1	6.7
Ni	130 ± 10	< 0.01	0.44	–
Pb	3500 ± 100	26 ± 3	2.3	11.3
Se	15 ± 1	< 0.02	0.15	–
Sn	630 ± 10	< 0.02	0.4	–
V	60 ± 2	< 0.05	1.8	–
Zn	19000 ± 200	21 ± 2	4.5	4.7

In addition to high metal concentrations, FA leachates after the standard leaching test contain large amounts of chloride (110 ± 10 g/kg) and sulfate (50 ± 1 g/kg). It is similar to the previous findings, where the effectiveness of a water treatment is shown[108,129–131]. However, the standard leaching test is not always sufficient to bring the sulfate content/leaching down to a level acceptable by the

environmental legislation[128]. Thus, from the values of leachable and bulk contents of PTEs, the standard leaching test should be complemented with a more detailed characterization.

Mineralogical composition and microstructure

According to the XRD data, the crystalline components of untreated FA are mainly anhydrite, quartz, halite, sylvite, and calcite. The pH 13 evidences that lime might be present as well. However, it gives very low XRD signals, probably due to fine dispersity, thus, its identification is hindered[132,133]. The changes due to treatments are presented below (Section 4.3.4).

Figure 4.3 presents a general overview of the untreated FA (< 500 μm). It consists of porous particles of irregular shape, and the fraction of fine particles (<50 μm) is very large, which agrees with the granulometric analysis (56.8% w/w is below 63 μm). To investigate if particle-size fractions of FA differ in the microstructure, the material was divided into three fractions: < 40, 40–250, and 250–355 μm.

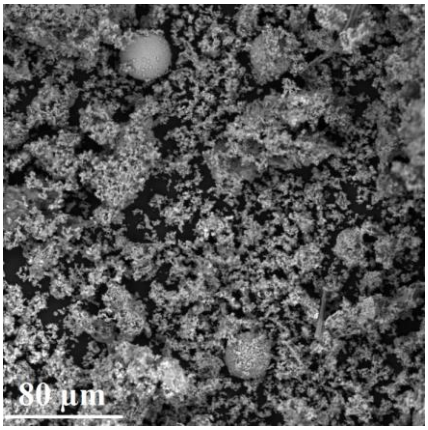

Figure 4.3 SEM-image of MSWI fly ash < 500 μm.

Figure 4.4 shows particles of irregular shape with a relatively small surface area. This fraction (40–250 μm) contains a larger number of spherical particles (about 10% v/v).

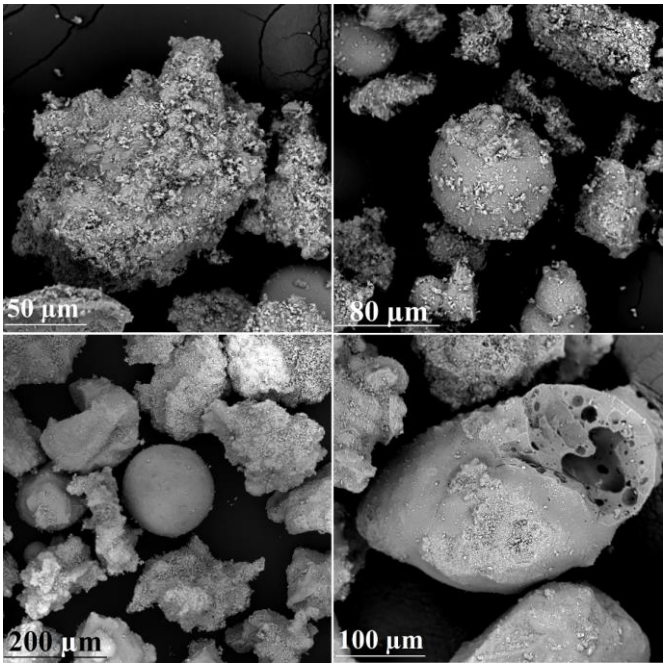

Figure 4.4 SEM-images of MSWI fly ash 40 - 250 µm.

Figure 4.5 portraits particles of the 250–355 µm fraction. In general, their shape resembles those from finer fractions. However, there are also agglomerates of smaller particles, glued together, including spherical (Figure 4.5, circled in white). There are also flat particles with porous structures. It is noteworthy that FA morphology does not change significantly in the range of 40–355 µm.

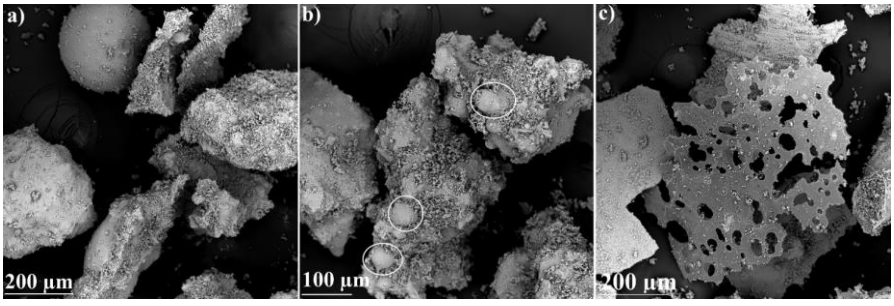

Figure 4.5 SEM-images of MSWI fly ash 250 - 355 µm.

4.3.2 Selection of complexing agents

Na-Gl and EDTA were selected because they are less aggressive than strong acids or bases, change the pH within 1.5 points only, which is important if being

compared with water, and show their effectiveness in the extraction of Zn and Pb from FA[107,129]. Thus, besides eliminating chloride and sulfate, these treatments elute PTEs. To test their effectivity, three independent treatments were performed (L/S 5; 20 min): water only, EDTA (0.05M), and Na-Gl (0.05M).

The results (Figure 4.6) show that, firstly, each of them efficiently elutes different metals, and secondly, they have different effects on the standard leaching test results for the treated material. Na-Gl is more effective in most cases (except for Ba, Sr, Mo, and Cd). It is vital to acknowledge its ability to elute major FA matrix elements, calcium, aluminum, and iron. This may lead to matrix decomposition releasing an additional portion of PTEs, which could not be released during the standard leaching test or treatment with water. PTEs, which showed the excess over the LL according to the standard leaching test, were Cr, Cd, Mo, Pb, and Zn. However, significant amounts of Cu (by Na-Gl) and Cd (by EDTA) can also be liberated from FA due to high complexation constants ($\log\beta_{1,\text{Cu-EDTA}} = 18$; $\log\beta_{1,\text{Cu-Gl}} = 36$; $\log\beta_{1,\text{Cd-EDTA}} = 17$; and $\log\beta_{1,\text{Cd-Gl}} = 10$)[134–136]. As agents complement one another, both reagents were used sequentially in one treatment (COMBY) to elute the maximum number of PTEs.

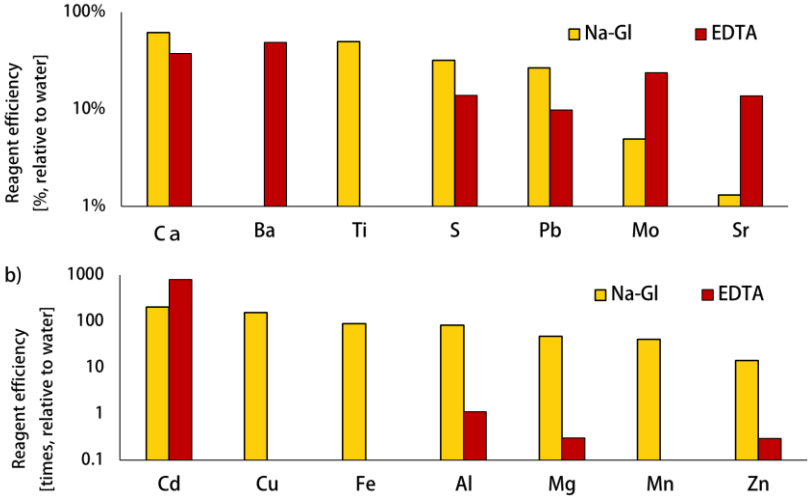

Figure 4.6 Reagents efficiency relative to water: a) for elements, it is comparable to water; b) for elements, it is much higher than for water

4.3.3 Components not present in leachates or washing waters

In this section, we sum up the data on the elements that were below the limit of quantification (LOQ, which for all the elements was lower than the LL) in the leachates for all the kinds of applied treatments.

Arsenic

According to the literature[137], the maximum leaching of As is observed at pH 10 and does not change significantly after the continuation of the leaching test for more than 22–23 hours. Thus, a standard leaching test (24 h) should be sufficient to detect and determine As. In general, the above-mentioned paper concludes that leaching increases with pH. However, another study[138] drew completely opposite conclusions. Eventually, it was concluded that several parameters are responsible for As leaching, and not just pH. Most likely, as As accumulates in different FA phases, its solubility is largely determined by the availability of those phases. In this study, the total amount of As in the FA is not so significant (about 60 mg/kg), and leaching is absent in all experiments. It seems that this might be attributed to the fact that As is encapsulated in the silicate matrix[139,140]. Thus, comparing the leaching test results with the total As content shows that As is quite firmly immobilized and does not pose a further threat.

Cobalt

The leaching of Co is minimal at pH 8–12[137]. On one hand, it seems that the leaching test is not able to adequately assess the environmental impact of cobalt because under standard (for ash) conditions Co should not be leached out (pH 10–13). On the other hand, it is noteworthy that the mass ratio of arsenic to cobalt in the FA is at the level of their ratios in such probable mineral phases as cobaltite CoAsS, safflorite $(Co,Fe)As_2$, or skutterudite $CoAs_3$. It might be assumed that cobalt can be enclosed together with arsenic in the silicate matrix, and thus, poses no further threat.

Nickel

According to the existing data, the maximum leaching of Ni is observed at pH 0–4 and 10–12[141]. At the same time, there are data reporting that nickel in FA is distributed between the silicate and magnetic fractions[142]. Judging by the fact that the leaching of Ni in all the samples is below LOQ, it can be concluded that it might be as well immured in the silicate matrix, dissolution of which in natural conditions is quite hindered.

Tin, Selenium, and Vanadium

Some studies[143,144] suggest that the ability of Sn to be mobilized is supposed to be high at pHs above 10. However, in this study, despite considerable total amount of Sn in the FA (around 0.6 g/kg), the leaching from all the samples was very low. Probably, it also indicates that the silicate matrix of FA is enriched with

Sn. Trace amounts of Se (15 mg/kg), as well as its leaching below the LOQ and LL for all the samples indicate that it is likely, in our case, that Se is also enclosed in the silicate matrix. It is reported[145] that the major source of vanadium in FA is glass. Given its trace contents in the investigated ash, as well as the lack of leaching in all samples, it can be concluded that it is also enclosed in the silicate matrix.

4.3.4 Two-reagent and water-only treatment comparison

Treatment parameters are the time of contact, L/S, and the number of steps. The priority task was to make a treatment which ensures the efficient chloride elution because its concentration is 100-fold higher than the LL. For a decrease in the chloride level by 98–99%, 15–30 min of washing is enough[18,122,129,130]. In several studies, several-steps washing with L/S 1–3 proved to be more efficient than single-step ones with larger L/S[18,130,146,147]. In most articles on this topic, the number of washing steps is limited to 2–3[122,130]. Given that the studied FA is severely polluted (Table 4.1) and retains a large water amount (about 30% w/w after being in contact with water for about 20 min), we used a three-step washing procedure to remove the contaminated water. To minimize its amount, L/S of 2 (relative to the initial sample mass) was used at each step. This ratio was selected empirically by obtaining a FA–water paste with a viscosity low enough for its rapid mixing. EDTA was used at the first step as it elutes large amounts of Cd (ca. 1000-fold higher than the LL), and this also required more iterations of rinsing out the contaminated water after this step. During the second step, Na-Gl was applied, and during the third, distilled water. All three steps together ((1) - EDTA/(2) - Na-Gl/(3) - water) comprise COMBY. For the sake of comparison, a WATER-3 treatment was applied. The procedure is the same as COMBY but instead of additives, only distilled water was used at all steps.

Treatment results (elution)

Figure 4.7 shows the step-by-step elution for certain elements during both treatments. Taking into consideration that, for almost all metals, each step provides a significant PTE liberation, the number of steps cannot be less than three. The elution character for these two treatments differs for all metals (Figure 4.7). For WATER-3, the concentrations of almost all the metals decrease in each step. This could be attributed to a change in pH at each step, however during COMBY pH drops are similar (see Figure 4.7 insets). For COMBY, the pH after the first step decreases more than with WATER-3. This probably occurs due to the removal of alkaline compounds (mainly Ca) with EDTA. A pH change after the second step is the same, so the elution of such metals as Pb and Zn would have to

be even less than in the first step[104], but it is the opposite. Thus, it is worthwhile to look for another reason for such an elution character.

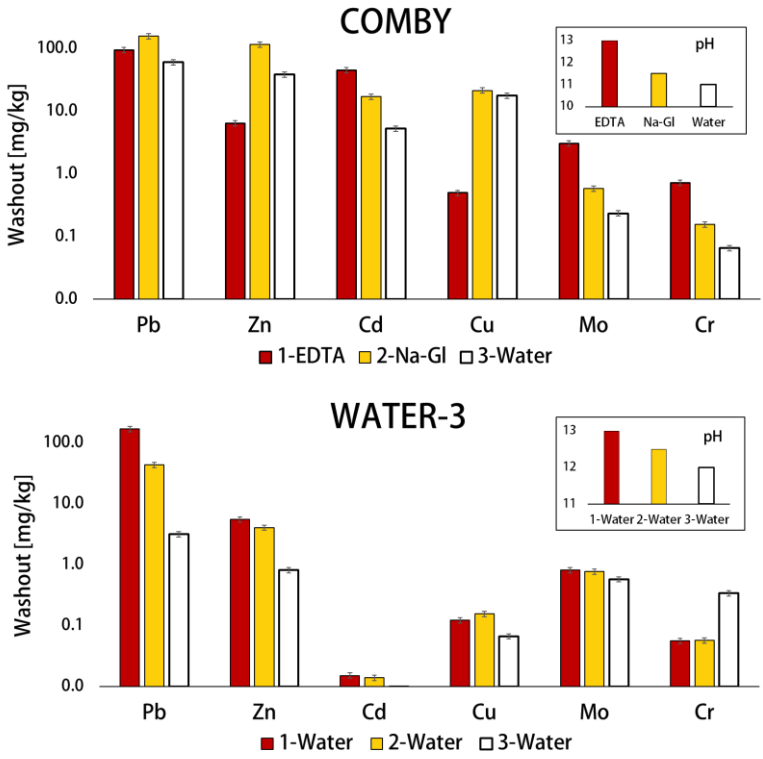

Figure 4.7 Elution of metals during WATER-3 and COMBY treatments for each step; insets: pH of the washing waters during each step.

Figure 4.8 illustrates the efficiency of COMBY and WATER-3 for chloride and sulfate.

For chloride, the difference is within the error range; but for sulfate, the difference in the second step is quite noticeable. More intensive sulfate leaching compared to water may be due to the chelation of calcium with Na-Gl, as anhydrite is one of FA main components. Figure 4.8 shows that three steps with L/S 2 are nearly sufficient for removing chloride from FA. In both treatments, a decrease in leachable sulfate concentration is evident; Na-Gl removes a larger amount of sulfate due to binding with calcium, and, unlike for chloride, still a significant amount of sulfate is liberated at the final stage of both treatments. The

value at the third step is in a rather good agreement with the solubility of $CaSO_4$ (2 g/L) produced from anhydrite.

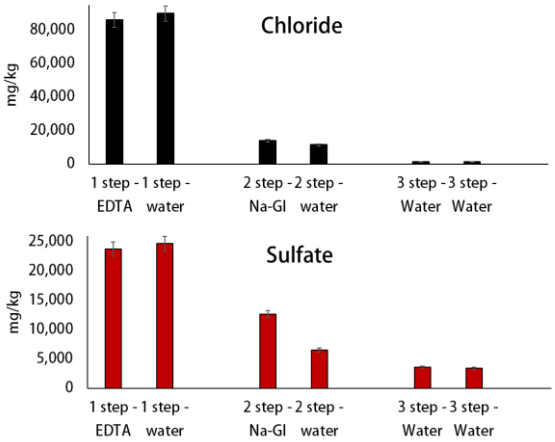

Figure 4.8 Elution of chloride and sulfate during WATER-3 and COMBY treatments for each step.

Mineralogical and element composition of treated FA

Figure 4.9 shows XRD spectra of treated FA in comparison with untreated FA, all samples were oven-dried (105°C). Table 4.2 indicates the relative peak heights to show how a treatment changes the FA matrix.

Table 4.2 Main minerals in untreated and treated FA.

Sample / Mineral	FA	FA-WATER-3	FA-COMBY
Halite	High	–	–
Anhydrite	Low	High	Medium
Sylvite	High	–	–
Calcite	Low	High	Medium
Quartz	Low	Medium	High

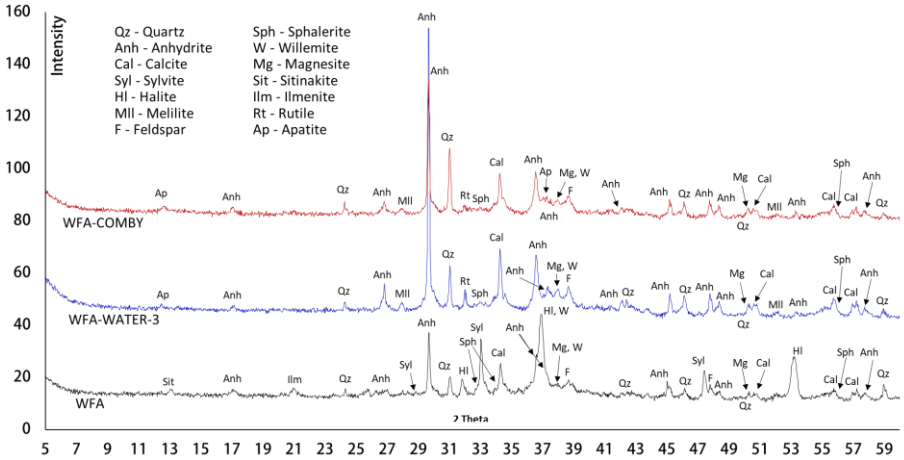

Figure 4.9 Diffractograms (Co radiation) of the untreated FA, and FA after WATER-3 and COMBY treatments; for the sake of convenience, the plots are shifted relative to each other; the intensity scale is given in square roots of original values.

A primary FA component is anhydrite[148,149]. It is worth mentioning how its share varies with the treatment type. It increases significantly both in FA-WATER-3 and FA-COMBY samples (due to the elution of readily soluble salts; approx. 20% w/w); however, the peak (ca. $2\theta = 29$) for FA-WATER-3 is much higher than for FA-COMBY. Thus, COMBY removes this component from the FA matrix much better than WATER-3 due to high chelatabilities of EDTA and gluconate with calcium[125,134]. Nevertheless, $CaSO_4$ remains to be the main component of treated samples. Because this compound simultaneously possesses good sorption properties and is capable of considerably dissolving in water, a very slow emission of PTEs into ground waters in the case of improper disposal cannot be excluded entirely.

The next main component is calcite[148,149]. Figure 4.9 shows that because of the sodium and potassium chloride elution, its share increases, and its content is higher for FA-WATER-3. This is confirmed by Figure 4.6, which shows the higher ability of COMBY to elute calcium compared to water.

High signals of halite (NaCl) and sylvite (KCl) are in line with the previous data[148,149], and agree with the leaching data for chloride (about 110 g/kg) and the total element composition (Na, ca. 75 g/kg; K, ca. 50 g/kg, Figure 4.10).

The last FA main component is quartz[148,149]. Its content also varies in concordance with a decrease in the contents of soluble salts (ca. 77 g/kg in

untreated and 93–96 g/kg in treated FA, Figure 4.10). Its share is larger after treatments, and the FA-COMBY sample has slightly more quartz due to a smaller share of anhydrite and other water-soluble phases.

All other minerals in Figure 4.9 are present in FA in fairly small amounts. No new phases are detected in the treated FA. A significant content of aluminum (33–45 g/kg) coincides with the presence of melilite and feldspar; sphalerite and willemite might be the origin of zinc (19–23 g/kg); the sources of iron (15–21 g/kg) and titanium (11–15 g/kg) are presumably ilmenite, rutile, and sitinakite; magnesite is for magnesium (12–17 g/kg); and the presence of apatite might explain moderate concentrations of phosphorus (7–10 g/kg).

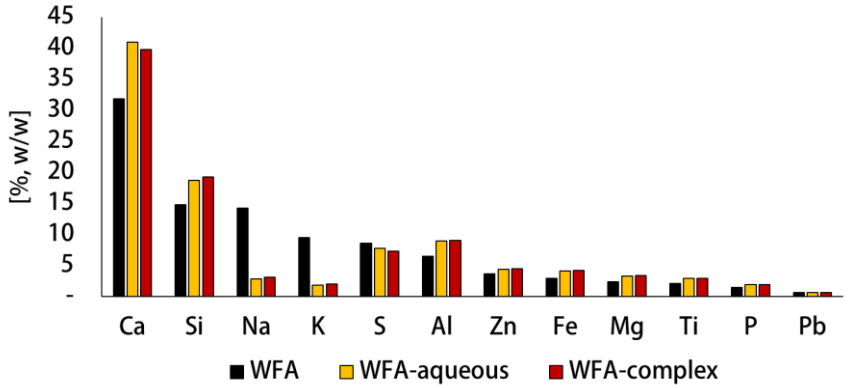

Figure 4.10 Total element composition (major components) of untreated FA, WATER-3-treated FA, and COMBY-treated FA.

Figure 4.10 shows the bulk FA composition after COMBY and WATER-3 treatments. It confirms the mineralogical analysis and leaching behavior. The contents of calcium and silicon are slightly higher in treated samples due to a noticeable decrease in the proportion of sodium, potassium (Figure 4.10), and chloride. Sulfur content (the main source is supposedly anhydrite) is slightly lower after treatments (by eluting sulfate, as shown above). The percentages of almost all the main components (Al, Zn, Fe, Mg, Ti, and P) are also slightly higher after treatments. While the elution of zinc during the treatments is abundant, a very significant Zn amount remains bound in the treated FA (22±1 g/kg) (Figure 4.10). After treatments, there is still also a high Pb content (3.2±0.2 g/kg). Because these elements pose a potential risk, even in a combination with the standard leaching test, the bulk element analysis is required to determine the treatment effectiveness, and to consider other ways of FA reuse because it contains large quantities of valuable metals.

Thus, both treatments show effective chloride removal. However, some differences in the treated FA due to the presence of EDTA and Na-Gl do not affect the final macro-composition considerably.

Microstructure of treated FA

As discussed earlier, the untreated FA consists of particles with a rather complex shape and a large surface area, which, nevertheless, has a fair share of smooth surface. Figure 4.11 illustrates the changes during the second and third steps of WATER-3. Spherical particles appear smoother as the porous outer layer is removed, and agglomerated particles are liberated. During this process, an increase in the number of particles, and, therefore, a new surface accessible for dissolution, might affect the PTE leaching.

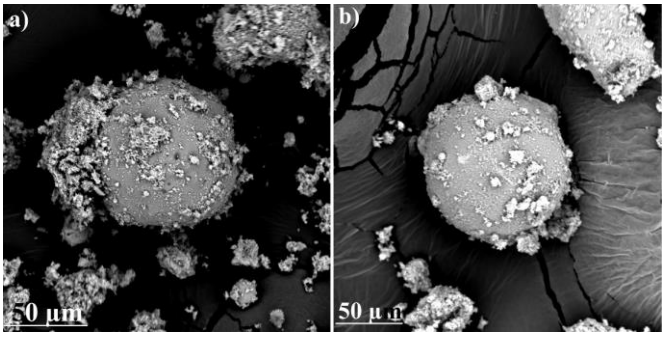

Figure 4.11 SEM-images of MSWI fly ash particles after the 2nd (a), and the 3rd steps of WATER-3 treatment.

Figure 4.12 shows changes in FA particles after washing the untreated FA with EDTA, Na-Gl, and water.

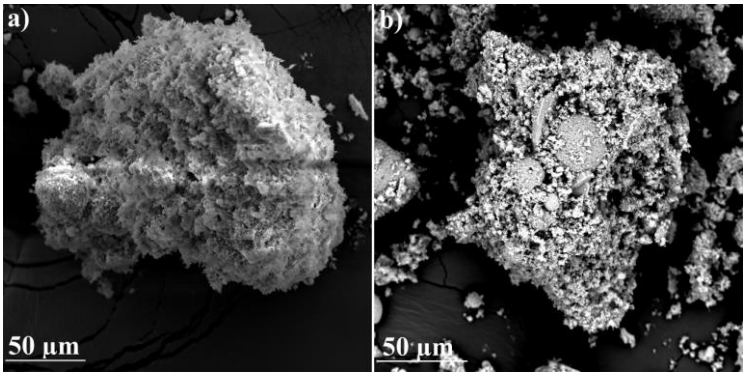

Figure 4.12 SEM-images of MSWI fly ash particles after the 2nd (a), and the 3rd steps of COMBY treatment.

Comparing this figure with Figure 4.4 and Figure 4.5 shows how much the surface of particles has changed. If a large part of the untreated FA was quite smooth (Figure 4.12), here the whole surface has become scabrous, so its surface area has increased significantly. This may explain PTE elution enhancement during the second step of COMBY. Figure 4.12b displays the shape of a FA particle after the last step of COMBY. To a relatively large porous particle, several small spherical particles are attached (in the center). This agglomerate may be formed during the drying process after treatment, or this structure was there originally, but only several washing steps have revealed it. During the further use or disposal, this agglomerated particle might fall apart completely, resulting in an increase in the number of particles, and, therefore, in the new surface available for PTE leaching.

Figure 4.13 shows a structure of particles after WATER-3 (all three steps). It is worth noting that such structures were not observed at any of the previous steps.

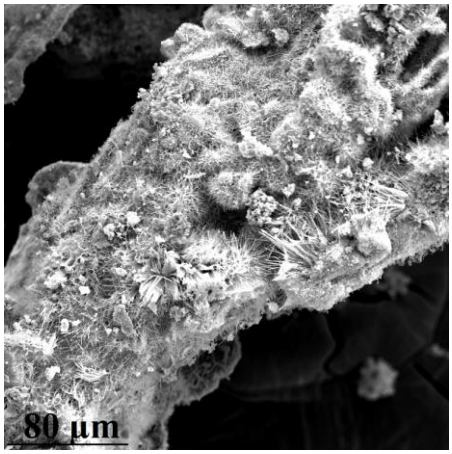

Figure 4.13 SEM-image of a MSWI fly ash particle after the last stage of COMBY treatment.

Based on XRD data, the formation of significant quantities (enough to form such large particles) of new phases was not observed during the treatment. Perhaps, it is a structure of some FA particles which was hidden before under the layers of soluble components. Only calcite of all main minerals that form FA can have a similar needle structure[150,151]. Besides, it would not dissolve in water (during treatments). It is possible that the reagents used in COMBY and contributing to the elution of calcium, help to dissolve such structures. Therefore, they are not observed in the case of COMBY. Another possible explanation of such

structures (yet demanding further research) might be the formation of hydration products[152]. It is important to come to understanding how such a vast formation of a new and very large surface would affect the leaching of PTEs.

Thus, during the treatments, the FA microstructure undergoes changes that may affect its further properties. Both treatments wash a rather deep surface layer off, significantly increasing the total surface area. During COMBY, the FA surface changes from partially smooth to rugged and scabrous compared to WATER-3.

Standard leaching test results on treated FA

Table 4.3 presents the standard leaching test results (L/S 10) for both treatments. Only elements with concentrations above the LL are shown. It is worthwhile to give a small remark regarding the LLs for chloride and sulfate. In this study, the environmental legislation for CCFA (LL (sulfate), 30,000 mg/kg; LL (chloride), 1000 mg/kg) could have been applied[153] because FA is closer in some properties to CCFA rather than to BA. However, because hereby no evidence of complete FA similarity to CCFA was presented, the legislation criteria for non-shaped building materials were used instead, see Table 4.3[128]. It is rather negligible in the context of this study because the goal was not to demonstrate the FA leaching results after a treatment, but to show what changes the FA undergoes. The treatment selection or other decision regarding the further utilization of FA can be made using these criteria though. Therefore, the LL values are taken for clarity, so that the challenge level can be estimated.

Table 4.3 Standard leaching test results for untreated FA and after treatments (for metals which concentrations exceed the legislation limit (LL)); underlined, more than the LL; bold, became worse after the treatment, $n = 5$, $P = 0.95$.

Element	Leaching test	LL	Leaching test results (after treatments)	
	FA untr.		COMBY	WATER-3
		mg/kg		
Cd	0.10 ± 0.01	0.04	**10 ± 1**	< 0.02
Cr	2.0 ± 0.2	0.63	0.50 ± 0.05	**4.4 ± 0.4**
Cu	0.10 ± 0.01	0.9	**3.6 ± 0.4**	< 0.02
Pb	21 ± 2	2.3	**85 ± 9**	< 0.05
Mo	6.7 ± 0.7	1	1.4 ± 0.2	3.3 ± 0.3
Zn	21 ± 2	4.5	**38 ± 4**	0.40 ± 0.04
		g/kg		
Cl^-	110 ± 10	0.62	1.6 ± 0.2	1.9 ± 0.2
SO_4^{2-}	50 ± 5	2.4	19 ± 2	16 ± 2

Table 4.3 shows that COMBY causes a strong increase in the PTE leaching except for Cr and Mo. In general, COMBY, which elutes matrix elements such as Ca, Fe, Al, Mg, and Zn, promotes the liberation of PTEs enclosed in the matrix (Figure 4.6). At the same time, WATER-3 elutes orders of magnitude less amounts of these matrix elements, keeping PTEs inside. Therefore, after WATER-3, the concentrations of a considerable number of PTEs (except for Cr and Mo) are below the LL. Both treatments were not targeted to completely elute anions. Table 4.3 shows that both treatments were similarly effective in eluting chloride (COMBY, 99%; WATER-3, 98%, w/w), and close to each other for sulfate elution (COMBY, 62%; WATER-3, 68%, w/w).

Table 4.3 shows that Cd leaching from the untreated FA (using the standard leaching test) is only twofold higher than the LL (0.10 mg/kg). However, COMBY increased Cd leaching by about 100 times (10 mg/kg), while during WATER-3 it has decreased by more than 5 times (< 0.02 mg/kg). At the first two steps of WATER-3, a very small amount of Cd was liberated (0.03 mg/kg, Figure 4.7), while during COMBY it was much larger at all the three steps (67.0 mg/kg). As at three steps of COMBY, the eluted Cd amount is decreasing (45, 17, and 5 mg/kg, respectively), while the matrix component elution at the 1st step for water and EDTA is similar, it might be concluded that EDTA transformed all available Cd to soluble species on the surface layers. If some additional Cd sources would have been uncovered by dissolving the matrix, an increase in its concentration at each subsequent step would have been observed. The ability of Na-Gl to elute Cd is also significant (0.10 mg/kg), although less than of EDTA due to a lower complexation constant (Section 4.3.2), and despite its use in the second step of COMBY, an increase in concentration also did not occur. As WATER-3 is reagent-free, only a small amount of soluble Cd got into the washing water (0.04 mg/kg), and the standard leaching test indicates FA-WATER-3 as apparently non-hazardous. However, a very significant increase in the cadmium leaching using chelating agents shows that such a "clean" FA may have a hazard under the action of environmental substances[126].

Figure 4.7 shows that a significant amount of Cr (0.7 mg/kg) is liberated at the 1st step of COMBY, less (0.2 mg/kg) at the second step, and at the third step a negligible amount (0.1 mg/kg) is eluted, and according to the standard leaching test results its level satisfies the regulations. At the same time, for WATER-3, a small amount (0.1 mg/kg) of Cr is liberated at the first two steps, and at the third step its amount increases threefold. Eventually, FA-WATER leaches twofold Cr (4.4 mg/kg) as the untreated FA (2.0 mg/kg). The solution pH decreases during the treatment; however, at pH 8–13, Cr leaching does not vary this much[104]. On the other hand, Figure 4.14 illustrating a comparison of Mg, Al, and Fe leaching

at all steps, reveals that it is 2-3-fold larger at the first step of COMBY (and Mg is not released at all at the first step of WATER-3), and at the 2nd and 3rd steps for COMBY, the elution of these components is 1–2 orders of magnitude higher than that of WATER-3. It might be suggested that Cr is encapsulated in the matrix. Thus, as for Cd, the standard leaching test with L/S 10 does not show how much Cr will potentially leach out later, during the use of FA-based materials.

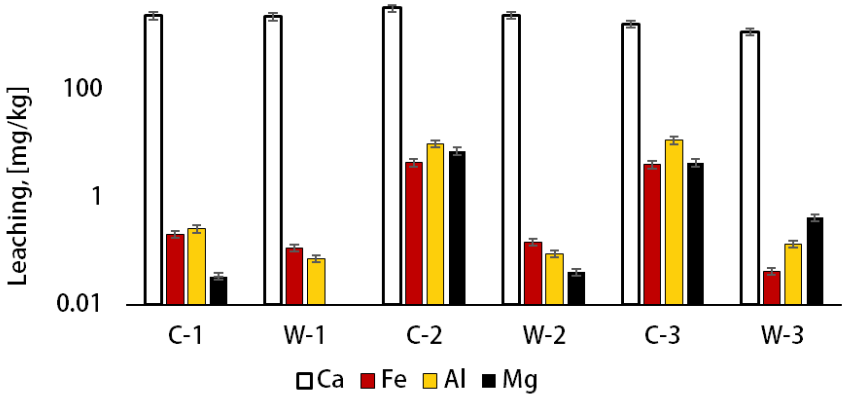

Figure 4.14 Matrix components elution during COMBY (marked C) and WATER-3 (marked W) treatments.

Considering the standard leaching test results (Table 4.3), for untreated FA Cu leaching was below the LL, but after COMBY it has increased significantly. The character of Cu elution differs from cadmium (for which the standard leaching test results after treatments were similar, Figure 4.7 and Table 4.3). Apart from very high complexation constants, the reason for such an elution character is also the matrix decomposition, elements are liberated 10-fold less effectively at the first step of COMBY, as if blocking Cu leaching. For WATER-3, these components are liberated only slightly, so approximately the same Cu elution is observed at all three steps.

After WATER-3, the concentration of Pb in leachates is less than the LL; however, after COMBY, the FA looks extremely hazardous (Table 4.3). In addition, even in the case of WATER-3, much more Pb is liberated at the first (168.8 mg/kg) and subsequent (43.5 and 3.2 mg/kg) stages than during the standard leaching test on the untreated FA (Figure 4.7, contact times are 20 min at every washing step, and 24 h for the standard leaching test). This can be explained by the fact that during the standard leaching test, calcium salts can re-precipitate (e.g., $CaSO_4$), with which Pb salts tend to co-precipitate[154]. Thus, in a

short time of COMBY this does not happen, and all available Pb transfers to the solution. This phenomenon is not observed for other metals because their chlorides and sulfates have rather high solubilities.

Mo concentration in leachates have decreased after both treatments, and for COMBY it was close to the LL (Table 4.3). The elution character in both cases as well indicates a link to the elution of matrix components: in WATER-3 it is slow, so at all steps a similar amount of metal is liberated (0.8, 0.8, and 0.6 mg/kg, respectively); for COMBY, a much larger amount is eluted immediately (3.1 mg/kg), presumably, because of a high complexation constant ($\log\beta_{1,\text{Mo-EDTA}} = 20$)[125], and at the following steps it decreases (0.6 and 0.2 mg/kg). The standard leaching test for the untreated FA showed 6.7±0.7 mg/kg of Mo, and the mass balance for treatments and liberated/left amounts for COMBY was 3.9±0.4/1.4±0.1 = 5.3±0.5 mg/kg, and for WATER-3 was 2.2±0.2/3.3±0.3 = 5.5±0.5 mg/kg, indicating that, probably, the rest of Mo (Table 4.1) is encapsulated in the silicate matrix and is unlikely to pose further threat.

For WATER-3, Zn level has decreased to an environmentally acceptable level (Table 4.3). However, for COMBY, it has become twofold worse than before the treatment. During WATER-3, it is very probable that only readily soluble Zn species are eluted, and at every step the elution decreases (5.5, 4.0, and 0.8 mg/kg). For COMBY, there is no significant Zn leaching at the first step (6.4 mg/kg), but at the second one, 18-fold higher amounts of the metal eluted (115.4 mg/kg). This can result from the matrix elements beginning to be effectively liberated at the Na-Gl step of COMBY, entailing enhanced Zn leaching.

4.4 Conclusions

Thus, mineralogical composition, total element content, leaching properties, and morphology of untreated and treated FA are studied. As a whole, the efficiency of such a three-step combined treatment with two complexing agents (EDTA and sodium gluconate) to increase the toxic-element elution from fly ash in contrast to conventional water-only treatments is shown.

- The main minerals found in the untreated FA are anhydrite, quartz, halite, sylvite, and calcite. The high pH of 13 might indicate the presence of lime.
- The FA major elements are Ca, Si, Na, K, S, and Al, and it is also enriched with Pb (3.5 g/kg) and Zn (19 g/kg).
- The FA mainly consists of particles with an irregularly developed shape (about 90% v/v) and spherical particles (about 10% v/v).

- The main cation contaminants in the FA are Cd, Cr, Mo, Pb, and Zn. Their leaching exceeds the legislation limits by 3–11 times. The leaching of anions exceeds the corresponding limits by 25–1000 times. Leaching of chloride is 110 g/kg, and sulfate is 50 g/kg.

- The ability of gluconate to elute metals from the FA is especially efficient (10–200 times higher than of water) for Cd, Cu, and Zn; and EDTA is the most efficient for Cd (800 times higher than of water).

- The ability of combined treatment to elute metals in comparison with water-only is 40% higher for Pb, 15 times higher for Zn, 1800 times higher for Cd, 115 times higher for Cu, and 2 times higher for Mo and Cr.

- During both treatments, the FA surface changes from smooth to scabrous. Both treatments wash a rather deep surface layer off, significantly increasing the surface area of the particles.

- As a result of combined treatment, the FA has become even more hazardous than before the treatment. In the case of water-only treatment, the FA appears to be much cleaner than before the treatment.

It is necessary to highlight that the same FA, which, according to the leaching test results, looks non-hazardous from almost all points after being washed with water, proves to be extremely hazardous (it matches the criteria for even more hazardous category than the untreated one). This study shows that it is beneficial not only to study the leaching of certain components and the factors which affect them, but also to pay attention to amounts of elements remaining in FA after treatments. Because the FA might have a latent hazard in some cases, and in some it is not hazardous after even minor processing. The aim underneath this research is to draw attention to the issue of FA processing once again. If the extraction of metals turns out to be economically feasible for a certain country, it would be rather insubstantial to incorporate the material in concrete. We believe that these findings will help in issues related to treating, processing, and utilizing FA. For further research, it is expedient to study the mechanisms of mutual elution of matrix components and PTEs in detail, as well as to investigate the structure of FA and how, if used as secondary building materials, it affects the final product properties.

CHAPTER 5

Physical and chemical properties of different types of MSWI BA fines for its application as a cement substituent (filler)

This chapter has been published as:

E. Loginova, K. Schollbach, M. Proskurnin, H.J.H. Brouwers, 2021. Municipal Solid Waste Incineration Bottom Ash Fines: Transformation into a Minor Additional Constituent for Cements. Resources, Conservation and Recycling. 166, p. 105354. doi: 10.1016/j.resconrec.2020.105354.

5.1 Introduction

Different particle-size fractions of BA are potentially attractive for various applications in the field of building materials[80]. Nowadays, the coarse fraction of BA (> 3–4 mm) is widely investigated as a substitute for natural aggregates in concrete[14,15]. For the fine fraction of BA (< 3 mm), which accounts for 50–60% of its total mass, there are several obstacles that still impede its use as secondary building materials[15,155].

There are three major problems related to the direct use of the BA fine fraction as aggregates. The first one is the high porosity, which increases the water demand and reduces the final product strength (concrete or mortar)[156,157]. The second challenge is metallic Al pieces in BA that can cause cracks (micro and macro) in concrete due to the formation of hydrogen gas as a result of the reaction between aluminum and the cement paste's alkaline environment[158,159]. The last obstacle is PTE leaching that sometimes exceeds the legislation limits[160,161].

To date, there are many papers devoted to solving these problems, and milling of BA seems particularly promising. It can reduce porosity and remove metallic Al, while, at the same time, making the material small enough to function as a cement replacement. Kim at al. studied 10–30% w/w cement replacement levels by ground BA (from an unmentioned fraction) and received unsatisfactory compressive strength of hardened pastes (loss of the strength from 30 to 10% w/w) mainly due to the presence of metallic Al[162]. Chen at al. studied the effect of different BA particle size fractions (untreated) on early hydration of cement and concluded that fine fractions, due to a higher sulfate content, inhibit the hydration more than coarse ones, although the difference turned out to be small[64]. In several papers, only one replacement level (30% w/w) was tested, and the compressive strength was unsatisfactory (either the compressive strength was significantly lower (> 16%), or the leaching of PTEs was too high)[155,161]. For this reason, researchers have investigated additional treatments. In one study, thermally treated, ground BA in the form of a slurry with an activator (up to 4% w/w $CaCl_2$) was investigated as a cement replacement (20–40% w/w) and showed satisfactory results for 20% w/w replacement levels. The same BA without an activator showed a significant decrease in compressive strength of about 40% w/w (21 days curing) observed for a 20% w/w replacement level[96]. However, the use of chlorides in concrete is generally avoided to prevent the corrosion of rebar. There are also studies conducted on the addition of acid-treated, ground, and sieved (0.074 mm) BA at the clinker production stage (with a replacement level of up to 3.5% w/w)[160,163]. But acid treatments generate highly contaminated waste solutions, which is not desirable.

It can be concluded that untreated milled BA without additives is unlikely to demonstrate good performance for higher replacement levels (10–20% w/w) and that additional treatments can have other drawbacks. However, according to regulations, it is possible to use a Minor Additional Constituent (MAC) in cement, which cannot exceed 5% w/w and have to be below 125 μm in size[39]. The usage of MAC reduces the costs related to the cement production (accompanied with the reduction of the carbon footprint) while utilizing the waste material. Low replacement levels are unlikely to have a noticeable detrimental effect. The Netherlands alone produce more than 1.4 million ton of cement per year. Using BA fines as a 5% w/w MAC replacement would make it possible to use around 70 thousand ton (more than 10% w/w) of the BA fines produced yearly. However, the studies on such a low range level of replacement (less than 10% w/w) are almost absent[40,41].

The aim of this part of the study is to demonstrate a novel approach for treating BA fines (0.125–3 mm) via milling close to cement size and using them as a MAC replacement material. The BA fraction of 0.125–3 mm is ground in three different ways to achieve the particle size below 125 μm and match the PSD of two different cement types (CEM I 52.5 R and CEM I 42.5 N). The properties of these milled fines are compared to the "natural" fine BA fraction (< 125 μm) from the same BA. A comparative analysis of chemical, physical, and morphological properties of all types of fines was carried out using ICP-AES, IC, XRF, XRD, SEM and other methods. Their effect on the cement hydration and mechanical properties of the final products (mortar) containing a 5% w/w cement replacement by BA was studied using isothermal calorimetry and a standard compressive-strength test.

5.2 Materials and methods

The general materials and methods are discussed in Chapter 2. Here, specific details and/or unique for the chapter procedures are presented.

5.2.1 Materials

BA fines (< 3 mm) were supplied by the municipal solid waste-to-energy incinerator plant of Mineralz (The Netherlands), where they underwent the standard washing and ferrous and non-ferrous metal removal process. The material was processed in the laboratory as depicted in Figure 5.1. Prior to each sieving step fines were oven-dried (105 °C).

CEM I 52.5 R and CEM I 42.5 N supplied by HeidelbergCement (The Netherlands) were used as binder for references and mixtures with ground and

non-treated BA fines (MCF, SOF-52, SOF-42, and BF, respectively). They have the same chemical composition but different PSDs.

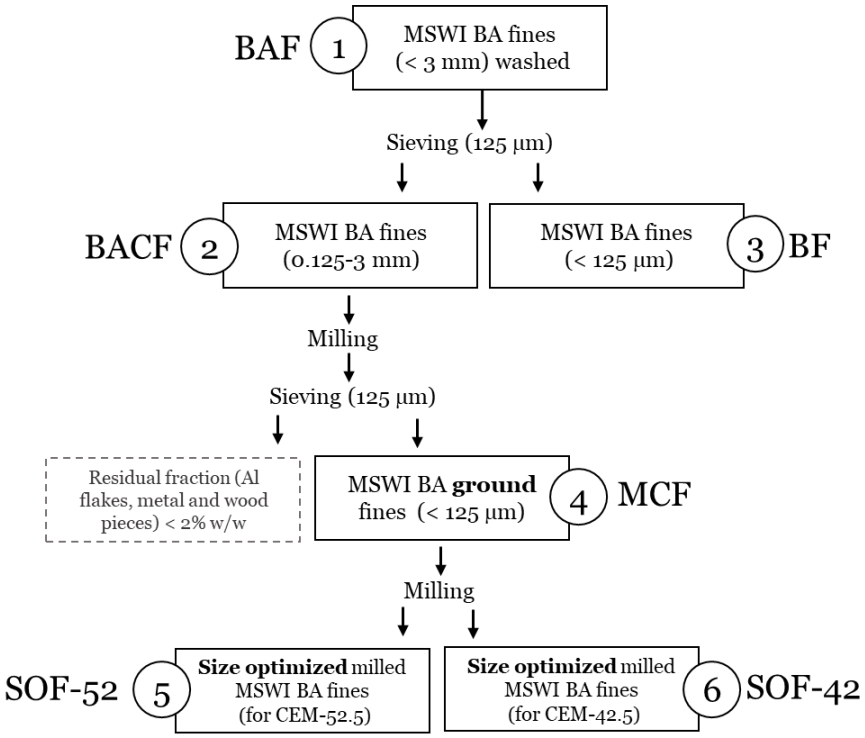

Figure 5.1 BA fines used in the study.

Figure 5.1 depicts the route for obtaining all the fines examined in the study. The starting material is BA fines (a fraction of BA < 3 mm, washed at the factory). Further, to obtain "natural" (unmilled) fines < 0.125 mm (BF, short for "basic fines"), the initial material was sieved with a 0.125 mm sieve. The remaining material of 0.125–3 mm (BACF – Bottom Ash Coarse Fines) was further milled to obtain "Milled Coarse Fines" (MCF). The material was then sieved again, and the residuals (> 0.125 mm) were sieved out because the filler should not contain particles > 0.125 mm. The last two steps consisted of additional grinding of MCF in two ways to match the particle size of the material with the particle size of the two cements. As a result, two materials were obtained: SOF-42, and SOF-52 (from "Size Optimized Fines", numbers indicating the standard compressive strength at 28 days), see Figure 5.1.

5.2.2 Procedures and treatments

Dry milling conditions

One of the main challenges of using BA fines as a substitute for cement or aggregates is their porosity and the subsequent high water demand. Milling not only reduces the particle size to the desired value, but also diminishes the rugosity of the particle surface (which contributes to the materials total SSA). In addition, during the milling process, metallic Al particles are flattened and can be removed via sieving (the residual fraction in Figure 1).

We aimed to reach the desired particle size with as little milling as possible to minimize the cost of milling. Thus, the first milling procedure was carried out in zirconia bawls in 4 cycles (10–10–20–20 min, 150 rpm), and after each cycle, the material was sieved through a 0.5-mm sieve (to remove flattened Al particles) and a 0.125-mm sieve to obtain the MCF fraction. This was done to remove softer particles that had already reached a desired size while harder ones were ground for longer to guarantee a uniform particle size. The MCF was then milled again for 85 and 210 additional minutes (300 rpm) for SOF-42 and SOF-52, respectively, to obtain particles in the range of CEM I 42.5 N or CEM I 52.5 N. SOF-52 was then mixed with CEM I 52.5 R, and SOF-42 with CEM I 42.5 N.

Standard leaching test

The standard leaching test[127] (24 h shaking, L/S 10, 200 rpm) was performed on sample groups denoted as 1-6 in Figure 5.1 (3 replicates of 30 g each) as well as hydrated cement pastes containing 5% w/w of fines 3-6 to evaluate the level of PTEs, chloride, and sulfate. Samples 1-6 were submitted to the test as is (coarse or fine powders), and cement pastes were crushed and sieved (after 28 days curing) below 4 mm prior to testing. After the test, the leachates were filtered through 0.2-µm filters to prepare solutions for IC and ICP–AES (later filtrates were acidified with nitric acid (69% w/w, for analysis, ISO grade, AppliChem Panreac).

Early day (72 h) hydration

The effect of MCF, BF, and SOF-52 as a partial replacement of cement in cement mixtures (0 and 5% w/w replacement) on the hydration process was studied by isothermal calorimetry (a TAM Air calorimeter). Mixtures were prepared with a water/powder ratio of 0.5. The additional reference used in the study was a sample containing 5% w/w quartz powder to control for the filler effect. The experiment was only performed on CEM I 52.5 R because the effect is easier to observe in more reactive cement.

5.3 Results and discussion

Four types of fines were analyzed for their properties and performance in cement mortars. Along with the assessment methods, a comprehensive portrait of physical, chemical, mineralogical, and morphological properties of all studied fines is presented. (The scheme of all the experiments can be found in Appendix B, Figure B.1).

5.3.1 Chemical properties of BA fines

Leaching

The leaching test on the initial materials (all types of fines and cement) was performed to estimate a potential environmental impact of the studied fines on their cement mixtures. All types of fines (Figure 5.1, units 1-6) were analyzed for the leaching of PTEs, sulfates and chlorides Table 5.1. The values for BF are above the LL for both anions. The BACF fraction, which was a precursor for MCF, is well below the limit for chlorides and above the limit for sulfates. Milling MCF to obtain two types of SOF resulted in a very slight increase in the leaching of both chlorides and sulfates with a decrease in the particle size.

The data for cement is presented here only for the sake of comparison. It can be seen that CEM I 52.5 R leaches a significant amount of Ba, while this is not the case for CEM I 42.5 N. CEM I 42.5 N also shows a much higher sulfate leaching than CEM I 52.5 R. The leaching of Ba^{2+} and sulfate may be connected as Ba^{2+} reacts with available SO_4^{2-} to form insoluble $BaSO_4$, which removes Ba^{2+} from the solution.

Regarding the leaching of PTEs of the initial fines: only BF shows leaching of Cu which is slightly above the limit (1.30 vs. 0.9 mg/kg). It is noteworthy that with an increase in the milling time, the leaching of Sb increased: for BACF it is below the detection limit; for MCF it is 0.7 mg/kg; for SOF-42, 0.80 mg/kg; and for SOF-52, 0.90 mg/kg, while the LL is 0.32 mg/kg. No other excess of the LL in the studied BA was observed.

Table 5.1 Leaching of sulfate and chloride, and present in the leachates cations for BA fines: fraction 0–3 mm (BA fines), fraction 0–0.125 mm (BF), fraction 0.125–3 mm (BACF), ground BACF (MCF); PSD-optimized to CEM I 42.5 N ground MCF (SOF-42), and PSD-optimized to CEM I 52.5 R, ground MCF (SOF-52); the units for concentrations given as mg per kg of dry solid, (n = 3, P = 0.95); LL is the legislation limit[128].

Fines	Chloride	Sulfate	Ba	Cr	Cu	Zn	Mo	Sb
				mg/kg$_{ds}$				
BA FINES	640 ± 60	5600 ± 600	0.40 ± 0.04	0.40 ± 0.04	0.80 ± 0.08	0.09 ± 0.009	< 0.01	< 0.01
BF	1200 ± 100	10000 ± 1000	0.30 ± 0.03	0.30 ± 0.03	1.30 ± 0.1	0.20 ± 0.02	< 0.01	< 0.01
BACF	470 ± 50	4400 ± 400	0.50 ± 0.05	0.30 ± 0.03	0.6 ± 0.06	0.06 ±0.006	< 0.01	< 0.01
MCF	500 ± 50	5400 ± 500	0.60 ± 0.06	< 0.02	0.7 ± 0.07	0.02 ± 0.002	0.40 ± 0.04	0.70 ± 0.07
SOF-42	590 ± 60	5800 ± 500	0.80 ± 0.08	< 0.02	0.7 ± 0.07	0.01 ± 0.001	0.60 ± 0.06	0.80 ± 0.08
SOF-52	650 ± 70	6200 ± 600	1.3 ± 0.1	< 0.02	0.8 ± 0.08	0.03 ± 0.003	0.90 ± 0.09	0.90 ± 0.09
CEM I 52.5 R	320 ± 30	50 ± 5	30 ± 3	0.50 ± 0.05	< 0.01	0.04 ± 0.004	0.20 ± 0.02	< 0.01
CEM I 42.5 N	180 ± 20	4700 ± 400	6.0 ± 0.6	6.6 ± 0.7	< 0.01	0.03 ± 0.003	0.80 ± 0.08	< 0.01
LL	616	2430	22.4	0.63	0.9	4.5	1	0.32

As can be seen from Table 5.1, the leaching of sulfate and chloride shows the same trend. Increased milling time leads to an increase in leaching. This is unexpected, since the solubility of chloride especially is very high and should be independent of milling time. An explanation is the fact that more contaminated small particles from the surface quenching layer are liberated during milling (Section 5.3.3). This quenching layer is very porous, and this porosity gets filled with the water used for BA quenching after incineration. The water tends to accumulate large quantities of chloride and other elements, because it is constantly reused. During drying and weathering, the porosity is partially closed, which creates small pockets inside the quenching layer that are rich in Cl. Normal washing is only partially effective in removing this physically trapped Cl, but it is made accessible by breaking up this layer during milling. This finding is consistent with literature[48,86].

Main oxide composition of fine BA

The main oxides of the investigated fines (BF and MCF) are depicted in Table 5.2. The compositions of SOF-42 and SOF-52 are the same as that of MCF because they are produced from the same material. CEM I 52.5 R and CEM I 42.5 N are also almost identical.

Table 5.2 Main oxides and LOI (% w/w) of BA fines in comparison with CEM I 52.5 R.

	BF	**MCF**	**CEM I 52.5 R**
SiO_2	35.1	50.7	20.1
CaO	20.1	12.9	64.0
Fe_2O_3	18.5	15.4	3.9
Al_2O_3	11.4	9.0	4.8
BaO	0.2	0.1	3.0
MgO	1.4	1.6	1.2
SO_3	1.1	0.8	2.8
Other	12.2	9.5	0.2
LOI	15	7.2	1.5

The most obvious differences are in SiO_2 and CaO contents. Both types of fines (BF and MCF) contain significantly lower amounts of CaO; 3 and 4 times, respectively, than cements. A large amount of it is present in the form of calcite. SiO_2 in BA fines is mainly present in the form of quartz (whose contribution to the hydration process is limited to providing nucleation sites only[164]).

The LOI should not exceed 5% w/w in cement (CEM I 52.5 R). Thus, all tested types of BA fines can be safely used. For MCF, SOF-42, and SOF-52 the LOIs in

the case of 5% w/w additions approx. 1.8% w/w, which is well below the standard requirement limit (max. 5% w/w).

As can be seen from Figure 5.2, these two BA fractions (MCF and BF) differ slightly. The predominant mineral of both fractions is quartz, which agrees with previously published works, as well as the results of XRF analysis[88,165]. In both fractions, various iron-containing minerals, such as magnetite, hematite, and wustite, are present in noticeable amounts[166]. Of the calcium-containing minerals, calcite, gypsum, anhydrite, and bassanite are found in both fractions, and in the BF fraction they appear to be present in larger quantities, which correlates with XRF data (Table 5.2) and the literature[167]. Silicates of different types, such as feldspar, pyroxene, and melilite are also present in small quantities in both fractions[90].

Mineralogical composition of BA fines

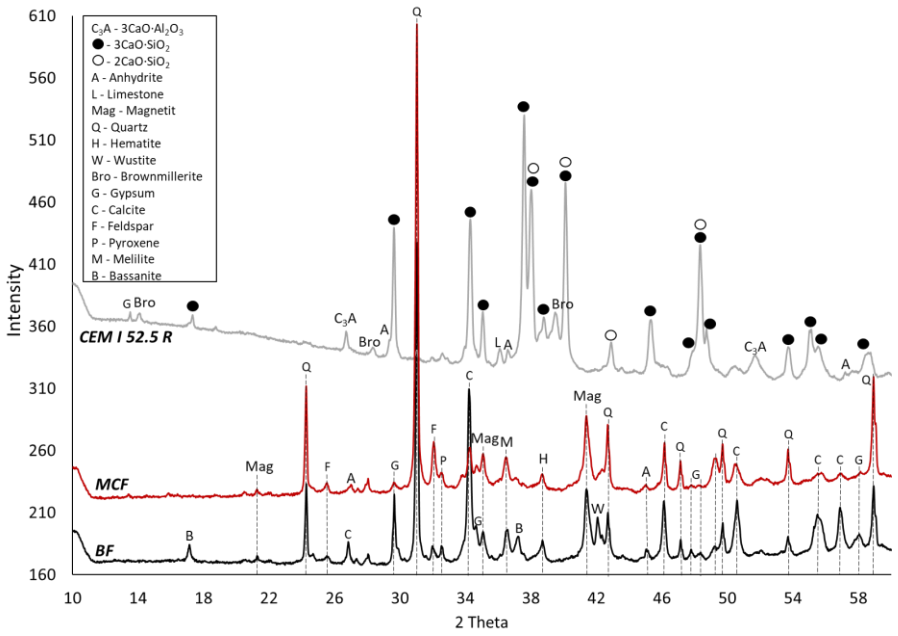

Figure 5.2 Diffractograms (Co radiation) of 2 BA fractions and cement (CEM I 52.5 R); for the sake of convenience, the plots are shifted relative to each other; the intensity scale is given in square roots of original values.

5.3.2 Physical properties of BA fines

Bulk and specific densities, water demand, PSD, and SSA were determined for all four types of fines (BF, MCF, SOF-42, and SOF-52) and cement (both types) for comparison (Table 5.3).

Table 5.3 Physical properties of BA fines and cement (n = 3, P = 0.95).

		Cement		BA FINES			
Property	**Units**	**I 52.5 R**	**I 42.5 N**	**BF**	**MCF**	**SOF-42**	**SOF-52**
B. density	**(g/cm³)**	1.1 ± 0.1	1.7 ± 0.1	1.2 ± 0.1	1.5 ± 0.1	1.6 ± 0.1	1.5 ± 0.1
Sp. density	**(g/cm³)**	3.10 ± 0.05	3.40 ± 0.05	2.90 ± 0.05	2.90 ± 0.05	2.90 ± 0.05	2.90 ± 0.05
W. demand	**(% w/w)**	22.0 ± 0.5	21.0 ± 0.5	40.0 ± 0.5	20 ± 0.5	22.0 ± 0.5	24.0 ± 0.5
SSA (BET)	**(m²/g)**	1.30 ± 0.05	1.0 ± 0.05	16.9 ± 0.05	6.9 ± 0.05	4.3 ± 0.05	4.8 ± 0.05
d (0.5)	**µm**	11	20	78	39	20	13
d (0.9)	**µm**	26	61	164	140	72	46

Water demand is an important parameter to consider for cement replacement materials such as BA. A high water demand will either lower workability or increase the water/binder ratio resulting in strength loss of the final product. Table 5.3 shows that the water demand of BF is two times larger than that of cement, and all milled fines (MCF, SOF-42, and SOF-52). Noteworthy, with a decrease in the particle size during milling, from MCF to SOF-42 and SOF-52, the water demand increases slightly, while the SSAs seem to decrease with the milling time. As mentioned in the previous sections, the unmilled BA particle normally has a solid core with a very fine particle layer attached to it. Presumably, the particles from this layer are being liberated during the milling, and then agglomerate[41]. The agglomeration might be due to the changes in the ratio of sulfate and OH-groups that are generated appearing during milling[168,169]. There is no literature found on these phenomena occurring with BA. However, similar observations have been mentioned in the literature with such materials as pulverized coal fly ash or clay. The emergence of such new mechano-activated groups may also result in binding very fine particles together (agglomeration, Section 5.3.3)[170,171].

In turn, all this might affect the availability of groups responsible for «wetting» the particles and nitrogen adsorption (in the BET measurements of the SSA) due to a presumed difference in the availability of the functional groups prone to react covalently (e.g., those that participate in the nitrogen exchange in BET), and groups responsible for adhesion of the water molecules. Therefore, we see a decrease in SSA, while the water demand changes little. This effect of milling on selective physicochemical activation is worth further studies.

Comparing SSA values of unmilled BA shows that the value for MCF is about 6 times higher than for cement, while the original fines (BF) have an SSA that is ca. 13 times higher. Such a high SSA in the latter case can be caused by either a high surface area due to small particle size or high porosity of the particles or both. In the case of BF, the high porosity appears to be the main contributing factor, because natural BA fines (< 0.125 mm) contain nearly only the porous outer layer of BA that was removed from larger particles during treatment at the plant[48]. The high porosity is expected to have no negative effects on the water demand/workability at MAC replacement levels. It may even be beneficial in terms of internal curing to reduced shrinkage[172], but more research is needed to determine this effect.

Figure 5.3 (upper part) shows that the PSDs of all fines are quite different from cement. MCF contains significantly larger particles (d (0.5) = 39 μm, d (0.9) = 140 μm) than cement (d (0.5) = 11 μm, d (0.9) = 26 μm) but the condition that all

particles should be in the range of < 125 µm was met[173]. It can also be seen that the PSD of MCF is closer to the cement PSD than the non-treated BF.

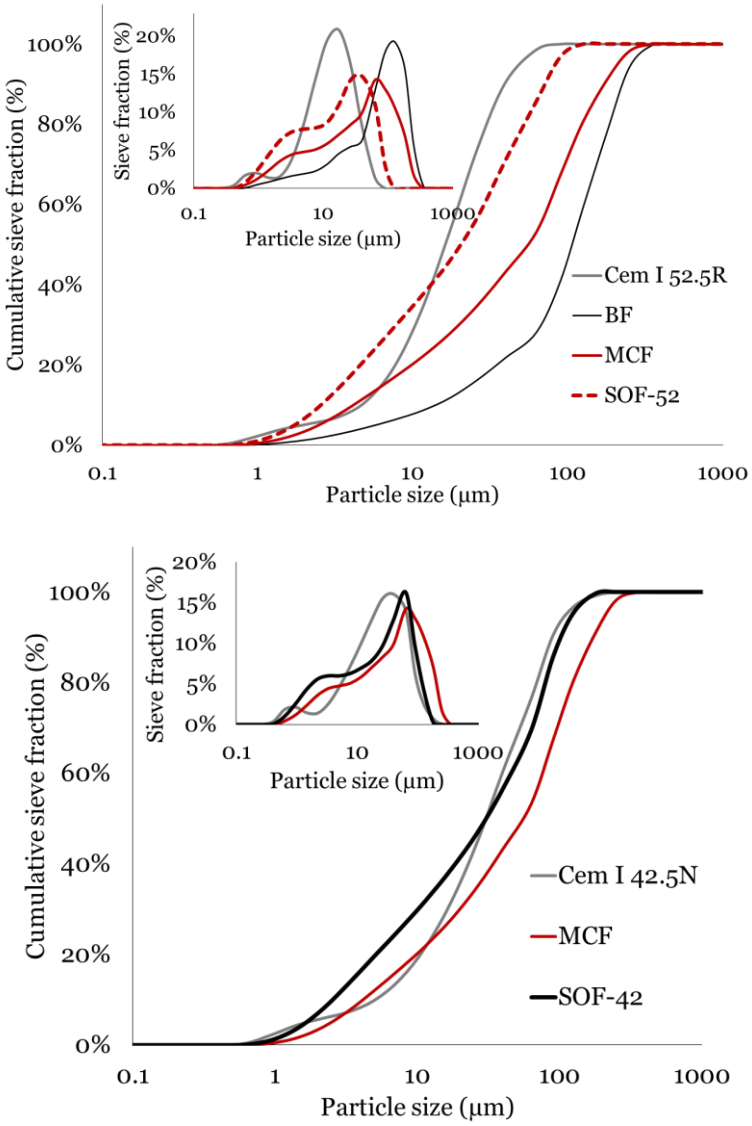

Figure 5.3 Upper part: Particle Size Distribution of CEM I 52.5 R, and MCF, SOF-52, and BF, cumulative and differential (inset). Lower part: Particle size distribution of CEM I 42.5 N, MCF and SOF-42.

Figure 5.3 (lower part) shows that the PSD of SOF-42 is close to the PSD of CEM I 42.5 N (d (0.5) = 20 μm, d (0.9) = 72 μm vs. d (0.5) 20 μm, d (0.9) 61 μm for CEM I 42.5 N). However, with increasing milling time from MCF to SOF-42, the amount of relatively large particles barely changes, while the number of small particles (1–10 μm) increases.

Even though the d-numbers appear to be close to those for cement (for SOF-52 d (0.5) = 13 μm, d (0.9) = 46 μm vs. for CEM I 52.5 R d (0.5) = 11 μm, d (0.9) = 26 μm), PSDs differ significantly.

5.3.3 Morphological properties of all fines

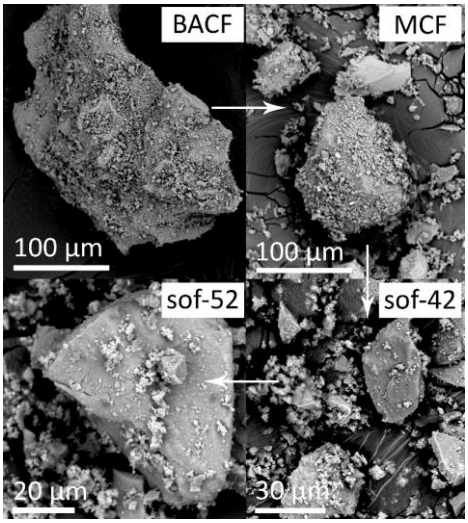

Figure 5.4 BA particles undergoing the milling treatment, clockwise from the upper left corner.

Changes in BA particles during the milling are shown in Figure 5.4. The upper left image is a representative particle from the original BA fraction of 0.125–3 mm. It has an irregular shape and is covered with a rough layer with high porosity previously reported as a "quenching layer"[85]. The upper right image is MCF, i.e. the material after the first stage of the initial milling of BACF. A smaller particle is visible that is still covered in a quenching layer. In SOF-42 (Figure 5.4, lower right), the size of particles has decreased significantly. In any case, both SOF-42 and SOF-52 show a cleaned particle surface free from the porous quenching layer. This effect explains the reduction in SSA with increased milling time (Table 5.3). Similar behavior has been reported previously with MSWI sludge[41]. Thus, it is likely that milling not only decreases the particle size due to fracturing, but also peels off small porous particles from presumably harder particles that then

agglomerate. This is consistent with the more pronounced bimodal size distribution of the fines with an increase in milling time (Section 5.3.2).

5.3.4 Effect of BA fines on cement hydration

Figure 5.5 depicts the effect of different types of BA fines (MCF, SOF-52, and BF) on the hydration of cement pastes. Cement with 5% w/w quartz is used as a reference with the same water/cement ratio. The difference between all fines is small and no significant negative effect on the hydration speed is observed at these replacement levels. Some delay could have been expected due to the presence of sulfates in the fines, but peak shapes and the absence of additional peaks indicate that there are no side reactions associated with a higher sulfate content in MCF compared to cement (2.83% for cement vs. 5.3% for MCF, 9.9% for BF, and 6.1% for SOF-52)[174].

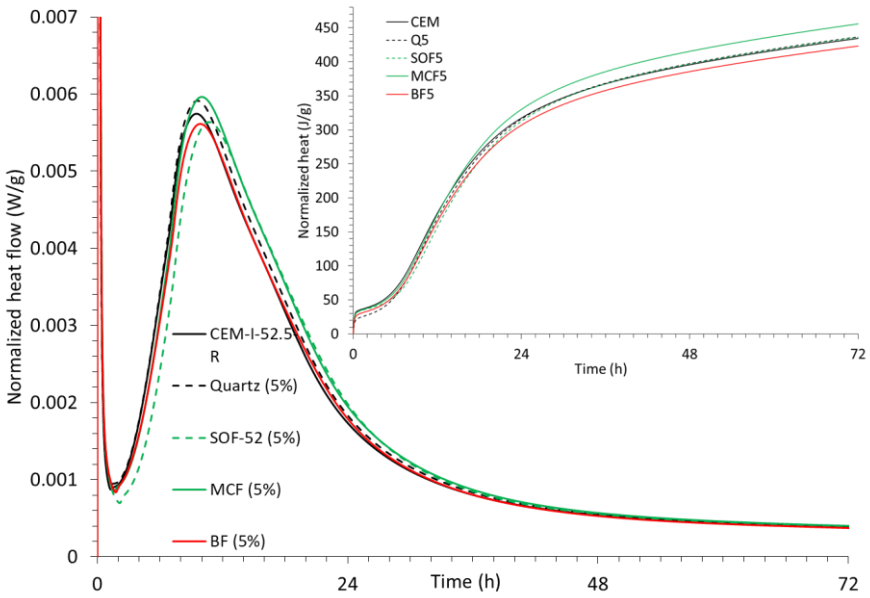

Figure 5.5 Effect of added BA fines on cement hydration (normalized by the cement weight).

Figure 5.5 also shows that the cumulative heat (normalized per cement) is the lowest for BF, suggesting that even though it does not lower the rate of cement hydration, it has a negative effect on the reaction degree. MCF shows the highest cumulative heat for reasons that are unclear. A higher cumulative heat could have been expected for SOF-52 as it has the smallest particle size and could therefore

be more reactive. But it is possible that the milling and the associated removing of the quenching layer releases not only more sulfate but also other components such as organic matter that have a negative influence.

5.3.5 Leaching properties of hardened pastes containing BA fines

Even though the initial BA fines contain some contaminants above the legislative limit, all pastes containing 5% w/w fines did not exceed the legislative limit after 2 and 28 days of curing. The concentrations of PTEs and anions are much lower than the limits or below the detection level, and are, therefore, not shown.

5.3.6 Mechanical properties of mortars containing BA fines as a filler

The suitability of fines to be used as a MAC was assessed by testing mechanical properties of mortars containing MCF, BF, SOF-42, and SOF-52 (Figure 5.6) After two days of hydration, SOF-52 shows the best results and reaches a compressive strength similar to the reference (100% cement), while MCF and BF are slightly lower and comparable to one another. All the samples are above the standard value for this type of cement (30 MPa). After 7 days, SOF-52 becomes comparable with the reference, and BF is noticeably lower. At 14 days, the difference between the reference and MCF becomes more obvious (as well as for BF). After 28 days, all the samples with additives are noticeably below the reference. However, all of them are still quite above the standard (52.5 MPa). Overall, at 28 days the strength reduction is 7, 11, and 9% for MCF, SOF-52, and BF, respectively. The situation is the same for 91 days.

The samples BF and MCF show the same starting strength that is lower than that for SOF-52 and the pure cement sample. The samples containing BF show the lowest overall strength increase over time and seems to stagnate at 91 days. The reason for this might be the high porosity and the presence of contaminants. MCF starts out at a similar strength but shows a much better strength increase over time and even surpasses SOF-52 at 28 days. This indicates some pozzolanic reactivity of the material. The strength gain over time for the sample containing SOF-52 is similar to that of MCF but is slightly lower at 28 and 91 days as mentioned. The reason for this is unclear but could be attributed to an increased release of compounds that delay the reaction in the course of milling. The strength of all mortars containing BA fines is somewhat below that of 100% cement samples.

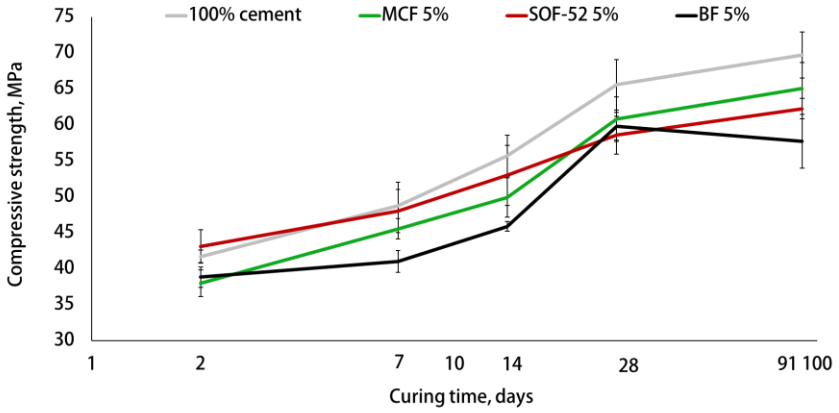

Figure 5.6 Compressive strength of mortars containing 5% w/w of MCF, SOF-52, and BF as a partial cement replacement at different curing times (from 2 to 91 days), $n = 18$, $P = 0.95$.

In comparison with the unexpected behavior of SOF-52 with CEM I 52.5 R, the performance of SOF-42 with CEM I 42.5 N appears to be more anticipated, i.e., the outcome at all the stages is lower in comparison with the reference (see Figure 5.7).

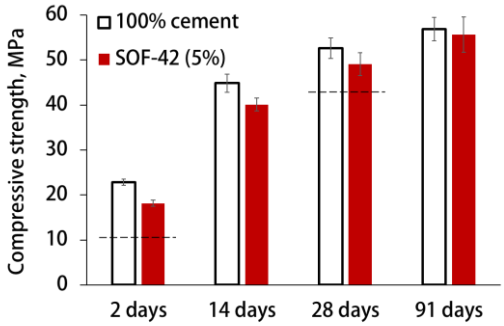

Figure 5.7 Compressive strength of mortars (CEM I 42.5 N) containing 0 and 5% w/w of SOF-42.

However, with the hydration continuation, the strength reduction is −21, −11, −7, and −2% for 2, 14, 28, and 91 days, respectively. The same numbers for SOF-52 are +3, −2, −5, and −11%, respectively. Therefore, even though the early compressive strength is even higher than of the reference, in a long term, this optimization appears to be more effective for a coarser and less reactive cement.

Changes in the flexural strength of all the samples do not appear to be governed by the addition of fines. They are on average within the experimental error and the flexural strength is not changing significantly from 14 to 91 days (Table 5.4).

Table 5.4 Flexural strength of mortars containing 5% w/w of MCF, SOF-52, and BF as a partial cement replacement at different curing times (from 2 to 91 days), $n = 3$, $P = 0.95$.

Days / Fines	2	7	14	28	91
100% cement	6.7 ± 0.7	8.1 ± 0.8	8.0 ± 0.7	8.1 ± 0.8	7.7 ± 0.8
MCF	6.5 ± 0.5	7.1 ± 0.7	7.5 ± 0.8	7.6 ± 0.8	7.7 ± 0.8
SOF-52	6.7 ± 0.7	7.0 ± 0.7	7.4 ± 0.7	7.7 ± 0.8	7.9 ± 0.8
BF	6.1 ± 0.6	6.8 ± 0.7	7.6 ± 0.8	8.0 ± 0.7	7.8 ± 0.7

Table 5.4 shows that the effect on the flexural strength of mortars containing 5% w/w of cement replaced with certain fines is almost negligible and within the experimental error.

5.4 Conclusions

Four types of BA fines were analyzed to assess their suitability and limitations as MAC in cement: “BF”, unprocessed fines < 0.125 mm (washed at the plant), and 3 derivatives from a fraction of “coarse” fines (0.125–3 mm); MCF (Milled Coarse Fines), SOF-42, and SOF-52 (Size Optimized Fines for CEM I 42.5 N, and CEM I 52.5 R, respectively). These fines were milled in 3 different ways to achieve a size distribution close to that of 2 types of cement.

Among the analyzed fines, MCF and SOF-52 gave the best results regarding compressive strength. However, MCF generates slightly more heat flow as measured with calorimetry. SOF-52 shows worse results than MCF (strength, in comparison to the cement reference) but taking into consideration that the material preparation is more intense, perhaps its use will not be justified (at least for such low replacement percentages). However, SOF-42 showed better results for the respective type of cement reducing the compressive strength of the sample at 28 days only by 2%. That might be due to the fact that CEM I 52.5 R is finer, and, therefore, more reactive than CEM I 42.5 N, so it is more sensitive to any negative influences the BA fines may have. Ergo, it is necessary to study this phenomenon further. Regarding the application of BF, it is necessary to take into account relatively high concentrations of certain metals (total composition)

(Chapter 3) which might exceed the limitations for cement even being added in small amounts.

The main results of this study can be summarized as follows:

- Mechanical treatment for the BA fraction of 0.125–3 mm was applied in several steps to generate fines that have a similar size distribution as CEM I 42.5 and CEM I 52.5 and can be used as a MAC, while also reducing porosity of the fines and removing metallic Al particles.
- The mechanical treatment results in polishing BA particles by removing the attached quenching layer from larger particles along with an overall size reduction. The breakup of the quenching layer results in increased leaching of chlorides and sulfates, while the surface area of the material decreases probably due to the agglomeration of small particles removed from the quenching layer.
- The hydration study has proven milled coarse BA fines (MCF) to be contributing the most to the cement hydration (+5% cumulative heat), while the "natural" unmilled fines (BF < 0.125 mm), slightly hindered the hydration (–2.5% cumulative heat) during the first 72 h.
- The compressive strength decrease for 28 days is 7% for milled coarse fines, 9% for non-treated fines, 11% for size optimized fines (for CEM I 52.5 R), and 7% for size-optimized fines (for CEM I 42.5 N). All the mortars showed the compressive strength above the standard with a minimum value of 58.5 MPa for a mixture with CEM I 52.5 R, and 49.1 MPa for a mixture with CEM I 42.5 N.
- The use of MCF fraction "as is" appears to be most suitable for a MAC application. Further milling to produce SOF-42 and SOF-52 does not appear to be beneficial based on the compressive-strength results. This is positive, as less energy and effort are required to produce this material.
- Physical, chemical, and mechanical properties suggest that all types of fines might be considered as potential MACs; however, milled coarse fines appear to be most desirable from two viewpoints: (i) its effect on the cement hydration, and, therefore, mechanical properties and (ii) its low environmental impact.

CHAPTER 6

Performance of differently ground coarse fine fraction of MSWI BA as filler in cement mortars

This chapter has been submitted for journal publication:

E. Loginova[1*], K. Schollbach[1], M. Proskurnin,[2] H.J.H. Brouwers[1], Waste recycling in structural building components: Mechanical performance and microstructural properties of cement mortars containing MSWI BA as a minor additional constituent (2022).

6.1 Introduction

There are three types of MSWI residues: air pollution control residues (APCr), fly ash (FA), and bottom ash (BA). MSWI APCr and FA are highly contaminated fractions and require a special treatment before being landfilled[24]. BA, composing ca. 80% w/w of all residues is a much cleaner product; although without treatment, it contains PTEs in concentrations that significantly exceed the legislation limits (LL)[98]. However, if the most contaminated BA fraction (<125 μm) is separated, the remaining material is clean enough to be used in various applications after washing out water-soluble salts (Chapter 3).

The BA part >125 μm can be divided into two fractions: below 3 mm (the fine fraction; 50–60% w/w of the total BA) and above 3 mm (the coarse fraction)[16].

Another possible application for the fine BA fraction is a cement substituent. Multiple studies investigated a partial cement replacement with BA; however, fairly significant amounts (from 10 to 50% w/w of BA in BA–cement mixtures) are usually used, which severely deteriorate the resulting concrete/mortar mechanical characteristics[159,161]. There are also studies reporting acceptable mechanical properties, where a 10–30% w/w BA caused a strength reduction of 10–31%, meaning the BA acted mostly as an inert filler. BA can also influence hydration rate negatively, and a 20% w/w replacement of cement with five untreated BA particle size fractions showed a delay in hydration up to 10 h for the finest fraction properties[64,162].

However, it might still be possible to use BA as a minor additional constituent (MAC) because cement standards allow the use of an inorganic additive of up to 5% w/w, and such low replacement levels should not have a negative effect on cement properties. As large additions of BA to cement results in a noticeable deterioration in concrete/mortar properties, and most studies do not consider low replacement levels (below 10% w/w), there are currently no cement products containing BA within the MAC range on the market.

Using BA as a MAC requires milling because the standard specifies that it should be < 125 μm in size. This has several advantages, because besides reducing the particle size, an optimized milling procedure might also help to remove pieces of metallic aluminum by flattening them and subsequently sieving them out and reduce the porosity and water demand of the BA itself[175].

However, previous research has mostly focused on milling BA without separating it into different fractions first, and the fine BA fraction (0.125–3 mm) has not been thoroughly studied. In another study, a fraction of 0.04–0.25 mm was investigated as a low-density binder with wood–cement boards analyzing

among others its properties as an insulation material[44]. Tang et al. focused on a combined milling and heating treatment at 550 and 750 °C (to increase reactivity and reduce the leaching) of a 0–2 mm BA fraction slowly milled to a size below 0.125 mm. Only a replacement level of 30% w/w was studied, and the reported mechanical properties were between 15–50% lower in comparison with a reference sample depending on the BA pretreatment prior to use[155]. The only paper dealing with different particle-size BA fractions (five fractions < 6.3 mm) milled below 150 μm made a study on hydration of mixtures but did not report the mechanical properties[64].

To summarize, to the best of authors' knowledge, there is almost no published research on the applications of the fine BA fraction (0.125–3 mm) as a MAC[176], which has the advantage of being significantly less contaminated than the finest fraction (< 125 μm) but cannot be recycled as a natural aggregate substitute.

The aim of this part of the thesis is therefore to analyze small replacement levels of differently ground BA fines (the fraction 0.125 – 3 mm) in a cement mixture in the MAC range (0–5% w/w), while higher replacement levels (up to 20% w/w) were used to demonstrate negative effects on the properties of mortars and pastes, which might not be visible at replacements within the MAC range. We aimed to determine the maximum BA content in cement mortars resulting in no detectable deterioration of properties (both mechanical and environmental). The second goal is to determine the maximum BA content that results in a satisfactory level of the final product (mortar) deterioration compared to the cement standard to discover whether the particle size distribution of BA fines tailored to a certain cement particle size influences a mortars mechanical performance. To achieve these goals, the mechanical properties of mortars containing BA fines (the MAC range: 1, 3, and 5; and the extended range: 10 and 20% w/w replacement level), leaching properties of dry mixtures and hardened crushed pastes, and hydration properties of pastes containing BA fines were analyzed. A microstructural analysis of mortars containing BA fines is also provided. We provided the data on all the properties for the extended range of additives (up to 20% w/w) to make changes in the structure and quality of resulted pastes/mortars clearly visible because in the MAC range some changes are very difficult to observe even though there is a detrimental effect. Thereby, this data also provides the deeper understanding on the impact of added BA milled fines.

6.2 Materials and methods

The general materials and methods are discussed in Chapter 2. Here, specific details and/or unique for the chapter procedures are presented.

6.2.1 Materials

Pre-treated (standard washed) BA fines (< 3 mm) were supplied by the MSW residues processing plant of Mineralz (the Netherlands). The material was sieved into two fractions: <125 μm and 0.125 μm – 3 mm, BA coarse fines. They were subsequently milled generating three final fine products: 1) MCF (Milled Coarse Fines), the BACF fraction milled to reduce the particle size below 125 μm; 2) SOF-52 milled to a PSD close to CEM I 52.5 R; 3) SOF-42 milled to a PSD close to CEM I 42.5 N. CEM I 52.5 R and CEM I 42.5 N supplied by HeidelbergCement (the Netherlands) were used as binders for references and mixtures with milled BA fines (MCF, SOF-52, SOF-42). The scheme of all BA fines used in the study can be found in Appendix B, Figure B.1.

6.2.2 Methods and procedures

Standard leaching test

The standard leaching test[127] (24 h shaking, L/S 10, 200 rpm) was performed on non-hydrated mixtures containing MCF, SOF-52, and SOF-42; as well as hardened cement pastes (crushed and sieved below 4 mm prior to testing) containing MCF (3 replicates of 30 g) to evaluate the level of PTEs, chloride, and sulfate, as well as to investigate the binding capacity of cement regarding the PTEs release at 28 days of curing. After the test, the leachates were filtered through 0.2 μm filters to prepare solutions for IC and ICP–AES (for the latter, filtrates were stabilized with nitric acid).

Determination of hydration delay

The effect of MCF and SOF-52 as a partial replacement of CEM I 52.5 R in cement mixtures (0 – 20% w/w replacement) on the hydration process was studied by isothermal calorimetry (a TAM Air calorimeter). Mixtures were prepared with a water/powder ratio of 0.5. Calorimetry measurement outcomes were normalized per cement mass in the sample.

Mortar preparation

Mortars with cement–BA mixtures were prepared according to EN-197-1. One batch was made from 450 g of a binder (either pure cement or cement + BA milled fines), 225 g of water, and 1350 g of sand. All mixtures (containing 1, 3, 5, 10, and 20% w/w of BA milled fines) were premixed and homogenized with a mixer prior to adding water.

The mortars were cast in Styrofoam molds and cured in water. Mortars that were used for the leaching test were cured at a high humidity without a direct contact to water.

Sample preparation and microstructural analysis

For microstructural analysis, paste samples containing MCF were prepared by the procedure described below. In a glass jar, water and cement-MCF powders were mixed (prepared in advance with the replacement level by weight), a water/powder ratio 0.5. After 24h, the jar was carefully removed, and the samples were placed in water for the remaining 6 days. After that, to stop the hydration, the samples were placed in isopropanol for 48 h and regularly mixed, and isopropanol was replaced every 12 h. After this procedure, the samples were polished using isopropanol to prevent hydration and provide a smooth surface without scratches.

Microphotographs of the samples were analyzed using ImageJ software, looking at representative areas, analyzing each area to differentiate three types of the matter in the paste: unhydrated cement, hydration products, and porosity. The results for each sample were averaged.

6.3 Results and discussion

6.3.1 Material characterization and properties of BA fines

Table 6.1 and Table 6.2 provide a summary of the main chemical and physical properties of the three types of milled BA fines used in the study. Most physical properties appear to be similar to the cement, therefore, the BA milled fines can be considered a suitable cement replacement material (Chapter 5).

Table 6.1 Leaching of sulfate and chloride, and cations present in the leachates for ground BA fines: MCF; PSD-optimized to CEM-I-42.5-N ground MCF (SOF-42); PSD-optimized to CEM-I-52.5-R, ground MCF (SOF-52); the units for concentrations given as mg per kg of dry solid. (n = 3, P = 0.95), (Chapter 5)).

	Chloride	Sulfate	Sb
Fines		**mg/kg$_{ds}$**	
MCF	500 ± 50	5400 ± 500	0.70 ± 0.07
SOF-42	590 ± 60	5800 ± 500	0.80 ± 0.08
SOF-52	650 ± 70	6200 ± 600	0.90 ± 0.09
LL	616	2430	0.32

Table 6.2 Physical properties of BA fines and cement (n = 3, P = 0.95).

		Cement		BA fines		
Property	**Units**	**I-52.5-R**	**I-42.5-N**	**MCF**	**SOF-42**	**SOF-52**
Bulk density	**(g/cm^3)**	1.1 ± 0.1	1.7 ± 0.1	1.5 ± 0.1	1.6 ± 0.1	1.5 ± 0.1
Water demand	**(% w/w)**	22.0 ± 0.5	21.0 ± 0.5	20 ± 0.5	22.0 ± 0.5	24.0 ± 0.5
D (0.5)	**µm**	11	20	39	20	13

6.3.2 Leaching of dry mixtures and hardened pastes, and mortars

To be able to use a material as a MAC, it should not influence the mechanical properties negatively and comply with local environmental LLs. Thus, it is important to examine the mortars, preferably at all stages of curing for their leaching properties.

In order to assess the environmental impact and potential risks of handling the cement containing BA, the leaching of the dry unhydrated cement mixtures was also determined even though the final assessment is made for a hydrated mortar or concrete. It is necessary to consider in what form and at what point, a cement product containing BA fines can be in contact with the soil (ground water) to prevent possible contamination.

Anion leaching of dry cement-BA mixtures

Figure 6.1 demonstrates the chloride and sulfate leaching from unreacted cement–BA mixtures. Note that for all replacement levels of SOF-52, the chloride leaching was at the same level as the initial leaching from the corresponding cement (CEM-I-52.5-R) and does not change. A very slight increase in concentrations is observed for SOF-42. For MCF (with CEM I 52.5 R), a slight decrease in chloride leaching for low replacement levels can be seen, and a slight increase in the large replacement level area (10–20% w/w) can be observed. Chloride leaching for all the mixtures is below the LL[128].

Sulfate leaching gradually decreases in all the cases when the BA share increases in the mixture, and in mixtures containing SOF-52 and MCF sulfate leaching is noticeably reduced compared to the leaching of pure fines, therefore, the main source of the leaching is cement, not BA. For pure SOF-42, the reduction in leaching is negligible. For a 1% w/w replacement, it is close to that of pure cement and then decreases with an increase in the share of SOF-42.

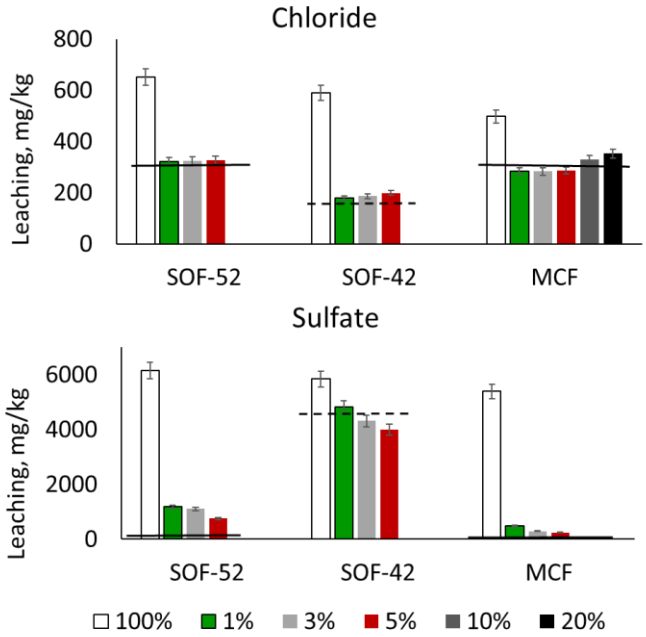

Figure 6.1 Leaching of chloride and sulfate from mixtures containing 0–20% w/w BA fines, only MCF were tested for replacements higher than 5% w/w; 100% corresponds to pure respective materials (BA fines). The level of anion leaching for CEM I 52.5 R is expressed with a black solid line; for CEM I 42.5 N, with a black dashed line.

PTEs leaching of dry cement-BA mixtures

Table 6.3 shows the leaching test results for PTEs that were either in concentrations above the LL or were high in the pure BA fines.

CEM I 52.5 R has a relatively high level of barium leaching (30 mg/kg dm), which becomes only half (15 mg/kg dm) with the addition of 1% w/w MCF, and even lower with the addition of 1% w/w SOF-52 (11 mg/kg dm). As the BA replacement level increases, Ba leaching increases too; and for MCF replacement levels of 10–20% w/w, they reach a level close to the leaching of pure CEM I 52.5R.

This can partially result from an increase in sulfate concentration due to the addition of fines, the excess of which reacts with the available barium to form $BaSO_4$, which has a very low solubility[177]. A slight difference in sulfate concentration of mixtures with MCF and SOF-52 is concordance with it, as the sulfate leaching from MCF is slightly lower in comparison with SOF-52.

Table 6.3 PTEs leaching of mixtures containing 0–20% w/w BA fines (recalculated to mg/kg); all values for Sb are below the detection limit; "b.d.l." denotes below the detection limit; (n = 3, P = 0.95)[128].

Sample	pH	Ba	Cr	Cu	Mo
CEM I 52.5 R	11 ± 0.1	30 ± 3	0.5 ± 0.05	b.d.l.	0.18 ± 0.02
MCF 1%	11 ± 0.1	15 ± 2	1.8 ± 0.2	0.05 ± 0.005	0.19 ± 0.02
MCF 3%	11 ± 0.1	18 ± 2	1.4 ± 0.1	0.07 ± 0.007	0.17 ± 0.02
MCF 5%	11 ± 0.1	19 ± 2	1.4 ± 0.1	0.13 ± 0.01	0.16 ± 0.02
MCF 10%	11 ± 0.1	31 ± 3	0.4 ± 0.04	0.16 ± 0.02	0.18 ± 0.02
MCF 20%	11 ± 0.2	32 ± 3	0.3 ± 0.03	0.28 ± 0.03	0.19 ± 0.02
SOF-52 1%	11 ± 0.1	11 ± 1	2.3 ± 0.2	b.d.l.	0.6 ± 0.06
SOF-52 3%	11 ± 0.1	17 ± 2	2.9 ± 0.3	0.08 ± 0.008	0.87 ± 0.09
SOF-52 5%	11 ± 0.1	19 ± 2	2.4 ± 0.2	0.11 ± 0.01	0.74 ± 0.07
CEM I 42.5 N	11.4 ± 0.1	6.0 ± 0.6	6.6 ± 0.7	b.d.l.	0.84 ± 0.08
SOF-42 1%	11.4 ± 0.1	7.0 ± 0.7	8.0 ± 0.8	b.d.l.	1.0 ± 0.1
SOF-42 3%	11.4 ± 0.1	7.7 ± 0.8	8 ± 0.8	b.d.l.	1.1 ± 0.1
SOF-42 5%	11.4 ± 0.1	8.0 ± 0.8	7.7 ± 0.8	0.05 ± 0.005	1.1 ± 0.1

As for the subsequent increase in the Ba^{2+} concentration with an increased cement replacement level, it might be assumed that it happens because the main source of Ba^{2+} is cement, and it is growing reaching a concentration peak at a 20% w/w replacement level. Additionally, in the case of SOF-42 and CEM I 42.5 N, barium concentrations are insignificant and are approximately at the same level for the entire range of additives.

Initially, chromium leaching was not detected in all the tested BA fines. Table 6.3 shows that the chromium leaching gradually increases in the row of MCF < SOF-42 < SOF-52 for the same cement substitution levels, although it is necessary to take into account that the CEM I 42.5 used for the SOF-42 samples leaches much more Cr (6.6 mg/kg) than the CEM I 52.5 (0.5 mg/kg). The emerging chromium leaching can be explained by a change in pH (from 8 ± 1 for pure BA fines to 11 ± 1 for cement–mixture leachates), and an increase in the solubility of chromium (III) hydrated oxide species in strong alkaline environments[178,179].

Copper was initially present in all the BA fines at the concentration level of 0.7 ± 0.1 mg/kg. Table 6.3 shows that the Cu^{2+} concentration in all the leachates is extremely low. Nevertheless, it is noticeable that in the MCF range of 1–20% w/w, the Cu concentration in the leachate slowly increases.

Molybdenum leaching was within the limit for all the BA fines (0.4, 0.6, and 0.9 mg/kg for MCF, SOF-42, and SOF-52, respectively); in all the samples containing MCF, molybdenum leaching is at the level of Mo leaching from CEM I 52.5 R and does not change as the MCF share in the mixture increases (Table 6.3). For SOF-52, the concentrations for the same replacement level with the same

cement are 4–5 times higher, although they are still below the legislation limit. For SOF-42, Mo concentrations are approximately the same for all the replacement levels, and slightly exceed the limit (1.0 mg/kg); however, it should be outlined that CEM I 42.5 N makes a significant contribution to the Mo leaching by itself.

Even though in all the samples (MCF, SOF-42, and SOF-52) antimony was present at a level exceeding the LL by 2–3 times, it was not found in any of the leachates of cement-mixtures.

Table 6.4 Relative leaching of PTEs (normalized per 1% w/w of added BA fines), mg/%. "b.d.l." denotes below the detection limit.

	Ba	**Cr**	**Cu**	**Mo**
MCF 1%	1.5	0.18	0.005	0.019
MCF 3%	0.60	0.047	0.002	0.006
MCF 5%	0.38	0.028	0.003	0.003
MCF 10%	0.31	0.004	0.002	0.002
MCF 20%	0.16	0.002	0.001	0.001
SOF-52 1%	1.1	0.23	b.d.l.	0.06
SOF-52 3%	0.57	0.097	0.003	0.029
SOF-52 5%	0.38	0.048	0.002	0.015
SOF-42 1%	0.70	0.80	b.d.l.	0.10
SOF-42 3%	0.26	0.27	b.d.l.	0.037
SOF-42 5%	0.16	0.15	0.005	0.022

Table 6.4 shows how PTEs are leaching normalized by the substitution level of MCF in the cement mixture. As can be seen, all dependences have a similar character with an abrupt drop within the 3% w/w replacement, then a gradual decrease until 10% followed with a plateau or a further slight decrease. It should be noted that even though the level of PTEs is not that high, their main source is cement, and this explains a decrease in concentrations as the share of cement in the mixture becomes smaller. However, as can be seen from Table 6.4, the values decrease much more than the share of cement (which changes from 100 to 80%), while the leaching is reduced by 60 to 100%.

Leaching of mortars containing MCF

No significant leaching of anions was detected for all mortars with a cement replacement level of up to 20% w/w after 2d of curing (chloride leaching, 40 – 100 mg/kg; sulfate leaching, 10 – 20 mg/kg), showing a high capacity of cement for chloride and sulfate binding. After 28 days of curing, the leaching of sulfate (10 – 40 mg/kg) and chloride (20 – 50 mg/kg) is even lower and in all cases well below the LLs (616 mg/kg for chloride and 2430 mg/kg for sulfate).

The leaching of PTEs in all mortars after 2 and 28 days of curing is also below the detection limits and, accordingly, below LLs. The only exception is Ba, the content of which is relatively high in the cement itself and is not caused by pollution from the BA.

6.3.3 Effect of BA fines on cement hydration (CEM I 52.5 R)

Figure 6.2-Figure 6.4 depict the effect of MCF and SOF-52 on the hydration of cement pastes. Replacements of 1, 3, and 5% w/w were used to analyze the MAC range (Figure 6.2), and 20% w/w to make detrimental effects more visible. MCF was also tested for a 10% w/w replacement. CEM I 52.5 R with 1, 3, 5, 10, and 20% w/w quartz powder replacements were used as additional references with the same water/powder ratio of 0.5.

The shapes of peaks and no extra peaks indicate that there are no side reactions associated with a higher sulfate content in BA fines compared to cement (2.83% w/w for cement vs. 5.3% w/w for MCF and 6.1% w/w for SOF-52)[174].

Figure 6.2 also shows that the cumulative heat (normalized per cement) is the highest for MCF for 1 and 5% w/w replacement for reasons unclear. A higher cumulative heat could have been expected for SOF-52 as it has the smallest particle size and could therefore be more reactive. However, it is possible that the milling and removal of the associated quenching layer releases not only more sulfate but also other components such as organic matter that might have a negative influence[64180].

For a 3% w/w replacement, the cumulative heat is almost the same, and for 10% w/w (as MCF is only compared with quartz), MCF cumulative heat is slightly higher than a 0% replacement, and almost the same as for 10% w/w quartz. Altogether, in the range of the replacement for MAC, there is no significant difference.

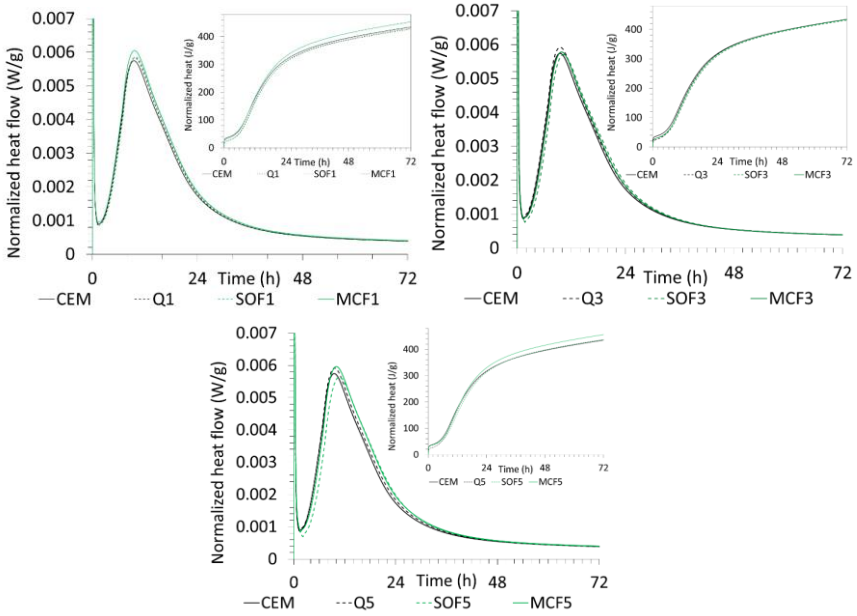

Figure 6.2 Effect of added BA fines on cement hydration (0–5% w/w replacements) normalized by the cement weight.

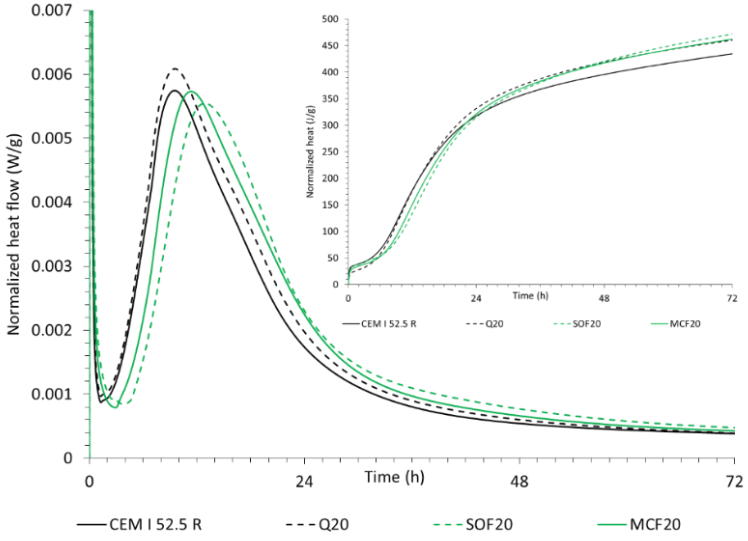

Figure 6.3 Effect of added BA fines on cement hydration (a 20% w/w replacement) normalized by the cement mass.

Figure 6.3 demonstrates more clearly the effect from BA fines on cement hydration. The addition of 20% w/w SOF-52 leads to a delay in hydration of ca. 4 h, the addition of 20% w/w MCF, ca. 2 h. The cumulative heat is almost the same for both types of fines and does not differ significantly from quartz (see Table 6.5).

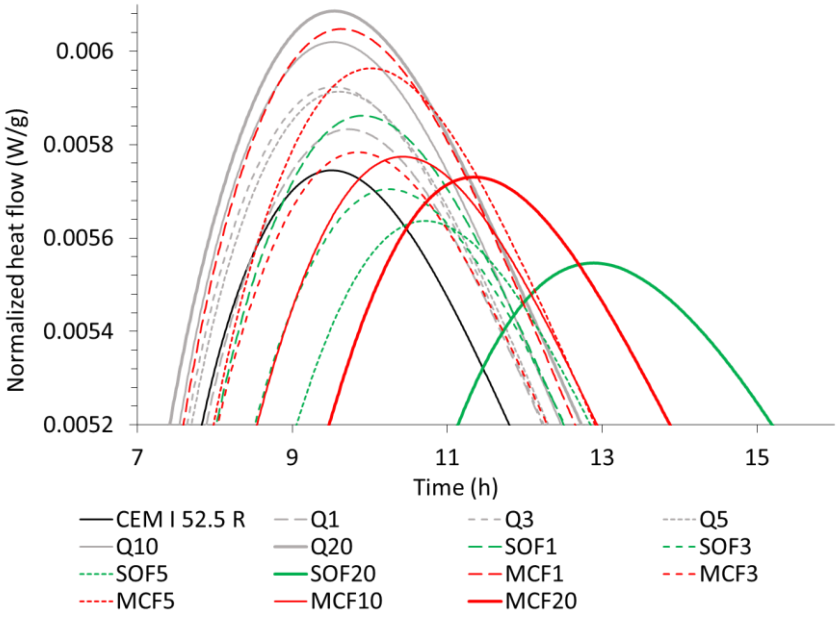

Figure 6.4 Effect of added BA fines on cement hydration (0–20% w/w replacements) normalized by the cement weight. The curves of those samples that show no significant differences compared to the reference (100% CEM 52.5) are shown as dashed lines.

Table 6.5 Total heat at 72 h for pastes containing BA fines and quartz normalized by the cement weight (J/g).

Sample / % w/w repl.	CEM 52.5	Quartz	MCF	SOF-52
0	432	-	-	-
1		425	450	428
3	-	432	431	428
5	-	434	453	433
10	-	441	443	-
20	-	457	459	468

Figure 6.3 and Figure 6.4 show that the longest delay in the hydration is observed for a 20% w/w replacement with SOF-52. This can be explained by additional sulfate (SOF-52 leaches about 13% more than MCF), and by the fact that at this replacement level the impact of other components in BA that may contributes to the delay becomes more noticeable. The leaching of SOF-52 is higher, because very fine particles are generated when the quenching layer is removed during the longer milling time[62,85]. Further delays in cement reaction are approx. 2 h for MCF (20% w/w), around 1 h for SOF-52 (5% w/w), and MCF (10% w/w), and around 30 min for SOF-52 (3% w/w). It is noteworthy that there are no significant delays observed for MCF in the MAC range. Table 6.5 shows the cumulative heat at 72 h for all the fines studied. Taking into consideration all above-mentioned data, it can be concluded that the most beneficial is the use of MCF with 1 or 5% w/w replacements.

6.3.4 Mechanical properties of MCF mortars (0–20% w/w)

The mechanical properties for mortars with a cement replacement level above the MAC range (> 5% w/w) were tested only for MCF and not for SOF-52 or SOF-42, as preliminary research showed that other properties of these fines would unlikely make them applicable in a large range of additives.

Strength development of MCF samples

In addition to the 28d strength, the early strength (2 days) was tested to ensure that the reaction delays visible with calorimetry do not have a negative influence on the strength development. As can be seen from Figure 6.5a, the 2-day compressive strength is acceptable up to a 10% w/w MCF replacement level according to the standard for CEM I 52.5 R (minimum compressive strength 30 MPa). After 28 days, only the samples with a replacement level up to 5% w/w show sufficient strength (the minimum compressive strength, 52.5 MPa).

For the flexural strength of 2-day hardened samples, a linear correlation with the replacement level is also observed (Figure 6.5b); however, at 28 days, the same general trend is visible. As it is for the compressive strength results, the harmful effect is minimal or absent only at a 1% w/w replacement level.

Additionally, it was noted that in most studies available on this topic, there is a place for some methodological changes related to testing certain replacement levels after a certain number of days of hardening. Almost none of the available papers revealed the data on mechanical properties of hardened cement products at the early stage (1–2 days), while for these terms most cements have the minimum requirements for the compressive strength[181].

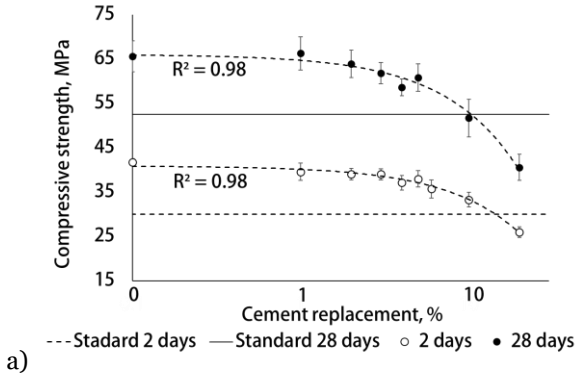

a)

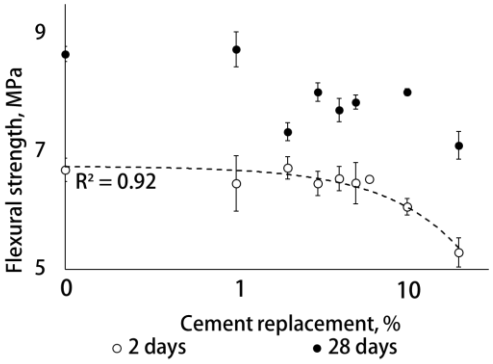

b)

Figure 6.5 Compressive (a) and flexural (b) strength of CEM I 52.5 R mortars containing MCF (from 0 to 20% w/w cement replacement). The X-axis is presented in a logarithmic scale. (n = 18, P = 0.95).

It appears beneficial if the use of any additive at any quantities would begin with testing the early compressive strength to continue the experiments only in the "working" concentration range. Figure 6.5a shows that the 2-day compressive strength is acceptable for this type of fines only within a 10% w/w replacement; after 28 days, it shifts to less than a 10% w/w replacement. It is possible that milling larger (coarser) fractions of ash would change the situation; however, this analysis suggests that with time the initial structural changes would lead to defect aggravation only. However, this issue requires further studies. Moreover, the compressive strength correlates with the replacement level, which may serve for predicting, and indicates the estimation of a potential effect of the additives on the mechanical performance.

Taking into consideration the fact that the strength analysis is made in the range of low replacement levels of fines in cement mixes, the difference between them is not expected to be significant. However, considering that one of the goals of this study is to determine the replacement level where no detectible difference with the reference sample can be observed, the insignificant difference of the absolute values will not be neglected in this case. Figure 6.6 shows the trends of the compressive strength for all the replacements (MCF) from 2 to 91 days.

At the early stage (2 days), all the replacement levels show results slightly worse than the reference. The replacement levels of 1–3% w/w show close results (a loss in compressive strength of 5–6%). By day 7, the 1% w/w sample is very close in strength to the reference; 2% w/w is slightly inferior to it (a 5% loss compared to the reference); and 3–5% w/w are still slightly lower (a 7–9% loss). By day 14, the difference between all the replacement levels becomes slightly more obvious, with 1% w/w showing even better results than the reference (a 5% gain), and 2 and 4% w/w are at the same level with it. Levels of 3 and 5% w/w have already noticeably lower compressive strength (4 and 10% losses, respectively).

By day 28 (the standard for cement), the best performing mortars are 1% w/w (a 1% gain) and the reference; 2% w/w is very close to them (a 3% loss); 3 and 5% w/w are slightly worse (6 and 7% losses, respectively); and 4% w/w shows the lowest strength (a 11% loss). By day 91, the best results are for the reference and 2% w/w (a 1% loss); 1% w/w is slightly worse (a 4% loss); and 3–5% w/w are approximately at the same level (a 7–8% loss). The apparent absence of changes from 28 to 91 days for the level of 1% w/w can be attributed to the experimental error (which can be within 10% according to the testing standard[39]), which almost does not go beyond the range of differences for all the replacement levels in this case.

6.3.5 Mechanical properties of the size optimized fines SOF-52 and SOF-42

The performance of various replacement levels of three types of BA fines (MCF, SOF-52, and SOF-42) was assessed in the MAC range (0–5% w/w). In the following subsections, two types (SOF-52, and SOF-42) are discussed separately, and MCF is compared with SOF-52 (as they were tested with the same cement type).

Because one of the objectives of this study was to find out whether the BA milling towards the particle size of the relevant cement beneficially affects the quality of fines as MAC, two types of fines with an increased milling time (SOF-52 and SOF-42) with two types of cement, which are similar in composition but

differ in PSD were compared. The goal here was to determine whether the mortars containing these fines vary in trends for mechanical performance with the changing cement reactivity.

Compressive strength (SOF-52)

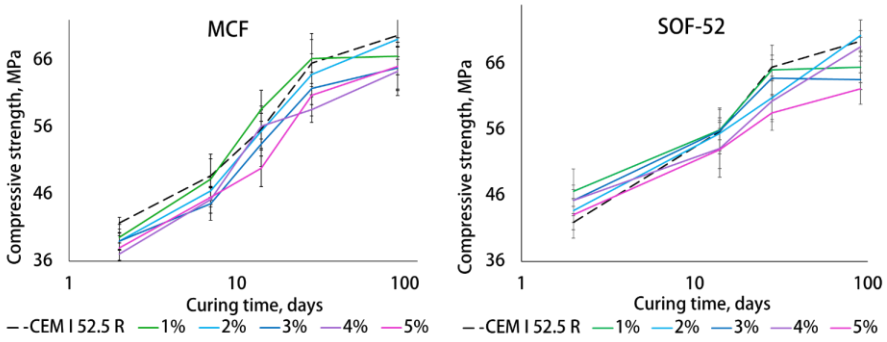

Figure 6.6 Compressive strength of mortars (CEM I 52.5 R) containing MCF (right), and SOF-52 (left) (0–5% w/w cement replacements); the data on the 5% w/w replacement solely can be found in Chapter 5.

Figure 6.6 shows the increasing trends of the compressive strength for all the replacement levels (SOF-52) from 2 to 91 days. Unlike for MCF, for SOF-52, at the early stage (2 days), all the replacement levels show a slightly higher compressive strength than the reference. Levels of 1, 3, and 4% w/w show similar maximum gains (8–11%). However, by day 14, levels 0–3% w/w almost do not differ (no gain or loss), while 4–5% w/w are noticeably worse (a 5% loss).

By day 28 (the standard for cement), the best performing mortars were 1% w/w (a 1% loss), 3% w/w (a 3% loss), and the reference. Slightly lower, with close values are 2 (a 7% loss) and 4% w/w (an 8% loss) and the level of 5% w/w showed the lowest compressive strength (a 11% loss). By day 91, the highest compressive strength is observed for the reference, 2, and 4% w/w (a 1% gain and a 1% loss, respectively). Levels of 1 and 3% w/w are slightly worse (6 and 8% losses). As in the previous case of MCF, only for 2% w/w the strength change between 28 and 91 days is not observed, while 5% w/w has the worst performance (a 10% loss). As it was discussed above, stagnation in the latter tested period of hydration can be attributed to the experimental error.

Compressive strength (SOF-42)

In the case of less reactive CEM I 42.5 N cement (Figure 6.7), the outcome is slightly different from the previous cases, although the general trends are similar. Unlike MCF and SOF-52, after 2 days of curing, replacement levels of 1–2% w/w show a compressive strength slightly higher than the reference (3 and 9% gains, respectively), while 3–5% w/w show significantly lower strength (a 13–21% loss in strength). However, after 14d curing, all replacement levels show worse performance in comparison with the reference, while levels of 1–2% w/w have a very similar strength (4 and 6% losses, respectively), and 3–5% w/w are slightly lower (a 10–13% loss).

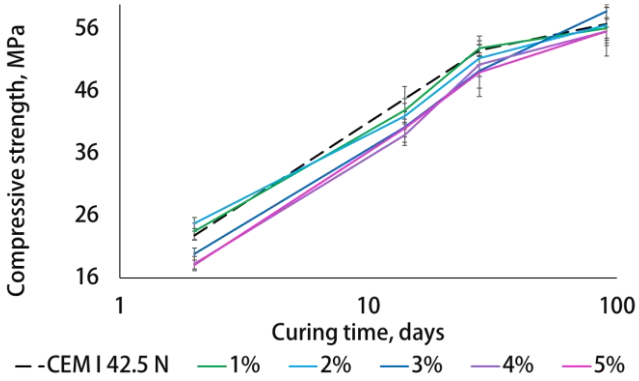

Figure 6.7 Compressive strength of mortars (CEM I 42.5 N) containing SOF-42 from 0 to 5% w/w cement replacement.

By day 28 (the standard for cement), the strength for the level of 1% w/w and the reference are almost the same (a 1% gain). They are followed by 2% w/w (a 2% loss), then 4% w/w (a 4% loss), and 3% w/w (a 6% loss); the level of 5% w/w shows the lowest compressive strength (a 7% loss). By day 91, almost all the replacement levels show the same strength, with 3% w/w being slightly above the reference (a 4% gain), and all the rest are statistically indistinguishable (a 0–2% loss). In this case, the stagnation is not observed for any replacement level for the period from 28 to 91 days. It is noteworthy that in the long-term perspective, the addition of this type of fines appears to be beneficial. This can be explained by the fact that a higher level of hydration is reached later for this cement than CEM I 52.5 R, it can be assumed that BA fines are incorporated into the cement matrix better, while with CEM I 52.5 R, with the ill-incorporated ash particles into the matrix, the negative effect of this phenomenon will become more noticeable over time.

Comparison of mechanical performance between MCF and SOF-52

Figure 6.8 shows the final mechanical performance result comparison of the two types of fines, MCF and SOF-52. As can be seen, at the early stage (2 days) for all the replacement levels, these fines show better results than MCF and the reference. By day 14, the same result is already observed only for 3 and 5% w/w, and for 2% w/w the results are roughly the same for both types of fines. By day 28, SOF-52 is still better at 3 and 4% w/w replacements. For 91 days, this is also true for 2 and 4% w/w. The general conclusion is that only with a replacement level of 1% w/w, a significant effect of fines on the final cement product properties is not observed. However, 2–3% w/w replacement levels also do not seem to pose a threat. The replacement levels of 4–5% w/w lead to a decrease in strength (28 days) by 8–10%, which is also not critical because that is within the allowed measurement error range of 10% but is no longer negligibly small. Taking into consideration that the preparation of SOF-52 requires additional time and energy costs, their use does not seem to be justified.

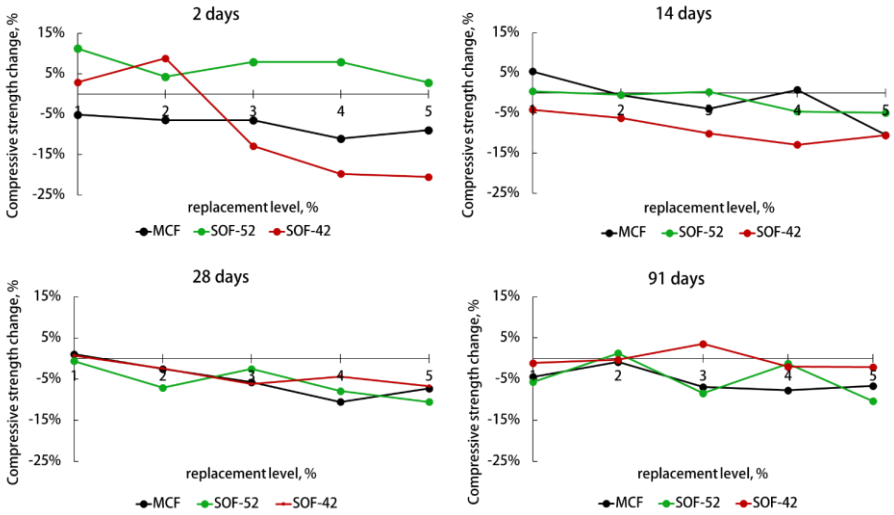

Figure 6.8 The compressive strength change in CEM I 52.5 R mortars containing MCF and SOF-52 (from 0 to 5% w/w cement replacements) relative to the corresponding reference.

6.3.6 Microstructural analysis of pastes containing BA fines

To gain more insight into the behavior of MCF on the cement microstructure, optical microscopy was used on cement pastes with different MCF replacement levels. Figure 6.9 shows the microstructure of a cement paste containing 0 (top)

and 20% w/w MCF (bottom) after 7 days of hydration. Each original image was segmented into 3 parts (porosity, reaction product, and unreacted cement/MCF) based on grey values using ImageJ software. Further, the lightest part (unhydrated cement or BA particles) was shown in red, the light-gray part (hydration products) in white, and the darkest areas (porosity) in black. This allows the quantification (area, %) of porosity and the general reaction degree of the sample and may give some insight into a decrease in the mechanical performance of mortars containing BA fines. Table 6.6 sums up the results.

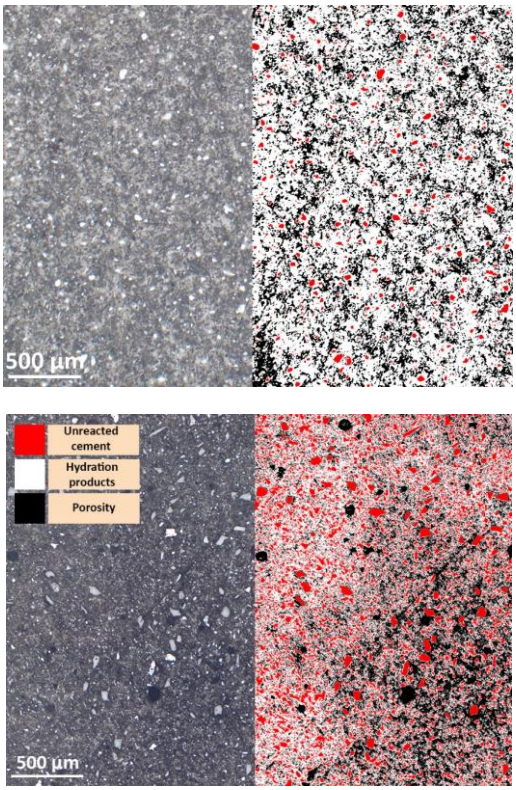

Figure 6.9 Microscopic photographs of pastes (a) 100% CEM I 52.5 R (b) 20% of MCF + 80% w/w of CEM I 52.5 R (7 days of hydration). The original photographs (left images) were segmented into 3 areas unhydrated cement or BA particles are marked red; white are hydration products; and black is pores.

Figure 6.9 and Table 6.6 reveal that an increase in the share of BA fines is accompanied with a significant increase in the porosity of the cement mixture. However, there is no linear dependence due to packing effects; and for the 5% w/w replacement level, the porosity is even slightly reduced. It also should be

considered that optical microscopy only detects porosity in the micrometer range. Nano-porosity that is a common C-S-H gel cannot be detected. But the heterogeneity of the hardened paste increases with the share of BA fines, and the material becomes extremely heterogeneous at a 20% w/w replacement (Figure 6.9). Table 6.6 shows that at all the replacement levels, the share of unreacted cement/MCF particles remains the same.

Table 6.6 Distribution of differently hydrated products in cement pastes (7 days hydration), containing 0–20% w/w cement replacement with MCF; On each photograph, 5 representative areas were selected and analyzed by ImageJ, the results were averaged (n = 5, P = 0.95).

% w/w MCF	Non-hydrated or BA	Reaction products	Porosity
	%		
0	3.5 ± 0.8	78 ± 4	18 ± 4
1	2.5 ± 0.2	79 ± 2	19 ± 2
5	6 ± 2	82 ± 4	12 ± 3
20	3 ± 1	60 ± 20	40 ± 20

Based on Table 6.6 data, the hardened paste structure of the reference and a sample containing 1% w/w MCF almost does not differ, neither in composition nor in homogeneity. The only difference is a slightly lower share of unhydrated cement, which can be explained by the fact that in the ash–cement mixture the water: cement ratio becomes slightly higher (as the water: powder ratio remains the same). This is confirmed by the mechanical performance (Section 6.3.4) and calorimetric data (Section 6.3.3). Even though for a 5% w/w replacement, the hydration product share increases, and the part of the porous zone diminishes, the heterogeneity of the mixture noticeably increases in comparison with the reference, which may cause the reduction in strength.

6.4 Conclusions

Three types of milled BA fines were compared on their performance in pastes and mortars to identify 1) the most suitable cement replacement level to be used as a MAC, the addition of which does not cause visible detrimental effects in the final products (mortars); 2) the maximum level of replacement by fines which would pass the cement requirements; 3) weather the approximation of the BA fine powder to the size of cement has a positive effect on the mechanical performance of mortars. Environmental properties of all types of BA fines as well as handling

a potential risk related to the leaching of dry cement–BA mixtures are discussed. The tested BA fines are three derivatives from a fraction of "coarse" BA fines (0.125–3 mm): MCF (the coarse fraction milled to the size below 125 μm); SOF-42 (MCF milled to approximate the particle size of CEM I 42.5 N); and SOF-52 (MCF milled to approximate the particle size of CEM I 52.5 R). The main results can be summarized as the following:

- The leachate analysis of hardened pastes (2 and 28 days) showed no cases when the legislation limit was exceeded; most elements were at a concentration level below the detection limit.
- Calorimetry showed that the detrimental effects are observed only with a large MCF share in the mixtures (> 10%, a noticeable hydration delay); while for SOF-52 this was observed already at a 5% w/w replacement. The smallest changes or beneficial effects were seen for MCF 1% and 5% w/w.
- Even though for some replacement levels, the compressive strength for SOF-52 appears to be better than for MCF (4% w/w, 28 and 91 days of hydration, and 3% w/w but only for 28 days), the reduction in this parameter is still greater for a 4% w/w replacement (about 8%) compared with 1% w/w MCF (an 1% increase in strength). The fact that the treatment of the material in the case of SOF-52 is more intense should be also considered.
- All investigated BA fines are satisfactory with respect to mechanical performance with a reduction in compression strength within 10% (28 days). However, the best results were for MCF 1% w/w with almost no change in the mechanical performance.
- Microstructural analysis of pastes containing MCF showed that on a significant increase in their share, the material porosity and heterogeneity increase significantly, which may deteriorate the mechanical properties of mortars containing BA fines.
- SOF-42, which was used only for the comparison of mechanical performance trends with a different type of cement (similar composition but less reactive), showed good results in the final stages of hardening, where 1–5% w/w replacements almost do not differ from the reference; compressive strength 98–104% of the reference at 91 days; 93–101%, at 28 days; 87–96%, at 14 days; and 80–109%, at 2 days. This might be because CEM I 52.5 R is finer and, therefore, more reactive than CEM I 42.5 N; any additional reactions or interactions would result in a more noticeable (harmful for the strength properties) effect. Therefore, it is necessary to study this phenomenon further.

In this chapter, a methodological feature was stated. It is proposed to use data on the mechanical performance at the early stage of hydration (2 days), which

significantly shortens further tests as well as the use of the material, because the failure to satisfy these conditions will be critical for using any material as a MAC.

The whole findings suggest that the MCF fraction “as is” (mildly milled BA fines) appears to be most suitable for a MAC application. Further milling to produce SOF-52 does not seem to be beneficial from the standpoint of the compressive strength results. This is positive as less energy and effort are required to produce this fraction.

The optimum replacement level where no changes are observed is 1% w/w. However, a 2–5% w/w replacement also provides good results passing the cement requirements. Various properties suggest that all types of fines might be considered as potential MACs; however, milled coarse fines look most attractive from two aspects: (i) its effect on the cement hydration and, therefore, mechanical properties and (ii) their low environmental impact.

CHAPTER 7

The connection between MSWI BA leaching and the quenching layer: empirical leaching model

This chapter has been submitted for journal publication:

E. Loginova[1*], K. Schollbach[1], M. Proskurnin,[2] H.J.H. Brouwers[1], The connection between MSWI BA leaching and the quenching layer: empirical leaching model (2022).

7.1 Introduction

Municipal Solid Waste Incineration Bottom Ash (BA) is one of the by-products of the incineration process to reduce the volume and mass of household waste[4]. In the last three decades, extensive research has dealt with various aspects of BA analysis, characterization, treatments, and applications. Specifically, numerous studies have focused on the leaching behavior of PTEs, factors affecting it, and approaches to mitigating it[101,103,182,183]. In addition, quite a few studies have focused on the physical, chemical, mineralogical, and morphological properties of BA[41,54,184,185]. Over the years, many treatments have been suggested to minimize the adverse effects of this material if it is recycled as aggregate, a road base material (coarse fraction) or cement replacement (fine fraction), such as thermal treatment, metal extraction to reduce the leaching, particle size separation, carbonation, etc[15,21,63,186–188].

It is challenging to reuse not only the coarse fractions of BA but also the fine fractions, which are, in comparison, more contaminated though can have potential as a cement replacement (Chapter 5). At the same time, PTE leaching remains one of the most acute challenges because of the high cost of treatments such as washing or sintering and the sometimes-limited effectiveness[62,189].

BA is highly inhomogeneous, consisting of various types of matter, including rocks, glass, metal, unburned organic matter, incineration, and weathering products[54]. The composition of the incineration product is affected by the starting composition of the household waste, the incineration conditions, and the cooling process. Most commonly the hot BA is cooled down by quenching water after the incineration. Many changes occur to BA during this procedure due to dissolution, precipitation, and the reaction of salts and minerals and their reabsorption by newly forming structures[54]. The quenching process results in a somewhat unstable quenching layer, encapsulating PTEs, salts from the quench water, and ash particles formed during incineration. Thus, quenched BA particles above a size of ~250 μm typically contain a solid core covered with this quenching layer with fine particles interspersed with newly formed hydrates[45,62]. BA particles below that size tend to consist primarily of this quenching layer (as large particles barely participate in the formation of the quench products). This means the finer the fraction, the more contaminated it is.

Several Ca-based minerals are formed only at the quenching stage, which can incorporate and immobilize PTEs. The literature mainly focuses on the behavior of chloride in this layer, as it tends to be the element leaching at the highest concentrations. Only limited information is available about other elements such as Cu, Zn, Ni, Cr, Sb, etc) (Chapter 3)[165,190]. One mineral crucial for chloride

immobilization is Friedel's salt, $3CaO{\cdot}Al_2O_3{\cdot}CaCl_2{\cdot}10H_2O$, which only forms during quenching and cannot be removed easily (even by thermal treatment at 1000 °C)[191]. It is considered the primary host of the insoluble Cl in BA. Yang et al. also demonstrated that the quench products are the primary source of chloride leaching in BA, resulting from the entrapment of tiny particles rich in Cl during the layer formation, found by SEM-EDX mapping analysis[191]. Inkaew et al. reproduced the quenching process under laboratory conditions to investigate its formation in-depth[85]. They showed that BA changes dramatically after the quenching due to the formation of amorphous and microcrystalline CSH phases and that the formation of the quenching layer is governed by the presence of fine particles (< 425 μm). Due to their chemical composition, those particles aid the formation of the quenching layer, and if separated from the coarser fraction before the quenching procedure, almost no layer is formed. They also found that the quenching layer is approx. 0.01–1 mm thick (for particles of a size of 2 to 4 mm)[85]. Additionally, quenching water raised some concern as an apparent secondary origin of chloride in BA[192].

It was discovered that slow milling performed on the BA fraction 0.125 – 3 mm, reduced the surface area of the grains by removing the quenching layer, while simultaneously increasing the leaching of the material (Chapter 5). This suggests that the quenching layer might be responsible for leaching from this material to a great extent and should be studied further to understand its influence. It might also be a key to estimating the leaching potential of BA and optimizing treatments that reduce leaching, such as grinding or washing.

One approach to study the influence of the quenching layer is modeling based on the analytical data. The existing data on the modeling of MSWI residue fractional composition and environmental impact, including BA, are numerous[56,59,124,193–196]. However, they are mainly focused on either the environmental impact related to the incineration process itself[197,198] or on how the leaching of hazardous metals is affected by pH during long term aging (weathering, carbonation, etc.)[199,200]. A great deal of research is based on chemical-equilibria models[101,201,202] or geological models[56,194–196].

In Chapter 3, S-shaped leaching patterns were obtained for multiple elements, yet the leaching data did not correlate with the SSA, or the particle size. There was also no correlation found between the total content of the element in the BA and its leachable amount. Because the pH of the studied leachates varied only within 8.8 – 9.2 interval, this parameter also could not explain the difference in the leaching among different particle-size fractions.

Park and Batchelor proposed a multi-component numerical leaching model and showed its potential to improve or substitute for a standard leaching test[203]. Also, Dijkstra et al. used a pH-dependent computer model to predict the PTE leaching from BA with an accuracy of approximately an order of magnitude[204]. Later, another multi-surface geochemical model was developed to predict the simultaneous leaching of a wide range of elements from BA[205]. However, these models did not pursue a goal of demonstrating the adverse effects of the quenching layer, and generally require in depth knowledge about the mineralogy of BA that is very complex and hard to determine. They are therefore hard to use in practice to estimate leaching behavior.

In this chapter, a semi-empirical leaching model is proposed to demonstrate the viability of the hypothesis that this quenching layer is greatly responsible for the leaching of certain elements (Chapter 5) and can be used to estimate the leaching of BA for these elements. The advantage of this model in comparison with previously suggested ones is its simplicity and potential as either a fast predictor of the leaching behavior of an entire BA batch (if differently processed, incinerated, or washed) or the estimation of the effectiveness of any treatments applied to reduce the leaching. Additionally, this model considers the particle size of the BA when predicting the leaching behavior.

The model is based on two sets of the leaching data of 18 BA particle size fractions: one for building the model and another one for validating it. Unlike previously developed models[203,204], this approach is based on the leaching data for the most contaminated fine fraction (< 63 μm) and the least contaminated large fraction (>22.4 mm) of the BA, which is then applied to the entire particle size range (18 fractions). The leaching data from the largest fraction is used as a "reference" or a background level of BA leaching, that is not or only very minorly affected by the quenching layer. At the same time, the finest fraction, mainly consisting of the quench product, represents the leaching of the quenching layer itself. The primary assumption of the model is that a BA grain consists of a core and a quenching layer with a certain thickness. The leachabilities of the quenching layer and the core are based on the smallest and largest BA fraction (determined with the one batch leaching test), and then the amount of quenching layer and leachability were calculated for each fraction. The calculated (modelled) values for the entire particle size range correlate well with the empirically obtained leaching data for certain elements (Na, K, SO_4^{2-}, Cl^-, Ca, Mg, Sr, Cu, Zn) indicating that this modelling approach could be a fast and simple method to determine the leaching potential of BA.

7.2 Materials and methods

The general materials and methods are discussed in Chapter 2. Here, specific details and/or unique for the chapter procedures are presented.

The untreated (unwashed) but water quenched and weathered BA was supplied by Mineralz (the Netherlands), two different batches were used. 3 replicas were used for each leaching test in the study (particle size range 0 – 22.4 mm, 15 kg each set).

7.2.1 Procedures

Sample preparation and analysis

The analyzed BA samples were initially pre-crushed at the plant to remove cemented matter and metals. Further, the material was oven-dried (105 °C; a UF 260 drying oven, Memmert) to a constant mass. Next, each set was sieved into 18 size fractions according to EN 933-1 (2012) and EN 933-2 (1995) with the additional sieves with the following mesh sizes: 22.4 mm, 11.2 mm, 5.6 mm, 2.8 mm, 1.4 mm, 710 μm, 355 μm, 180 μm, and 90 μm to obtain a better specification within the general BA fraction. Each fraction of both sets was divided with sample splitters (15-D0438 riffle boxes, CONTROLS Group) into 4 parts, 3 of which were used for the standard leaching test [127], 24 h shaking, L/S 10, 200 rpm on an SM-30 shaking table (Edmund Bühler GmbH). After the test, the leachates were filtered through 0.2-μm filters to prepare solutions for IC and ICP–AES (for the latter, filtrates were stabilized with nitric acid). Further ICP-AES analyses were performed by an ICP–OES 5100 SVDV spectrometer (Agilent Technologies); IC analysis by a Thermo Scientific Dionex ion chromatograph 1100. Specific densities of dried samples were measured by a Helium pycnometer (AccuPyc II 1340).

Density and pH

The density did not vary significantly throughout the particle size range of the studied BA, but generally it cannot be assumed that unprocessed BA fractions would always have the same density due to differences in the treatment during and after the incineration. In fact, lower temperatures and incineration time might leave a higher degree of unburnt organic matter, or metal extraction can be more or less effective at different plants, therefore, it might be considered as an additional step to include the density correction in the calculations.

Table 7.1 Median particle size and specific density for each sieve fraction as well as the pH of the leachate after the standard leaching test[127].

	µm											mm									
Sieve size	63	90	125	180	250	355	500	710	1000	1.4	2	2.8	4	5.6	8	11.2	22.4	31			
Med. Part. size	31	77	108	153	215	302	427	605	855	1.2	1.7	2.4	3.4	4.8	6.8	9.6	16.8	22.4			
Sp. Dens. (g/cm³)	2.6	2.6	2.7	2.7	2.7	2.7	2.7	2.7	2.8	2.9	2.8	2.9	2.8	2.8	2.7	2.7	2.8	2.9			
pH	8.9	8.9	8.8	8.8	8.8	8.8	8.8	8.9	8.9	9.1	9.1	9.0	9.2	9.1	9.1	9.1	9.1	9.2			

7.3 Results

7.3.1 Model concept and assumptions

Specific leaching patterns (S-shaped curves with the maximum for the finest fraction and the minimum for the largest for most elements and anions, see Figure 7.2) throughout the particle size range were observed previously (Chapter 3). It was shown that the leaching curves throughout the fraction range for many elements are similar in shape, yet no correlation was observed with either particle size or surface area[43,87,165].

Additionally, it was observed that slow milling led to a decrease in surface are but an increase in leaching, due to the breakup and removal of the quenching layer from the larger grains. Therefore, it can be assumed that surface area alone is not a suitable predictor for leachability (Chapter 5).

Therefore, the concept of the proposed model is to incorporate the leaching data from the entire particle size-fraction range to estimate the influence of the quenching layer in PTE leaching. Figure 7.1 shows the abstraction made from real particles of BA to the model ones and the main assumptions made in the model.

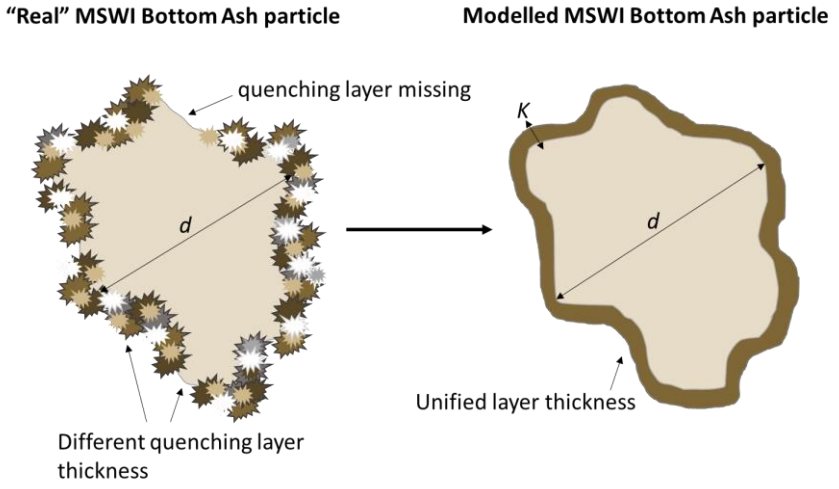

Figure 7.1 Schematic representation of a BA particle, "real" (left), modelled (right). K represents an equal thickness of the quenching layer for all BA particles throughout the fractions for modelling.

The model assumes that all particles, regardless their size, have a quenching layer of equal thickness. A range of values is provided by the literature[85]. The particles of a size fraction are assigned an average size which is the arithmetic

mean of minimum and maximum size of such fraction. Every size fraction has a specific range (e.g., a fraction named «180 μm» has a range from 125 to 180 μm), and therefore the arithmetic mean is 152.5 μm. The model is based on the idea that leaching occurs primarily from a quenching layer of a certain thickness, but also the potential leaching provided by the core is considered.

7.3.2 Leaching estimation

The leaching of the finest fraction (< 63 μm) was taken as representative for the leaching of the quenching layer, because it can be assumed to consist mostly of broken-off quench product. The largest fraction is the least affected by the presence of the quench products and therefore its leaching value was used as the background leaching of the core material.

Further, two numbers are necessary to calculate the final modelled leaching value ($M_{quench\ total}$): ratios of $R_{quench} = V_{quench} / V_{part}$ and $R_{core} = V_{core} / V_{part}$ for each fraction. As core particle and the whole particle have similar shapes, it follows that

$$R_{quench} = 1 - \sqrt[3]{\frac{r-K}{r}} \tag{7.1}$$

and

$$R_{core} = \sqrt[3]{\frac{r-K}{r}} \tag{7.2}$$

where r is half the particle size (a characteristic size) and K the quenching layer thickness. Further each R_{quench} was normalized to the R_{quench} of the finest fraction, and the same was done to R_{core} but to the R_{core} of the largest fraction. This way, the range of values was obtained for each fractions indicating how the amount of the quenching layer and the core changing depending on the particle size. Because the ratio between the leaching volume and the core decreases with increasing particle size, the leaching of the largest fraction is lowest. The model applies the ratios of the quench part (leaching of the most contaminated fine fraction) and the core (leaching of the least contaminated coarse fraction) to the overall volume of the particle for each fraction. The model predicts the leaching value of a target fraction (semi-empirical prediction) according to:

$$M_{frX} = R_{quench.norm} \times L_{finest} + R_{core.norm} \times L_{largest} \tag{7.3}$$

Here, M_{frX} is the leaching value for the target fraction; L_{finest} and $L_{largest}$ are leaching values of the finest and the largest fractions, respectively, determined experimentally. The density of the core and the quenching layers might differ

slightly, yet the data on the specific density indicates that the difference is insignificant, therefore the same density for the core and the quenching layer is used in this model.

For each element in this study, M_{frX} was calculated for each fraction to obtain the range of "modelled" leaching values, altogether for each element they were portrayed as a curve and compared to the values from the experimental sets.

K, the model layer thickness, is established by fitting the layer thickness to the empirically obtained leaching values. The result is 20 µm, which gives the best fit for all elements and which is subsequently used for the second data set. The values for the quenching layer thickness suggested by the literature are 0.01 – 100 µm[85], which agrees well with the results of the present model.

7.3.3 Experimental and calculated leaching curves

Two sets of the leaching data for different particle size fractions are presented (sieve size: 63, 90, 125, 180, 250, 355, 500, 710 µm, and 1, 1.4, 2, 2.8, 4, 5.6, 8, 11.2, 22.4 mm), one of which was used to create the model, and the other one was used to validate it.

The main objective of this study was to demonstrate the effect of the quenching layer on the short-term leaching (24 h shaking) through the entire range of fractions. Thus, the calculation given in Eq. (7.3) was made for the entire set of elements for each fraction. The leaching behavior of chloride and sulfate, Na, Mg, Ca, Sr, Ba, Cu, Mn, Ni, Zn, and Sb were considered typical elements present in BA. Co, Cr, Pb, Sn, Ti, and V were not considered as they are accumulated mainly in fly ash[206,207]. Fe, Al, and Si were also disregarded, as they do not leach significantly from BA. For validation, the model was tested with another set of data for a second batch of BA.

Figure 7.2 illustrates the graphical model representation including calculated data points. Figure 7.3–Figure 7.8 present the graphical representation of the leaching results from data set 1 and 2 and the modelling results. The leaching curve shape of most of the selected elements agrees well with the existing data[81,95]. The model shows a good fit for chloride, sulfate, Na^+, K^+, Ca^{2+}, Mg^{2+}, Sr^{2+} (Figure 7.4 and Figure 7.6), overestimated values for Ba^{2+}, Zn^{2+} and Sb^{2+}, underestimated values for Cu^{2+} (Figure 7.7 - Figure 7.8), and no fit for Mn^{2+} and Ni^{2+} (Figure 7.5).

Table 7.2 presents the coefficient of correlation of the model curves, sums of RSDs for each curve (element/ion), and overall, the leaching errors, to objectively assess the quality provided by the model describing the leaching behavior of a particular element. It was calculated by obtaining the RSDs for all the data points

of the 2 curves (sets 1 and 2), and then summing them up for one element. The dependences of the errors for modelled values on the particle size are given in the Appendix C, Figure C.1.

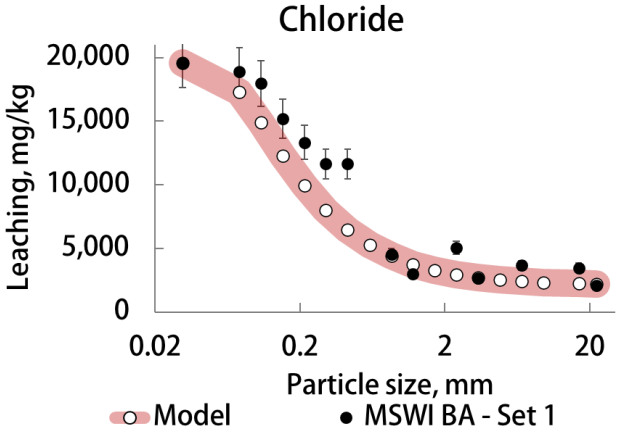

Figure 7.2 Example of the modeled and measured leaching values. The error bars are the standard deviation as each measurement was done in triplicate.

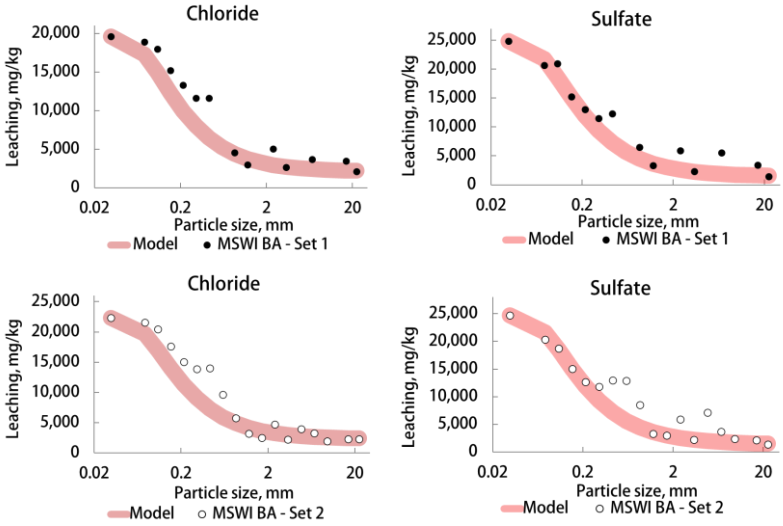

Figure 7.3 The graphical model representation for chloride and sulfate. Set 1 is the experimental set and Set 2 is the validation set. The black and white data points are the measured leaching values for all fractions; the colored curves are the calculated leaching values based on the model.

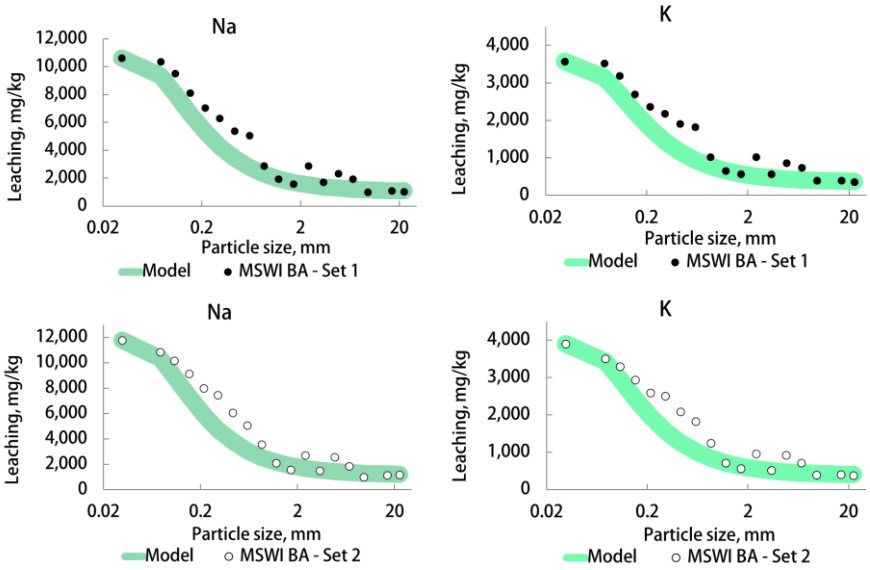

Figure 7.4 The graphical model representation for Na and K; Set 1 is the experimental set, Set 2 is the validation set.

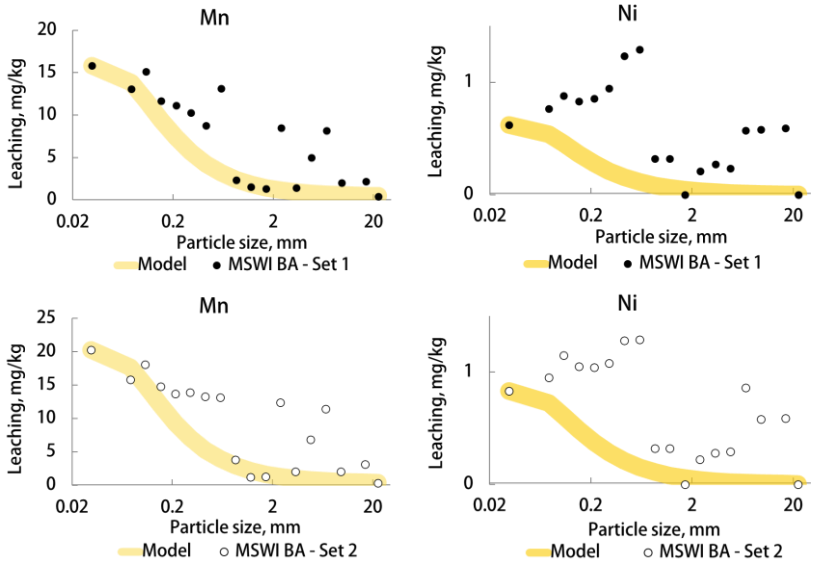

Figure 7.5 The graphical model representation for Mn and Ni, Set 1 is the experimental set, Set 2 is the validation set.

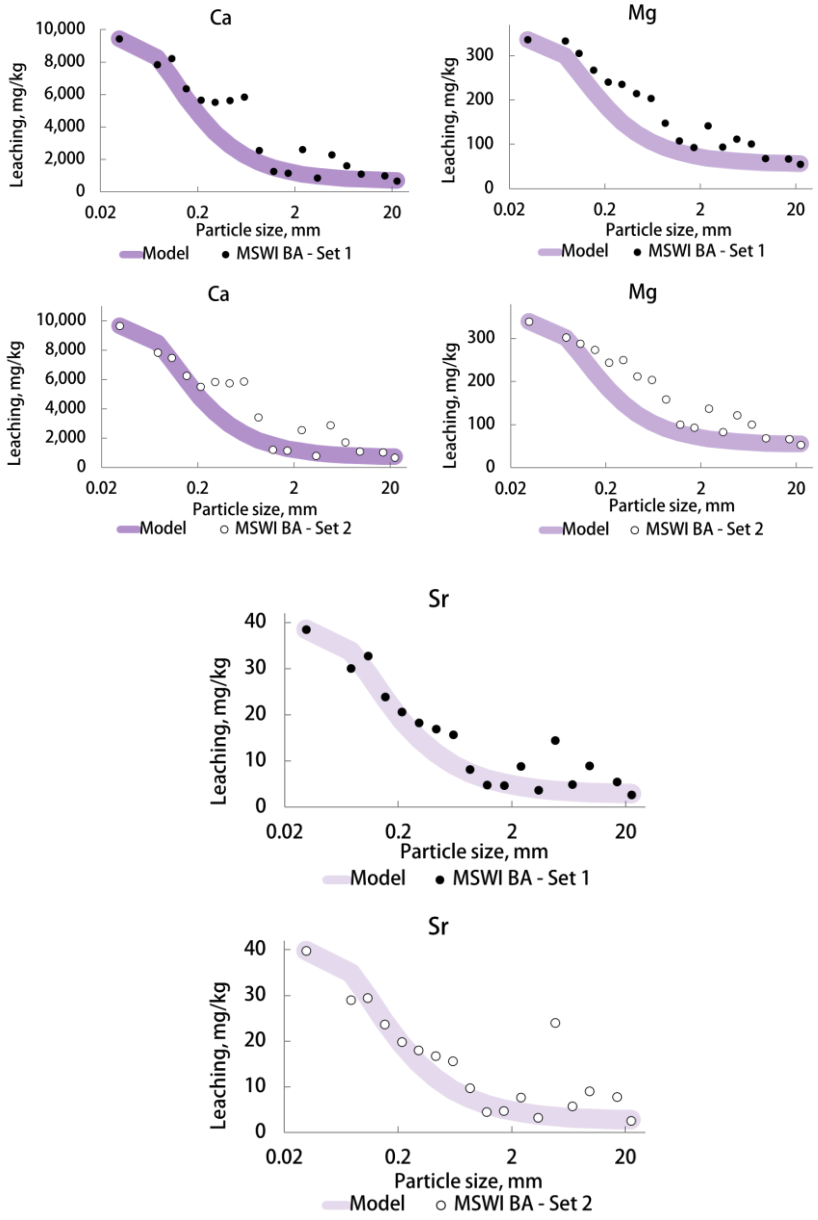

Figure 7.6 The graphical model representation for Ca, Mg, and Sr, Set 1 is the experimental set, Set 2 is the validation set.

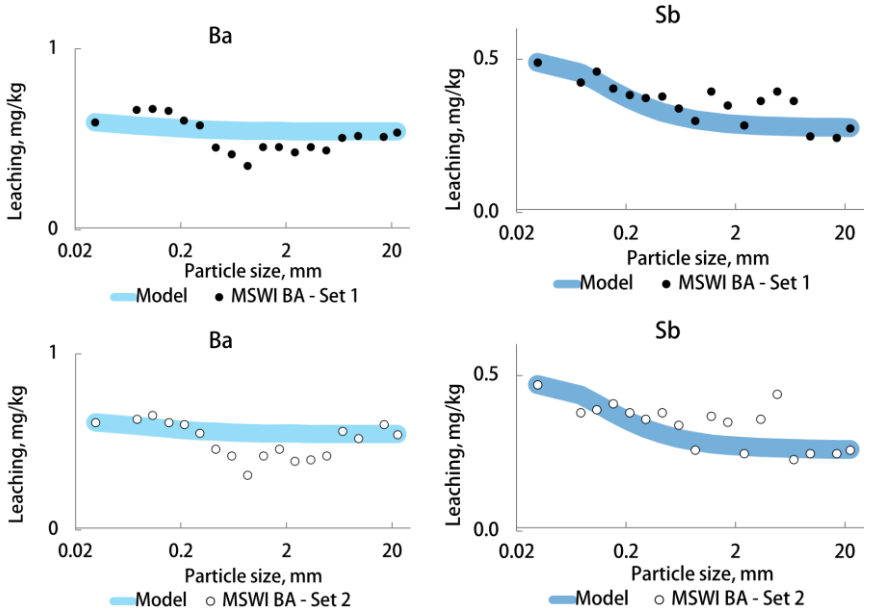

Figure 7.7 The graphical model representation for Ba and Sb, Set 1 is the experimental set, Set 2 is the validation set.

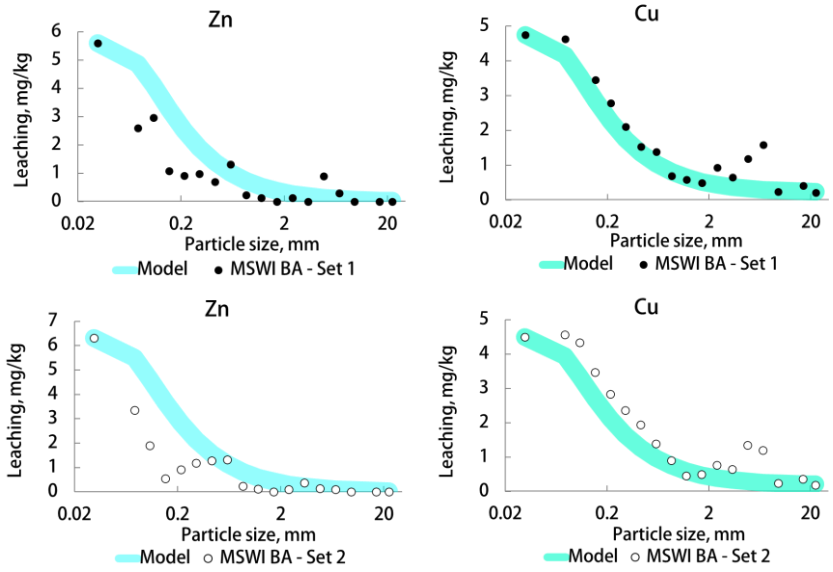

Figure 7.8 The graphical model representation for Zn and Cu, Set 1 is the experimental set, Set 2 is the validation set.

To assess the model accuracy for each element, the sum of the RSDs was calculated for the data points (pairs) for all particle size fractions, obtained in the experiment, and modelled.

Table 7.2 Accuracy of the leaching model including the sum of RSD for all data points, and *R* (correlation coefficient between the model and the empirical set) are given for each element.

Element	Calculation set			Validation set		
	R	The sum of RSD for all fractions	Total estimation error,%	R	The sum of RSD for all fractions	Total estimation error,%
Sodium	0.98	0.93	-13.3%	0.98	0.90	-11.2%
Potassium	0.98	1.07	-15.1%	0.97	0.97	-12.7%
Sulfate	0.98	1.23	-8.3%	0.95	1.88	-13.8%
Chloride	0.97	0.90	-15.3%	0.97	1.35	-10.5%
Magnesium	0.96	1.16	-17.0%	0.95	1.30	-16.8%
Strontium	0.96	1.90	-10.4%	0.89	2.50	-11.5%
Copper	0.96	2.07	-16.8%	0.97	2.40	-23.0%
Calcium	0.94	1.88	-17.0%	0.93	2.22	-16.3%
Zinc	0.89	33.59	54.6%	0.86	74.22	73.9%
Manganese	0.82	4.78	-35.6%	0.81	6.60	-37.1%
Antimony	0.80	0.28	-1.8%	0.65	0.39	1.9%
Barium	0.73	2.46	29.7%	0.56	3.65	33.2%
Nickel	0.39	9.68	-71.4%	0.58	9.00	-66.2%

7.4 Discussion

Table 7.2 shows the overall coefficient of correlation and the total relative residual sum of errors; based on this data, all the considered elements in BA can be separated into three groups. The first group shows a good fit and low total errors (10 – 20%). It is comprised of anions (chloride and sulfate), alkali metals (Na^+ and K^+), and alkaline-earth elements (Mg^{2+}, Ca^{2+}, and Sr^{2+}) as well as Cu^{2+}. The second group unites elements with a good fit and more significant total error (approx. 30%): Ba^{2+}, Zn^{2+}, Sb^{2+}. Finally, the third group of Mn^{2+} and Ni^{2+} shows lower coefficients of correlation and/or significant total errors (>50%). Considering the complex nature of the BA, multiple factors, which play a role in the leaching of a specific element, and simplification of the BA provided by the model, the scale of errors appears to be satisfactory.

7.4.1 Elements with the leaching behavior described well by the model / Cl^-, SO_4^{2-}, Na^+, K^+, Mg^{2+}, Ca^{2+}, Sr^{2+}, and Cu^{2+}

Chloride

As shown in Figure 7.3, a slight underestimation in the 0.3 – 0.5 mm range is noticeable (Appendix C, Figure C.1). A similar outcome can be observed for the validation set. The coefficient of correlation for the experimental set (Set 1) is 0.97, and the validation set (Set 2) is the same. The RSD sum for the Set 1 is 0.9 and for the Set 2 is 1.35, thus underestimating the total leaching of the entire range by about 15% for the Set 1 and 10% for the Set 2. For chloride, most fractions are estimated fairly accurately by the model (RSD < 0.1 for most of the fractions), the most deviating fraction is 355 – 500 μm with a RSD of 0.17. For the Set 2, the least accurately described fraction is 1.4 – 2 mm with an RSD of 0.34.

Sulfate

The sulfate leaching is also underestimated for several fractions. For the validation set, the result is similar, but underestimation is observed for more points. The coefficient of correlation for the Set 1 is 0.98, and for the Set 2 is 0.95. The RSD sum for the Set 1 is 1.23, and for the Set 2 is 1.88, thus underestimating the leaching of the entire range by about 8% for the Set 1 and 14% for the Set 2. Overall, the leaching of the fractions is estimated fairly accurately by the model (RSD < 0.1 for most of the data points), the most deviating fraction is 5.6 – 8.4 mm with the RSD of 0.42. For the Set 2, the least accurately described fraction is 4 – 5.6 mm with an RSD of 0.50.

Figure 7.4 presents the data on a group of cations, for which the shape of the leaching curves throughout the fraction range was similar. The same slight

underestimation is observed for the particle size range of 0.3 – 0.7 mm. For Ca, the underestimation in this range is higher.

Sodium

The coefficient of correlation for the Set 1 is 0.98, and for the Set 2 is the same. The RSD sum for the Set 1 is 0.98, and for the Set 2 is 0.9, thus underestimating the entire leaching range by about 13% for the Set 1 and 11% for the Set 2. For Na^+, nearly all the fractions are estimated fairly accurately by the model (RSD < 0.1 for most of the data points); the most deviating fractions are 2 – 2.8 mm and 4 – 5.6 mm with RSDs of 0.19. For the Set 2, the least accurately described fraction is 4 – 5.6 mm with an RSD of 0.18.

Potassium

The coefficient of correlation for the Set 1 is 0.98, and for the Set 2 is 0.97. The RSD sum for the Set 1 is 1.07, and for the Set 2 is 0.97, thus underestimating the entire range leaching by about 15% for the Set 1 and 13% for the Set 2. For K^+, most of the fractions are estimated fairly accurately by the model (RSD < 0.1 for most of the data points); the most deviating fractions are 4 – 5.6 mm and 5.6 – 8 mm with the RSDs of 0.22 and 0.18, respectively. For the Set 2, the least accurately described fraction is 4 – 5.6 mm with an RSD of 0.22.

The obtained data agrees well with the literature because sodium and potassium are mainly present in salts with high solubility[192]. Therefore, the more soluble the compounds for a particular element are, the better the model is going to describe their behavior.

Calcium

The coefficient of correlation for the Set 1 is 0.94, and for the Set 2 is 0.93. The RSD sum for the Set 1 is 1.88, and for the Set 2 is 2.22, thus underestimating the entire range leaching by about 17% for the Set 1 and 16% for the Set 2. As for all cases described above, the calcium leaching for most of the fractions is estimated fairly accurately by the model (RSD < 0.1 for most of the data points), the most deviating fraction are 0.71 – 1 mm and 4 – 5.6 mm with the RSDs of 0.32, and 0.35, respectively. For the Set 2, the least accurately described fraction is 4 – 5.6 mm with an RSD of 0.45.

Magnesium

The coefficient of correlation for the Set 1 is 0.96, and for the Set 2 is 0.95. The RSD sum for the Set 1 is 1.16, and for the Set 2 is 1.3, thus underestimating the entire range leaching by about 17% for both sets. As for all cases described above,

for magnesium, most of the fractions are estimated fairly accurately by the model (RSD < 0.1 for most of the data points), the most deviating fraction is 2 – 2.8 mm with the RSD of 0.23. For the Set 2, the least accurately described fraction is 4 – 5.6 mm with an RSD of 0.23.

Strontium

The coefficient of correlation for the Set 1 is 0.96, and for the Set 2 is 0.89. The RSD sum for the Set 1 is 1.90, and for the Set 2 is 2.5, thus underestimating the entire range leaching for about 10% for the Set 1 and 11% for the Set 2. For Sr^{2+}, the fine fraction range up to 1 mm is described well by the model (RSD < 0.1 for most of the data points), but larger fractions show a high deviation. Three fractions out of 18 have the RSD in the range of 0.15 – 0.2, and the two most deviating fractions are 8 – 11.2 mm and 4 – 5.6 mm, with the RSDs of 0.4 and 0.54, respectively. For the Set 2, the least accurately described fractions are the same with the RSDs of 0.42 and 0.71, respectively.

Copper

The coefficient of correlation for the Set 1 is 0.96, and for the Set 2 is 0.97. The RSD sum for the Set 1 is 2.07, and for the Set 2 is 2.4, thus underestimating the entire range leaching for about 17% for the Set 1 and 23% for the Set 2. For Cu^{2+}, the fine fraction range up to 2 mm is described well by the model (RSD < 0.1 for most points). Further, more than half of the fractions have RSDs in the range of 0.13 – 0.64 for Set 1 and 0.15 – 0.60 for the Set 2. The two most deviating fractions for the Set 1 are 4 – 5.6 and 5.6 – 8 mm, and with the RSDs of 0.49 and 0.64, respectively. For the Set 2, the least accurately described fractions are the same with the RSDs of 0.60.

As can be seen on nearly all plots of the elements of the first group, both anions and cations, the model describes well the range of fine fractions and the large one, but for different elements, the artifacts in the ranges 0.3 – 0.7 mm remain unexplained. One of the possible explanations would be improper sieving, for example if tiny, contaminated particles adhere to larger particles due to electrostatic effects[62]. This adherence could result in the over-contamination of those fractions and their non-fitting to the proposed model. Figure 7.6 provides another example of the phenomenon mentioned above.

7.4.2 Medium fit elements (modelling of the leaching behavior is limited), Ba and Sb

The model for Ba and Sb is presented in Figure 7.7. In this case, the leaching for the most contaminated fraction and the largest fraction do not differ

significantly. Unlike the above-described elements, where the difference between the most and the slightest contaminated fractions would be in the range of an order of magnitude, for Sb, it is only about two times, and for Ba, it is approximately the same. One of the possible explanations for this phenomenon would be the size of those cations, their "hardness" (by Lewis-Pearson), and their tendency to form poorly soluble compounds[208]. Therefore, they might form their phases and/or precipitate on the quenching layer but not be adsorbed by it during quenching. This way, through precipitation, they appear in all fractions. It is also the reason to include the leaching of the least contaminated fraction in the model calculation, to account not for adsorbed compounds only but also for precipitated ones that explain the change in these model curve shape.

Barium

The coefficient of correlation for the Set 1 is 0.73, and for the Set 2 is 0.56. Thus, the RSD sum for the Set 1 is 2.46, and for the Set 2 is 3.65. For Ba, this results in overestimating the entire range of leaching values by about 30% for the Set 1 and 33% for the Set 2. For $Sr^{2+,}$ the large-fraction range from 1.4 mm is described well by the model (RSD < 0.1 for most of the data points), but the fine-fraction range is not described so accurately. For the Set 2, the situation is similar. The two most deviating fractions are 500 – 710 μm and 0.71 – 1 mm with RSDs of 0.32 and 0.59, respectively. For the Set 2, the least accurately described fractions are 63 – 125 μm and 0.71 – 1 mm with the RSDs of 0.42 and 1.06, respectively.

Antimony

The coefficient of correlation for the Set 1 is 0.8, and for the Set 2 is 0.65. The RSD sum for the Set 1 is 0.28, and for the Set 2 is 0.39. For Sb, this results in underestimating the entire range leaching for about 6% for the Set 1 while overestimating for about 2% for the Set 2. For Sb, the model describes all the fractions well (RSD < 0.1 for all the points). The situation is the same for the Set 2: except one, the most deviating fraction with the RSD of 0.13.

7.4.3 Elements that are not described well by the model - Zn, Mn, and Ni

Figure 7.5 and Figure 7.8 show the leaching patterns of elements which are poorly described by the model. Zinc shows much higher values for fine fractions, while nickel and manganese does not follow the S-shape leaching curve due to reason described below, which correlates with previous findings[124]. The reason for the insufficient fit of the model for Mn and Ni might lie in the fact that they tend to form complex insoluble compounds with iron. Combined with the

heterogeneity of the BA, and presence of these elements at least partially in metallic form results in the decrease of the model accuracy for those elements (the results presented in Table 7.2 confirm that).

For Zn (Figure 7.8), the model does not describe the leaching behavior satisfactorily; however, without an increase in the range of 4 – 5 mm, the model curve would have been very close to both sets of data. One of the many reasons for that could be the difference of this fraction (based on visual inspection) in comparison with the fine fractions (looking like dark gray sand), and the coarse fractions (particles of rocks, glass, ceramics, etc). Therefore, this fraction might be an outlier. Metallic zinc is highly volatile compared to other many other elements and evaporates during incineration, emerging in high quantities in FA (Chapter 4). However, a part of the evaporated zinc may be absorbed on the surface of BA particles, especially the finest fraction as the surface area is the highest. Further, very little Zn leaching is observed throughout all fractions, and for the particle size range from 1 to 22.4 mm, the values are fairly similar, and close to zero, unlike the descending trend among large fractions, which can be observed for elements with a good fit[209]. Additionally, the metal extraction treatment after the incineration might play a role in it.

The coefficient of correlation for the Set 1 is 0.89, and for the Set 2 is 0.86. The RSD sums are significantly more than for previously described elements; for the Set 1, it is 33.59, and for the Set 2, it is 74.22. This results in overestimating the entire range of leaching by about 55% for the Set 1 and 74% for the Set 2. For Zn, nearly all fractions deviate significantly from the model. For the Set 1, only two points have the RSD < 0.15, and for the Set 2, this number is five. The two most deviating fractions are 1 – 1.4 mm and 0.71 – 1 mm with the RSDs of 14 and 5.9, respectively. For the Set 2, the least accurately described fractions are 1 – 1.4 mm and 125 - 180 μm, with the RSDs of 19 and 34, respectively.

For Mn, the coefficient of correlation for the Set 1 is 0.82, and for the Set 2 is 0.81. The RSD sums are 4.78 for the Set 1 and 6.6 for the Set 2, thus underestimating the entire range leaching for about 36% for the Set 1 and 37% for the Set 2. For Mn, a fine-fraction range (up to 355 μm) is described well for both sets, but for coarser fractions, accurately estimated fractions are alternating with significantly deviating for the Set 1, and for the Set 2, everything in the range of 1 – 22 mm is not described accurately, RSDs are in the range 0.16 – 1.24. The two most deviating fractions are 2 – 2.8 mm and 5.6 - 8 mm, with the RSDs of 0.72 and 0.83, respectively. For the Set 2, the least accurately described fractions are 1 – 1.4 mm and 5.6 - 8 mm, with the RSDs of 1.24 and 0.88, respectively.

For Ni, the coefficient of correlation for the Set 1 is 0.39, and for the Set 2 is 0.58. The RSD sums are 9.68 for the Set 1 and 9.0 for the Set 2, thus underestimating the entire range leaching for about 71% for the Set 1 and 66% for the Set 2. For Ni, nearly none of the fractions is described accurately by the model. The range of large fractions (2 – 22.4 mm) deviates the most, with RSDs in the range of 0.7 – 0.98 for the Set 1 and 0.62 – 0.98 for the Set 2.

7.4.4 Overall model evaluation

As can be seen, the best results are obtained for alkali-metal cations and anions; the worst results are observed for Ni. It demonstrates that despite the BA complexity, a simple model can predict the leaching behavior of many elements using a limited set of experimental data.

As can be observed from the above, for nearly all elements, the model does not describe the fraction 4 – 5.6 mm very well, for some elements the fraction 5.6 – 8 mm is also affected. This might be due to the relatively small amounts of these fractions in the BA. It was also visibly different after sieving, containing much more leaves, threads, etc. This fraction could therefore be an outlier. A noticeable number of deviations is also observed for fractions of 0.71 – 1 mm and 1 – 1.4 mm. One of the possible explanations might be found in the loss-on-ignition (LOI) data for both sets of the BA. Figure 7.9 demonstrates the LOI for all particle size fractions. As can be seen, with the increase in the particle size, the LOI decreases. However, the fractions between 710 μm and 8 mm have an increased LOI compared to the surrounding fractions. This is especially noticeable in the range of 2 – 5.6 mm. These deviations might come from the relatively high amount of unburnt organic matter (leaves, treads, fabrics, etc.) present in these BA fractions (Chapter 3). It is likely that they get enriched in this fraction due to their similar size after incineration. These materials might impact the overall leaching because they could disrupt the packing of MSWI particles due to being shaped very differently from the proposed model shape but the regular shape of the BA particles.

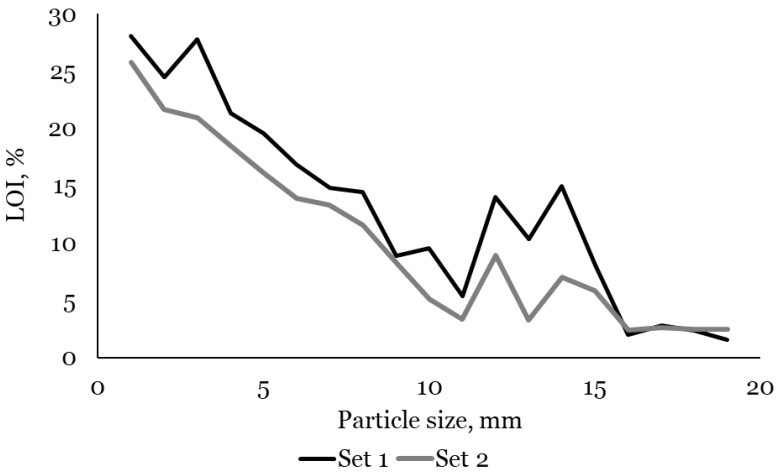

Figure 7.9 LOI of the Set 1 (experimental set) and the Set 2 (validation set) of the data used in modeling.

Even though the model simplifies the real BA particles to a great extent, it can be used to predict leaching of certain elements using only the leaching values of the largest (> 22.4 mm) and smallest fraction (< 0.63 µm) as input and serves as additional proof of the adverse effect of the quenching layer on the leaching. This approach would allow the rapid screening of BA regarding its contamination and an easy assessment of the effectiveness of treatment procedures such as washing or grinding that affect/remove the quenching layer [102,210].

To further improve the model and to take the high variability of BA into account more data sets from other countries and incineration plants should be incorporated in the future. It would also be interesting to compare data from different incinerators in different countries to see if the model is applicable in these cases.

7.5 Conclusions

The objective was to develop a simple model for estimating the leaching of BA based on the amount of particle core and quenching layer present in different size fractions. The model calculates the ratio between the volume of the quenching layer and the entire volume of the particle for each BA size fraction assuming a uniform thickness. Additionally, it takes into account a "background" leaching provided by the core. The leaching value for each fraction corresponds to the volume share of the quenching layer and the core in the particle. The finest fraction is mostly composed of the quenching layer, so its leaching value is

assumed to be representative for the leaching of the quenching layer in other fractions and used for calculating the amount of PTEs leaching from the quenching layer. The largest fraction contains very little quenching layer, and its leaching value is therefore taken as the background leaching of BA without quench present.

The model demonstrated promising results for various elements (chloride and sulfate, Na, K, Ca, Mg, Sr, Cu), supporting the idea that the quenching layer has significant influence on the leaching of BA. The model predicts the leaching behavior of the entire particle size range with an error within 10–20% for these ions. For Ba, Sr, and Sb, the model also shows satisfactory results with a total error of ca. 30%, and for Ni, Mn, and Zn, the model does not work sufficiently (significant total errors, > 50%). To summarize, the model predicts the leaching of certain elements well when it is clearly influenced by the composition of the quenching layer, while the leaching of other elements is influenced by other factors such as presence of metallic forms of elements throughout fractions.

The proposed approach of taking the quenching layer into account seems to be a promising, novel, and easy way to estimate the leaching potential of BA fractions, which makes it easier to apply the BA, and to select a fraction that needs further treatment to remove this quenching layer such as washing or grinding.

It appears that during the quenching procedure, the BA transforms into a more contaminated product with poorer physicochemical properties. Therefore, the further treatment aimed to improve the quality of the quenched BA essentially is to undo the damage caused by the quenching procedure. It appears to be vital to illustrate the full responsibility of the quenching layer in the leaching of the elements which are crucial for the further use in secondary building materials (such as Cl), but also PTEs, as to whether BA be landfilled or reused, it must match the environmental legislation limits. The comparison with air-quenched materials in the future could also be helpful to better understand the influence of the quenching layer.

To estimate the severity of the “quenching problem” and demonstrate once again that this way of handling the BA prevents it from being easily transformed into a secondary material and requires several decontamination steps. The purpose was to demonstrate a potential link between the presence of the quenching layer on the BA particles and the leaching. It was done by developing a simple semi-empirical model.

CHAPTER 8

Conclusions and recommendations

8.1 Summary

The aim of this thesis was to examine the entire range of the Municipal Solid Waste Incineration (MSWI) residues, including MSWI Fly Ash (FA) and MSWI Bottom Ash (BA). Previously, the question of whether these by-products can be used in applications such as building materials was not properly answered. Thus, it was essential to obtain a comprehensive picture of the properties of those materials taking into consideration the fact that the material properties substantially vary throughout the particle-size range. The goal was then to develop tailored treatments based on the property analysis to estimate the recycle potential for specific fractions of MSWI residues to determine which of them appear to be the most promising.

A comprehensive study of the particle size range of BA < 22.4 mm and MSWI FA allows us to draw several conclusions. MSWI FA was severely contaminated (especially with chloride) and does not appear to be a reliable source for secondary building materials due to the leaching above the limit set by the government (in the Netherlands). However, high contents of valuable metals, such as Zn and Pb make this material attractive for metal extraction. Regarding BA, almost the entire range of particle size fractions can be used as substitutes for concrete/mortar components. However, the fraction BA < 0.125 mm appears to be the least suitable because of a very high contamination level and a noticeable deterioration of the mechanical properties of cement products containing this fraction due to the high value of water adsorption, among other factors.

Based on this analysis, the BA fraction 0.125 < X < 3 mm was further investigated as a cement substitute, as it does not have the disadvantages of contamination compared to the finest fraction, and, at the same time, is not a suitable substitute for fine aggregates in concrete due to high porosity, presence of metallic aluminum, etc.

Eventually, a mechanical treatment was developed for the BA fraction 0.125 < X < 3 mm to reduce the size and porosity and extract flattened Al pieces to obtain the material which can be used as a MAC for cements.

The final part of the thesis was devoted to the development of a leaching model based on the leaching data from the investigated particle-size ranges. It has the potential to predict the leaching of a certain BA fraction, as well as an argument regarding the adverse effect of the quenching procedure.

Further parts summarize the conclusions from all the steps of the study in more detail.

8.2 Characterization of MSWI BA

Chapter 3 provided a full analysis of 14 particle-size fractions of BA. There, the total element composition, minerology, and leaching properties were investigated to propose the justified division of BA bulk for analysis, treatment, and possible applications. The analysis has shown that for further processing from any viewpoint it would be beneficial to divide BA into three fractions: fine (below 0.125 mm), medium (0.125 – 1 mm), and coarse (> 1 mm). The separation at the size 0.125 mm is conditioned by an abrupt decrease of the PTE leaching at this point, therefore, removing this fraction purifies the rest of the material immensely. Regarding the second "division": the analysis showed that the properties of the fractions above 1 mm do not differ significantly, while the total composition, minerology, and leaching of the medium fraction still allow for a separation from both fractions (above and below). The essential point is to separate BA from the most contaminated fraction below 0.125 mm because, if not removed, it may contaminate coarse fractions, while, if the separation is made, coarse fractions will require no or just minor water-washing treatment to pass the environmental legislation.

8.3 Characterization of MSWI FA

In Chapter 4, MSWI FA was at the same time analyzed and treated. The leaching test and total content analyses showed that MSWI FA is highly contaminated, especially with chloride, Pb, Zn, and Cd. To remove the contamination, two chemical agents were evaluated and compared with water. At first, the elution abilities of demineralized water, sodium gluconate, and EDTA solutions were analyzed. Subsequently, two three-step treatments were performed: (1) With chelatants at the first two steps, and water at the third, and (2) three-step water treatment. This was done to obtain the data regarding the effect of two different treatments on the total element composition and the leaching of MSWI FA.

The developed three-step water treatment dealt quite successfully with the removal of salts like chloride and sulfate; however, it was far less effective in eluting metals. Chemical treatment was also effective towards chloride, and eluted significant amounts of metals. However, due to partial dissolution of the MSWI FA matrix by chelatants, not only more metals were extracted but also, supposedly because of opening closed pores, the latter treatment led to increased leaching of contaminants (more than for the material before treatment). Therefore, considering that MSWI FA, unlike BA, contains substantial amounts of such metals as Pb, Cd, and Zn, the matrix decomposition in a natural environment or cement might lead to a severe leaching, even though the results

for the three-step water-washed FA were almost satisfactory from the environmental-use viewpoint. Because the latent hazard of MSWI FA is incomparably more than of BA, at this moment, it does not appear to be beneficial to develop treatments for its further use in building materials.

8.4 MSWI BA fines

After analyzing both MSWI by-products, we focused further on the fine fraction of BA because unlike the coarse fraction, it has very limited application. With the information regarding the total element content and leaching properties from the previous part of this study, the fraction 0.125 – 3 mm was selected because it is unsuitable as an aggregate alternative; however, it has a potential for application as a MAC. A milling treatment was developed to transform this fraction into a finely dispersed material. The milling pursued three goals: the size reduction to pass 0.125 mm, the reduction of porosity, and the removal of flattened Al bids (by sieving). The fraction below 0.125 mm was used for the sake of comparison, without any treatment.

The analysis of physical properties of the BA fractions below 0.125 mm and 0.125 – 3mm showed that they are rather similar to those of cement(s); however, contents of main oxides differed significantly: SiO_2 content was nearly 50% w/w for the coarser fraction, while for the finer it was around 35% w/w; CaO content was much higher for the finer fraction. The hydration and strength analyses for mortars and pastes showed that the reactivity of both types of fines is limited, and it acts mostly as a filler. The overall outcome of this investigation (Chapters 5 and 6) is that on one hand, nearly all studied BA fines (even unprocessed, below 0.125 mm) could be used as MACs because the mechanical performance is satisfactory for cement replacement according to the standard, provided the replacement level does not exceed 5% w/w. However, for most types of fines (unprocessed, milled, or milled to be close to the cement particle size), the reduction of the compressive strength of mortars containing those fines is worse than the expected proportionately, e.g., it drops by more percent than the replacement level. The additional milling of BA fines to reduce the size (as a result it would be closer to cement) appears to be inadvisable providing no increase in the strength but also increasing the leaching of these fines. Hypothetically, these phenomena are related to liberating the outer layer of particles (the quenching layer), which supposedly has higher leaching, and differs in properties with the core of the fines from the fraction 0.125 – 3 mm. The liberated quench-layer particles are far more similar to the fraction below 0.125 mm, and, therefore, bring with them higher contamination, and other disadvantages such as high porosity. Their share is most likely rather insignificant; therefore, it does not affect the strength (especially with

such low levels of replacement) and increase the leaching only slightly. Thus, if there is no added value, or maybe a minor detrimental effect from the additional milling, it should be advised against using it.

8.5 Leaching model

In Chapter 7, because of the findings on the leaching of BA during this study, a semi-empirical leaching model was developed. The concept was to demonstrate by the model that the quenching layer formed by the quenching process is in large part responsible for the leaching of PTEs. The calculations for the model assumed that a BA particle has a core and an outer layer, where the core has the same leaching as the least contaminated fraction (22.4 mm), and the leaching of the layer corresponds to the leaching of the most contaminated fraction (below 63 micrometers). The amount of the outer layer was calculated for each size fraction assuming the same thickness for each fraction. Based on this, the leaching was estimated. The model showed suitable results for alkali and alkaline-earth cations, chloride, sulfate, Cu, and Zn. Considering these findings, it is possible to argue that the quenching procedure greatly impacts on the contamination of BA. In addition, the simplicity of the proposed model in comparison with other more complex approaches allows for its potential use in predicting the leaching properties of this type of the materials.

8.6 General observations and practical recommendations

The suggestions on the implementation of the findings within the scope of the thesis or close to it can be summed up as follows.

Better waste handling and separation

Visual inspection of BA used in this study combined with the literature analysis of the waste management in the Netherlands suggest that the immense decrease of BA amounts is possible through the reduction of the amount of the residual combustible waste. The BA is quite rich on various organic matter and materials (wood, leaves, threads, fabric, etc.), broken glass, and ceramics. The latter two, if separated prior to the incineration, reduce incineration costs, and potentially can be used further as building-material substitutes with a minimum washing treatment (which anyway would have to be applied later to BA containing those materials).

Separation of the fines from the bulk

Another point, which has also been suggested in previous research on the topic, is that it is vital to separate and not mix fines (below 0.125 mm) with coarser fractions. This way, the contamination of a coarse fraction would be avoided,

which will reduce costs of the washing treatment, and improve its physical properties, while the fine fraction can be dealt separately with treatments and application. The most important outcome is that a pure coarse fraction is almost readily suitable "as is" as a material substitute, while a coarse fraction mixed with fines requires further treatment. Now (2022), the separation is performed at the size 3–4 mm, and the finer fraction is landfilled. However, should this separation occur at 0.125 mm (or slightly higher, considering practical difficulties), the part of the material between 3–4 mm, and above 0.125 mm will become available for further processing and reuse. Taking into consideration the fact that the material properties substantially vary throughout the particle-size range, considering them as the same for the entire range and applying one treatment would lead to increased costs and reduced overall quality of treated products, which is not desirable.

Dry vs. wet quenching

In several parts of this thesis, it has been shown that the quenching procedure might have adverse effects on the quality of BA by creating a quenching layer. This especially affects the leaching of the fine fractions of BA due to formation of new mineral phases upon immersion of hot BA into the quenching water (the latter is used multiple times; therefore, has high to moderate concentrations of salts, particularly, chloride). Unfortunately, the literature body on this topic is scarce. It can be carefully suggested for consideration that should water quenching be substituted with a dry cooling process, the level of contamination of BA could drop drastically, especially, for chloride (which is the main problem often requiring a washing treatment). Thus, the material will require less measures to pass the environmental legislation.

It appears now that a large part of the BA treatment is targeted to undo the damage (mostly related to contamination) from the way of handling the material at nearly all previous steps (waste collection, waste separation, incineration, mixing BA fines with the coarse fraction, and water quenching). Therefore, an interesting route of the future research would be to study how various handling at all steps contributes to the final properties of BA. This requires going a few steps back to begin with the waste and simulate various processes on a laboratory scale, but the outcome might be a great reduction of the residual part, generation of several streams of valuable recyclable materials, and either improved qualities of BA or a major decrease in the volume of the residuals.

8.7 Recommendations for further research

Overall, the original aim of this thesis is mainly achieved. It shows that BA can be used as a secondary building material. However, it requires several-step processing even for the application with a limited amount of the material. Regarding the fine part of the material, it requires at least washing, milling, and sieving to be further successfully applied.

However, there are options that would either provide a much better-quality BA (cleaner, less contamination from undesirable materials such as organic matter) or enormously reduce the yield of this by-product due to more rigorous segregation of the residual waste. Perhaps, the points summed up above in the previous section would be economically feasible only in decades from now, but the growing population combined with overproduction and overconsumption unavoidably lead to an increase in the amount of incinerated waste and therefore the amounts of its by-products. Unfortunately, some changes go beyond the scope of this thesis and towards social and economic aspects, thus, they are not discussed here. However, especially now, the classic RRR (Reduce-Reuse-Recycle) should get improvements concerning avoiding unnecessary consumption and production in nearly all areas of everyday life.

Future work as a continuation of this study or the research on BA might include comparative studies with points mentioned above. It is important to understand the difference in chemical and physical properties of different BA (for instance, after wet and dry quenching), as well as the effect of various properties on the mechanical performance of the material. It is interesting to study first the mechanical/through-separation/segregation purification of BA to understand which part of the material contributes most to good mechanical properties, and which part causes the most damage (e.g., glass, ceramics, minerals, etc.).

The coarse fraction of BA at the time of this study had been already thoroughly investigated and partially used as a substitute for natural aggregates. Therefore, it was not included for the treatment and application development plan. However, the author believes that this range of fractions or parts of it might have a potential as a filler/fine aggregate substitute after milling. This requires further research.

Also, studying the difference in the microstructure of cement pastes containing milled large fractions of BA (> 4 mm) with/without the segregation into streams, appears to be of interest to investigate if this step of BA handling provides a desirable improvement in the structure of cements with such additives.

Overall, the most essential point would be to prevent spoilage of the material at a particular stage of handling, and before developing the treatment or

application for a given BA mechanically minimizing the adverse effect brought by the previous step.

References

1. Eurostat - Data Explorer. https://appsso.eurostat.ec.europa.eu/nui/show.do?dataset=env_wasgen&lang=en.

2. Nicholls, R. J., Beaven, R.P., Stringfellow, A., Monfort, D., Le Cozannet, G., Wahl, T., Gebert, J., Wadey, M., Arns, A., Spencer, K.L., Reinhart, D., Heimovaara, T., Santos, V.M., Enríquez, A.R. & Cope, S. Coastal Landfills and Rising Sea Levels: A Challenge for the 21st Century. *Front Mar Sci* **8**, (2021).

3. DeMarco, J. Advanced techniques for incineration of municipal solid wastes. *AMER.INST.CHEM.ENGNS SYMP.SER.* **70**, 481–484 (1974).

4. Wiles, C.C. Municipal solid waste combustion ash: State of the knowledge. *Journal of Hazardous Materials* **3894**, 20 (1995).

5. Eurostat. Eurostat Statistic explained. (2017).

6. Tyrer, M. Municipal solid waste incinerator (MSWI) concrete. *Eco-Efficient Concrete* 273–310 (2013) doi:10.1533/9780857098993.3.273.

7. van der Sloot, H.A. Comparison of the characteristic leaching behavior of cements using standard (EN 196-1) cement mortar and an assessment of their long-term environmental behavior in construction products during service life and recycling. *Cement and Concrete Research* **30**, 1079–1096 (2000).

8. *Soil Quality Decree*. (VROM, Den Haag: Ruimte en Milieu. Ministerie van Volkshuisvesting, Ruimtelijke Ordeling en Milieubeheer, 2013).

9. Ministry of Economic Affairs, Ministry of Infrastructure and the Environment & Relations, M. of I. and K. Green Deals Overview. (2015).

10. Verbinnen, B., Billen, P., van Caneghem, J. & Vandecasteele, C. Recycling of MSWI Bottom Ash: A Review of Chemical Barriers, Engineering Applications and Treatment Technologies. *Waste and Biomass Valorization* **8**, 1453–1466 (2017).

11. Berg, E.R. & Neal, J.A. Municipal Solid Waste Bottom Ash as Portland Cement Concrete Ingredient. *Journal of Materials in Civil Engineering* **10**, 168–173 (1998).

12. Xie, Y., Wu, X.M., Fan, Y.M., Yu, Q.J., Huang, J. & Kuang, Z.R. Investigation into incineration bottom ash of municipal solid waste used as cement admixture. *Huanan Ligong Daxue Xuebao/Journal of South China University of Technology (Natural Science)* **37**, 37–43 (2009).

13. Mary Joseph, A., Snellings, R., Nielsen, P., Matthys, S. & de Belie, N. Pre-treatment and utilisation of municipal solid waste incineration bottom ashes towards a circular economy. *Construction and Building Materials* **260**, (2020).

14. Jurič, B., Hanžič, L., Ilić, R. & Samec, N. Utilization of municipal solid waste bottom ash and recycled aggregate in concrete. *Waste Management* **26**, 1436–1442 (2006).

15. Keulen, A., van Zomeren, A., Harpe, P., Aarnink, W., Simons, H.A.E. & Brouwers, H.J.H. High performance of treated and washed MSWI bottom ash granulates as natural aggregate replacement within earth-moist concrete. *Waste Management* **49**, 83–95 (2016).

16. van de Wouw, P.M.F., Florea, M.V.A. & Brouwers, H.J.H. Crushing of MSWI bottom ash towards material purification. *AInternational Conference on Advances in Cement and Concrete Technology in Africa, Dar es Salaam, Tanzania,* accepted in October 2015 (2016).

17. Zhang, T. & Zhao, Z. Optimal Use of MSWI Bottom Ash in Concrete. *International Journal of Concrete Structures and Materials* **8**, 173–182 (2014).

18. Mangialardi, T. Effects of a washing pre-treatment of municipal solid waste incineration fly ash on the hydration behaviour and properties of ash—Portland cement mixtures. *Advances in Cement Research* **16**, 45–54 (2004).

19. Ginés, O., Chimenos, J. M., Vizcarro, A., Formosa, J. & Rosell, J.R. Combined use of MSWI bottom ash and fly ash as aggregate in concrete formulation: Environmental and mechanical considerations. *Journal of Hazardous Materials* **169**, 643–650 (2009).

20. Saikia, N., Kato, S. & Kojima, T. Production of cement clinkers from municipal solid waste incineration (MSWI) fly ash. *Waste Management* **27**, 1178–1189 (2007).

21. Bertolini, L., Carsana, M., Cassago, D., Quadrio Curzio, A. & Collepardi, M. MSWI ashes as mineral additions in concrete. *Cement and Concrete Research* **34**, 1899–1906 (2004).

22. Kamon, M., Katsumi, T. & Sano, Y. MSW fly ash stabilized with coal ash for geotechnical application. *Journal of Hazardous Materials* **76**, 265–283 (2000).

23. Nowak, B., Aschenbrenner, P. & Winter, F. Heavy metal removal from sewage sludge ash and municipal solid waste fly ash — A comparison. *Fuel Processing Technology* **105**, 195–201 (2013).

24. van der Bruggen, B., Vogels, G., van Herck, P. & Vandecasteele, C. Simulation of acid washing of municipal solid waste incineration fly ashes in order to remove heavy metals. *Journal of Hazardous Materials* **57**, 127–144 (1998).

25. Buclet, N. & Godard, O. The evolution of municipal waste management in Europe: How different are national regimes? *Journal of Environmental Policy and Planning* **3**, 303–317 (2001).

26. Goorhuis, M., Reus, P., Nieuwenhuis, E., Spanbroek, N., Sol, M. & Van Rijn, J. New developments in waste management in the Netherlands. *Waste Management and Research* **30**, 67–77 (2012).

27. van der Sloot, H.A. Present status of waste management in the Netherlands. *Waste Management* **16**, 375–383 (1996).

28. van der Sloot, H.A., Comans, R.N.J. & Hjelmar, O. Similarities in the leaching behaviour of trace contaminants from waste, stabilized waste, construction materials and soils. *Science of The Total Environment* **178**, 111–126 (1996).

29. Waste-to-Energy: How It Works - Deltaway. https://deltawayenergy.com/2018/08/waste-to-energy-how-it-works/.

30. Aubert, J.E., Husson, B. & Sarramone, N. Utilization of municipal solid waste incineration (MSWI) fly ash in blended cement: Part 1: Processing and characterization of MSWI fly ash. *Journal of Hazardous Materials* **136**, 624–631 (2006).

31. Sormunen, L.A., Kalliainen, A., Kolisoja, P. & Rantsi, R. Combining Mineral Fractions of Recovered MSWI Bottom Ash: Improvement for Utilization in Civil Engineering Structures. *Waste and Biomass Valorization* **8**, 1467–1478 (2017).

32. Yao, J., Kong, Q., Zhu, H., Long, Y. & Shen, D. Content and fractionation of Cu, Zn and Cd in size fractionated municipal solid waste incineration bottom ash. *Ecotoxicology and Environmental Safety* **94**, 131–137 (2013).

33. Taylor, H.F.W. Cement chemistry. 2nd Edition, Thomas Telford Publishing, London, 361 pp. (1997) doi:10.1680/CC.25929.

34. ASTM C150 / C150M-19a, Standard Specification for Portland Cement, ASTM International, West Conshohocken, PA. 1–10 Preprint at https://doi.org/10.1520/C0150_C0150M-19A (2019).

35. Faleschini, F., Toska, K., Zanini, M.A., Andreose, F., Settimi, A.G., Brunelli, K. & Pellegrino, C. Assessment of a municipal solid waste

incinerator bottom ash as a candidate pozzolanic material: Comparison of test methods. *Sustainability (Switzerland)* **13**, (2021).

36. Lin, K.L., Chang, W.C. & Lin, D.F. Pozzolanic characteristics of pulverized incinerator bottom ash slag. *Construction and Building Materials* **22**, 324–329 (2008).

37. Lin, K.L. & Lin, D.F. Hydration characteristics of municipal solid waste incinerator bottom ash slag as a pozzolanic material for use in cement. *Cement and Concrete Composites* **28**, 817–823 (2006).

38. Polettini, A., Pomi, R. & Carcani, G. The effect of Na and Ca salts on MSWI bottom ash activation for reuse as a pozzolanic admixture. *Resources, Conservation and Recycling* **43**, 403–418 (2005).

39. EN 197-1. *European standards*. 1–29 (2000).

40. Caprai, V. Treatment and valorization of Municipal Solid Waste Incineration bottom ash: applications in cement-based materials. PhD thesis, Eindhoven University of Technology (2019).

41. Caprai, V., Florea, M.V.A. & Brouwers, H.J.H. Evaluation of the influence of mechanical activation on physical and chemical properties of municipal solid waste incineration sludge. *Journal of Environmental Management* **216**, 133–144 (2018).

42. van Gerven, T., Van Keer, E., Arickx, S., Jaspers, M., Wauters, G. Vandecasteele, C. & Vandecasteele, C. Carbonation of MSWI-bottom ash to decrease heavy metal leaching, in view of recycling. *Waste Management* **25**, 291–300 (2005).

43. Liu, Y., Li, Y., Li, X. & Jiang, Y. Leaching behavior of heavy metals and PAHs from MSWI bottom ash in a long-term static immersing experiment. *Waste Management* **28**, 1126–1136 (2008).

44. Caprai, V., Gauvin, F., Schollbach, K. & Brouwers, H.J.H. MSWI bottom ash as binder replacement in wood cement composites. *Construction and Building Materials* **196**, 672–680 (2019).

45. Saffarzadeh, A., Shimaoka, T., Wei, Y., Gardner, K. H. & Musselman, C. N. Impacts of natural weathering on the transformation/neoformation processes in landfilled MSWI bottom ash: A geoenvironmental perspective. *Waste Management* **31**, 2440–2454 (2011).

46. Arm, M. Variation in deformation properties of processed MSWI bottom ash: Results from triaxial tests. *Waste Management* **24**, 1035–1042 (2004).

47. Shim, Y.-S., Rhee, S.-W. & Lee, W.-K. Comparison of leaching characteristics of heavy metals from bottom and fly ashes in Korea and Japan. *Waste Management* **25**, 473–480 (2005).

48. Alam, Q., Lazaro, A., Schollbach, K. & Brouwers, H.J.H. Chemical speciation, distribution and leaching behavior of chlorides from municipal solid waste incineration bottom ash. *Chemosphere* **241**, 124985 (2020).

49. Shim, Y.-S., Kim, Y.-K., Kong, S.-H., Rhee, S.-W. & Lee, W.-K. The adsorption characteristics of heavy metals by various particle sizes of MSWI bottom ash. *Waste Management* **23**, 851–857 (2003).

50. Karlfeldt Fedje, K., Ekberg, C., Skarnemark, G. & Steenari, B.-M. Removal of hazardous metals from MSW fly ash—An evaluation of ash leaching methods. *Journal of Hazardous Materials* **173**, 310–317 (2010).

51. van der Sloot, H.A., Heasman, L. & Quevauviller, P. Harmonization of Leaching/Extraction tests. *Studies in Environmental Science* vol. Volume 70 280 Preprint at https://doi.org/10.1016/S0166-1116(97)80109-4 (1997).

52. Li, X.-G., Lv, Y., Ma, B.-G., Chen, Q.-B., Yin, X.-B. & Jian, S.-W. Utilization of municipal solid waste incineration bottom ash in blended cement. *Journal of Cleaner Production* **32**, 96–100 (2012).

53. Yan, K., Sun, H., Gao, F., Ge, D. & You, L. Assessment and mechanism analysis of municipal solid waste incineration bottom ash as aggregate in cement stabilized macadam. *Journal of Cleaner Production* **244**, (2020).

54. Speiser, C., Baumann, T. & Niessner, R. Morphological and chemical characterization of calcium-hydrate phases formed in alteration processes of deposited municipal solid waste incinerator bottom ash. *Environmental Science and Technology* **34**, 5030–5037 (2000).

55. Weibel, G., Eggenberger, U., Schlumberger, S. & Mäder, U.K. Chemical associations and mobilization of heavy metals in fly ash from municipal solid waste incineration. *Waste Management* **62**, 147–159 (2017).

56. Müller, U. & Rübner, K. The microstructure of concrete made with municipal waste incinerator bottom ash as an aggregate component. *Cement and Concrete Research* **36**, 1434–1443 (2006).

57. Saffarzadeh, A., Arumugam, N. & Shimaoka, T. Aluminum and aluminum alloys in municipal solid waste incineration (MSWI) bottom ash: A potential source for the production of hydrogen gas. *International Journal of Hydrogen Energy* **41**, 820–831 (2016).

58. Song, Y., Li, B., Yang, E.H., Liu, Y. & Ding, T. Feasibility study on utilization of municipal solid waste incineration bottom ash as aerating agent for the production of autoclaved aerated concrete. *Cement and Concrete Composites* **56**, 51–58 (2015).

59. Chimenos, J., Segarra, M., Fernández, M. & Espiell, F. Characterization of the bottom ash in municipal solid waste incinerator. *Journal of Hazardous Materials* **64**, 211–222 (1999).

60. Nesterov, I., Jensen, P.A. & Dam-Johansen, K. Literature review – Incineration bottom ash leaching properties. *Improved electrical efficiency and bottom ash quality on waste combustion plants* Preprint at (2010).

61. Astrup, T., Muntoni, A., Polettini, A., Pomi, R., Van Gerven, T. & van Zomeren, A. Treatment and Reuse of Incineration Bottom Ash. in *Environmental Materials and Waste: Resource Recovery and Pollution Prevention* (2016). doi:10.1016/B978-0-12-803837-6.00024-X.

62. Alam, Q., Florea, M.V.A., Schollbach, K. & Brouwers, H.J.H. A two-stage treatment for Municipal Solid Waste Incineration (MSWI) bottom ash to remove agglomerated fine particles and leachable contaminants. *Waste Management* **67**, 181–192 (2017).

63. Arickx, S., van Gerven, T. & Vandecasteele, C. Accelerated carbonation for treatment of MSWI bottom ash. *Journal of Hazardous Materials* **137**, 235–243 (2006).

64. Chen, Z. & Yang, E.-H. Early age hydration of blended cement with different size fractions of municipal solid waste incineration bottom ash. *Construction and Building Materials* **156**, 880–890 (2017).

65. Lee, J.B., Kim, S.S., Lee, J.Y. & Ryou, J.S. Study on the pozzolanic activity of finely ground bottom ash for cement replacement. *Journal of Ceramic Processing Research* **18**, 291–300 (2017).

66. Jing, Z., Fan, X., Zhou, L., Fan, J., Zhang, Y., Pan, X. & Ishida, E.H. Hydrothermal solidification behavior of municipal solid waste incineration bottom ash without any additives. *Waste Management* **33**, (2013).

67. Alba, N., Gassó, S., Lacorte, T. & Baldasano, J.M. Characterization of Municipal Solid Waste Incineration Residues From Facilities with Different Air Pollution Control Systems. *J Air Waste Manage Assoc* **47**, 1170–1179 (1997).

68. Saqib, N. & Bäckström, M. Chemical association and mobility of trace elements in 13 different fuel incineration bottom ashes. *Fuel* **172**, (2016).

69. Matusiewicz, H. Sample Preparation for Inorganic Trace Element Analysis. *Physical Sciences Reviews* **2**, 5 (2017).

70. Iwata, S., Chiba, K., Haraguchi, H., Fujimori, E. & Minamoto, K. Enrichment of elements in industrial waste incineration bottom ashes obtained from three different types of incinerators, as studied by ICP-AES and ICP-MS. *Journal of Material Cycles and Waste Management* **6**, 73–79 (2004).

71. Fällman, A.M. & Hartlén, J. Leaching of slags and ashes - controlling factors in field experiments versus in laboratory tests. *Studies in Environmental Science* **60**, 39–54 (1994).

72. Abbas, Z., Moghaddam, A.P. & Steenari, B.-M. Release of salts from municipal solid waste combustion residues. *Waste Management* **23**, 291–305 (2003).

73. Xing, W. & Hendriks, C. Decontamination of granular wastes by mining separation techniques. *Journal of Cleaner Production* **14**, 748–753 (2006).

74. Hunger, M. & Brouwers, H.J.H. Flow analysis of water-powder mixtures: Application to specific surface area and shape factor. *Cement and Concrete Composites* **31**, 39–59 (2009).

75. Wei, Y., Shimaoka, T., Saffarzadeh, A. & Takahashi, F. Mineralogical characterization of municipal solid waste incineration bottom ash with an emphasis on heavy metal-bearing phases. *Journal of Hazardous Materials* **187**, 534–543 (2011).

76. Speiser, C., Baumann, T. & Niessner, R. Characterization of municipal solid waste incineration (MSWI) bottom ash by scanning electron microscopy and quantitative energy dispersive X-ray microanalysis (SEM/EDX). *Fresenius' Journal of Analytical Chemistry* **370**, 752–759 (2001).

77. Wu, B., Wang, D., Chai, X., Takahashi, F. & Shimaoka, T. Characterization of chlorine and heavy metals for the potential recycling of bottom ash from municipal solid waste incinerators as cement additives. *Frontiers of Environmental Science & Engineering* **10**, 8 (2016).

78. Tasneem, K.M., Nam, B.H. & Eun, J. Sustainable Utilization of MSWI Bottom Ash as Road Construction Materials, Part II: Chemical and Environmental Characterization. in *Airfield and Highway Pavements 2015* 593–604 (American Society of Civil Engineers, 2015). doi:10.1061/9780784479216.053.

79. Schollbach, K., Alam, Q., Caprai, V., Florea, M.V.A., van der Laan, S.R., van Hoek, C.J.G. & Brouwers, H.J.H. Combined characterisation of MSWI

bottom ash. in *Proceedings of the thirty-eighth international conference on cement microscopy, April 17 – April 21, 2016, Lyon, France* 74–82 (2016). doi:ISBN: 1-930787-12-X.

80. Zhu, W., Chen, X., Struble, L.J. & Yang, E.-H. Characterization of calcium-containing phases in alkali-activated municipal solid waste incineration bottom ash binder through chemical extraction and deconvoluted Fourier transform infrared spectra. *Journal of Cleaner Production* **192**, 782–789 (2018).

81. del Valle-Zermeño, R., Gómez-Manrique, J., Giro-Paloma, J., Formosa, J. & Chimenos, J.M. Material characterization of the MSWI bottom ash as a function of particle size. Effects of glass recycling over time. *Science of The Total Environment* **581–582**, 897–905 (2017).

82. Tang, P., Florea, M.V.A. & Brouwers, H.J.H. Employing cold bonded pelletization to produce lightweight aggregates from incineration fine bottom ash. *Journal of Cleaner Production* **165**, 1371–1384 (2017).

83. Gao, X., Yuan, B., Yu, Q.L. & Brouwers, H.J.H. Characterization and application of municipal solid waste incineration (MSWI) bottom ash and waste granite powder in alkali activated slag. *Journal of Cleaner Production* **164**, 410–419 (2017).

84. Wongsa, A., Boonserm, K., Waisurasingha, C., Sata, V. & Chindaprasirt, P. Use of municipal solid waste incinerator (MSWI) bottom ash in high calcium fly ash geopolymer matrix. *Journal of Cleaner Production* **148**, 49–59 (2017).

85. Inkaew, K., Saffarzadeh, A. & Shimaoka, T. Modeling the formation of the quench product in municipal solid waste incineration (MSWI) bottom ash. *Waste Management* **52**, 159–168 (2016).

86. Marchese, F. & Genon, G. Effect of leaching behaviour by quenching of bottom ash from MSW incineration. **29**, 39–47 (2011).

87. Dabo, D., Badreddine, R., De Windt, L. & Drouadaine, I. Ten-year chemical evolution of leachate and municipal solid waste incineration bottom ash used in a test road site. *Journal of Hazardous Materials* **172**, 904–913 (2009).

88. Minane, J.R., Becquart, F., Abriak, N.E. & Deboffe, C. Upgraded Mineral Sand Fraction from MSWI Bottom Ash: An Alternative Solution for the Substitution of Natural Aggregates in Concrete Applications. *Procedia Engineering* **180**, 1213–1220 (2017).

89. Lin, W.Y., Heng, K.S., Sun, X. & Wang, J.-Y. Accelerated carbonation of different size fractions of MSW IBA and the effect on leaching. *Waste Management* **41**, 75–84 (2015).

90. Dabo, D., Raimbault, L., Badreddine, R., Chaurand, P., Rose, J. & Windt, L.D. Characterisation of glassy and heterogeneous cementing phases of municipal solid waste of incineration (MSWI) bottom ash. in *Australasian Institute of Mining and Metallurgy Publication Series,* 95–100 (2008).

91. Hui, K.S. & Chao, C.Y.H. Pure, single phase, high crystalline, chamfered-edge zeolite 4A synthesized from coal fly ash for use as a builder in detergents. *Journal of Hazardous Materials* **137**, 401–409 (2006).

92. Vasiliev, L.L., Kanonchik, L.E., Antuh, A.A. & Kulakov, A.G. NaX zeolite, carbon fibre and CaCl2 ammonia reactors for heat pumps and refrigerators. *Adsorption* **2**, 311–316 (1996).

93. Grossman, D.G. Machinable Glass-Ceramics Based on Tetrasilicic Mica. *Journal of the American Ceramic Society* **55**, 446–449 (1972).

94. Zevenbergen, C., Wood, T.V., van der Broeck, P.F.C.W., Orbons, A.J. & van Reeuwijk, L.P. Morphological and Chemical Properties of MSWI Bottom Ash with Respect to the Glassy Constituents. *Hazardous Waste and Hazardous Materials* **11**, 371–383 (1994).

95. Dahl, O., Nurmesniemi, H., Pöykiö, R. & Watkins, G. Comparison of the characteristics of bottom ash and fly ash from a medium-size (32 MW) municipal district heating plant incinerating forest residues and peat in a fluidized-bed boiler. *Fuel Processing Technology* **90**, 871–878 (2009).

96. Polettini, A., Pomi, R. & Fortuna, E. Chemical activation in view of MSWI bottom ash recycling in cement-based systems. *Journal of Hazardous Materials* **162**, 1292–1299 (2009).

97. Yao, J., Li, W.B, Tang, M., Fang, C.R., Feng, H.J., & Shen, D.S. Effect of weathering treatment on the fractionation and leaching behavior of copper in municipal solid waste incinerator bottom ash. *Chemosphere* **81**, 571–576 (2010).

98. Meima, J.A. & Comans, R.N. The leaching of trace elements from municipal solid waste incinerator bottom ash at different stages of weathering. *Applied Geochemistry* **14**, 159–171 (1999).

99. Sunda, W.G. & Lewis, J.A.M. Effect of complexation by natural organic ligands on the toxicity of copper to a unicellular alga, *Monochrysis lutheri* 1. *Limnology and Oceanography* **23**, 870–876 (1978).

100. Lam, C.H.K., Ip, A.W.M., Barford, J.P. & McKay, G. Use of Incineration MSW Ash: A Review. *Sustainability* **2**, 1943–1968 (2010).

101. Dijkstra, J.J., van der Sloot, H.A. & Comans, R.N.J. The leaching of major and trace elements from MSWI bottom ash as a function of pH and time. *Applied Geochemistry* **21**, 335–351 (2006).

102. Cornelis, G., Gerven, T.V. & Vandecasteele, C. Antimony leaching from MSWI bottom ash: Modelling of the effect of pH and carbonation. *Waste Management* **32**, 278–286 (2012).

103. Verbinnen, B., Van Caneghem, J., Billen, P. & Vandecasteele, C. Long Term Leaching Behavior of Antimony from MSWI Bottom Ash: Influence of Mineral Additives and of Organic Acids. *Waste and Biomass Valorization* **8**, 2545–2552 (2017).

104. Quina, M.J., Bordado, J.C.M. & Quinta-Ferreira, R.M. The influence of pH on the leaching behaviour of inorganic components from municipal solid waste APC residues. *Waste Management* **29**, 2483–2493 (2009).

105. Goumans, J.J.J.M., van der Sloot, H.A. & Aalbers, Th.G. Waste materials in construction. in *Proceedings of the International Conference on Environmental Implications of Construction with Waste Materials* 672 (Elsevier, 1991).

106. Lovell, C.W., Ke, T.C., Huang, W.H. & Lovel, J.E. Bottom ash as highway material. in *70th annual meeting of the transportation research board* 106–116 (Transportation Research Board, 1991).

107. Ferreira, C., Ribeiro, A.B. & Ottosen, L.M. Study of different assisting agents for the removal of heavy metals from MSW fly ashes. in *Waste Management and the Environment* (eds. Almorza, D., Brebbia, C. A., Sales, D. & Popov, V.) 171–179 (WIT Press, 2002).

108. Mangialardi, T. Disposal of MSWI fly ash through a combined washing-immobilisation process. *Journal of Hazardous Materials* **98**, 225–240 (2003).

109. Eighmy, T.T., Crannell, B.S., Butler, L.G., Cartledge, F.K., Emery, E.F., Oblas, D., Krzanowski, J.E., Eusden, J.D., Shaw, E.L. & Francis, C.A. Heavy metal stabilization in municipal solid waste combustion dry scrubber residue using soluble phosphate. *Environmental Science and Technology* **31**, 3330–3338 (1998).

110. Quina, M.J., Bordado, J.C.M. & Quinta-Ferreira, R.M. Chemical stabilization of air pollution control residues from municipal solid waste incineration. *J Hazard Mater* **179**, 382–92 (2010).

111. Li, X., Chen, Q., Zhou, Y., Tyrer, M. & Yu, Y. Stabilization of heavy metals in MSWI fly ash using silica fume. *Waste Management* **34**, 2494–2504 (2014).

112. Ecke, H. Sequestration of metals in carbonated municipal solid waste incineration (MSWI) fly ash. *Waste Management* **23**, 631–640 (2003).

113. De Boom, A., Aubert, J.-E. & Degrez, M. Carbonation of municipal solid waste incineration electrostatic precipitator fly ashes in solution. *Waste Management & Research* **32**, 406–413 (2014).

114. Wey, M.-Y., Liu, K.-Y., Tsai, T.-H. & Chou, J.-T. Thermal treatment of the fly ash from municipal solid waste incinerator with rotary kiln. *Journal of Hazardous Materials* **137**, 981–989 (2006).

115. Huber, F., Blasenbauer, D., Mallow, O., Lederer, J., Winter, F. & Fellner, J. Thermal co-treatment of combustible hazardous waste and waste incineration fly ash in a rotary kiln. *Waste Management* **58**, 181–190 (2016).

116. Pedersen, A.J. Evaluation of assisting agents for electrodialytic removal of Cd, Pb, Zn, Cu and Cr from MSWI fly ash. *Journal of Hazardous Materials* **95**, 185–198 (2002).

117. Kersch, C., Woerlee, G.F. & Witkamp, G.J. Supercritical Fluid Extraction of Heavy Metals from Fly Ash. *Industrial & Engineering Chemistry Research* **43(1)**, 190–196 (2003).

118. Karlfeldt Fedje, K., Ekberg, C., Skarnemark, G., Pires, E. & Steenari, B.-M. Initial studies of the recovery of Cu from MSWI fly ash leachates using solvent extraction. *Waste Management & Research* **30**, 1072–1080 (2012).

119. Tang, J. & Steenari, B.M. Solvent extraction separation of copper and zinc from MSWI fly ash leachates. *Waste Management* **44**, (2015).

120. Tang, J., Petranikova, M., Ekberg, C. & Steenari, B.-M. Mixer-settler system for the recovery of copper and zinc from MSWI fly ash leachates: An evaluation of a hydrometallurgical process. *Journal of Cleaner Production* **148**, 595–605 (2017).

121. Colangelo, F., Messina, F. & Cioffi, R. Recycling of MSWI fly ash by means of cementitious double step cold bonding pelletization: Technological assessment for the production of lightweight artificial aggregates. *Journal of Hazardous Materials* **299**, 181–191 (2015).

122. Hoi, C., Lam, K., Patrick, J., Bullet, B. & Mckay, G. Utilization of municipal solid waste incineration ash in Portland cement clinker. *Clean Technologies and Environmental Policy* **13**, 607–615 (2011).

123. Mishra, D.P. & Das, S.K. A study of physico-chemical and mineralogical properties of Talcher coal fly ash for stowing in underground coal mines. *Materials Characterization* **61**, 1252–1259 (2010).

124. Kitamura, H., Sawada, T., Shimaoka, T. & Takahashi, F. Geochemically structural characteristics of municipal solid waste incineration fly ash particles and mineralogical surface conversions by chelate treatment. *Environmental Science and Pollution Research* **23**, 734–743 (2016).

125. Martell, A.E. & Sillén, L.G. Stability Constants of Metal-ion Complexes: Inorganic ligands. (Chemical Society, 1971).

126. EN 12457-4. Characterisation of waste - Leaching - Compliance test for leaching of granular waste materials and sludges. (CEN, 2002).

127. Dutch Soil Quality Decree. Regulation of the State Secretary for Housing, Planning and the Environment and the State Secretary for Transport, Public Works and Water Management, The Netherlands. (Staatscourant nr. 469, 3 December 2007, 2007).

128. Colangelo, F., Cioffi, R., Montagnaro, F. & Santoro, L. Soluble salt removal from MSWI fly ash and its stabilization for safer disposal and recovery as road basement material. *Waste Management* **32**, 1179–1185 (2012).

129. De Boom, A. & Degrez, M. Combining sieving and washing, a way to treat MSWI boiler fly ash. *Waste Management* **39**, (2015).

130. Mulder, E. Pre-Treatment of MSWI fly ash for useful application. *Waste Management* **16**, 181–184 (1996).

131. Thongsanitgarn, P., Wongkeo, W. & Chaipanich, A. Hydration and Compressive Strength of Blended Cement Containing Fly Ash and Limestone as Cement Replacement. *Journal of Materials in Civil Engineering* **26**, 401–408 (2014).

132. Wang, L., Jin, Y. & Nie, Y. Investigation of accelerated and natural carbonation of MSWI fly ash with a high content of Ca. *Journal of Hazardous Materials* **174**, 334–343 (2010).

133. Sawyer, D.T. Metal-Gluconate Complexes. *Chemical Reviews* **64**, 633–643 (1964).

134. Warwick, P., Evans, N. & Vines, S. Studies on metal gluconic acid complexes. *29th International Symposium on the Scientific Basis for Nuclear Waste Management* **932**, 959–966 (2005).

135. Dojindo. Metal Chelates. *Analytical & Biological Products* **13**, 252–253 (2017).

136. Jankowski, J., Ward, C.R., French, D. & Groves, S. Mobility of trace elements from selected Australian fly ashes and its potential impact on aquatic ecosystems. *Fuel* **85**, 243–256 (2006).

137. van der Hoek, E.E., Bonouvrie, P.A. & Comans, R.N.J. Sorption of As and Se on mineral components of fly ash: Relevance for leaching processes. *Applied Geochemistry* **9**, 403–412 (1994).

138. Hulett, L.D., Weinberger, A.J., Northcutt, K.J. & Ferguson, M. Chemical Species in Fly Ash from Coal-Burning Power Plants. *Science (1979)* **210**, 1356–1358 (1980).

139. Senior, C.L., Bool, L.E. & Morency, J.R. Laboratory study of trace element vaporization from combustion of pulverized coal. *Fuel Processing Technology* **63**, 109–124 (2000).

140. Dijkstra, J.J., Meeussen, J.C.L. & Comans, R.N.J. Leaching of Heavy Metals from Contaminated Soils: An Experimental and Modeling Study. *Environmental Science & Technology* **38**, 4390–4395 (2004).

141. Izquierdo, M. & Querol, X. Leaching behaviour of elements from coal combustion fly ash: An overview. *International Journal of Coal Geology* **94**, 54–66 (2012).

142. Jung, C.-H. & Osako, M. Leaching characteristics of rare metal elements and chlorine in fly ash from ash melting plants for metal recovery. *Waste Management* **29**, 1532–1540 (2009).

143. Hou, H., Takamatsu, T., Koshikawa, M.K. & Hosomi, M. Concentrations of Ag, In, Sn, Sb and Bi, and their chemical fractionation in typical soils in Japan. *European Journal of Soil Science* **57**, 214–227 (2006).

144. Spears, D.A. The use of laser ablation inductively coupled plasma-mass spectrometry (LA ICP-MS) for the analysis of fly ash. *Fuel* **83**, 1765–1770 (2004).

145. Vu, D.H., Wang, K.-S., Chen, J.-H., Nam, B.X. & Bac, B.H. Glass–ceramic from mixtures of bottom ash and fly ash. *Waste Management* **32**, 2306–2314 (2012).

146. Ferone, C., Colangelo, F., Messina, F., Santoro, L. & Cioffi, R. Recycling of Pre-Washed Municipal Solid Waste Incinerator Fly Ash in the Manufacturing of Low Temperature Setting Geopolymer Materials. *Materials* **6**, 3420–3437 (2013).

147. Wan, X., Wang, W., Ye, T., Guo, Y. & Gao, X. A study on the chemical and mineralogical characterization of MSWI fly ash using a sequential extraction procedure. *Journal of Hazardous Materials* **134**, 197–201 (2006).

148. Bayuseno, A.P. & Schmahl, W.W. Characterization of MSWI fly ash through mineralogy and water extraction. *Resources, Conservation and Recycling* **55**, 524–534 (2011).

149. Braissant, O., Cailleau, G., Dupraz, C. & Verrecchia, E.P. Bacterially Induced Mineralization of Calcium Carbonate in Terrestrial Environments: The Role of Exopolysaccharides and Amino Acids. *Journal of Sedimentary Research* **73**, 485–490 (2003).

150. Wang, L., Sondi, I. & Matijević, E. Preparation of Uniform Needle-Like Aragonite Particles by Homogeneous Precipitation. *Journal of Colloid and Interface Science* **218**, 545–553 (1999).

151. Wang, X., Ye, J., Wang, Y., Wu, X. & Bai, B. Control of crystallinity of hydrated products in a calcium phosphate bone cement. *Journal of Biomedical Materials Research Part A* **81A**, 781–790 (2007).

152. Doudart de la Grée, G.C.H., Florea, M.V.A., Keulen, A. & Brouwers, H.J.H. Contaminated biomass fly ashes - Characterization and treatment optimization for reuse as building materials. *Waste Management* **49**, 96–109 (2015).

153. Buffle, J., Greter, F.L. & Haerdi, W. Measurement of complexation properties of humic and fulvic acids in natural waters with lead and copper ion-selective electrodes. *Analytical Chemistry* **49**, 216–222 (1977).

154. Lu, H., Zhang, W., Yang, Y., Huang, X., Wang, S. & Qiu, R. Relative distribution of Pb2+ sorption mechanisms by sludge-derived biochar. *Water Research* **46**, 854–862 (2012).

155. Tang, P., Florea, M.V.A., Spiesz, P. & Brouwers, H.J.H. Application of thermally activated municipal solid waste incineration (MSWI) bottom ash fines as binder substitute. *Cement and Concrete Composites* **70**, 194–205 (2016).

156. Kim, H.K., Jeon, J.H. & Lee, H.K. Flow, water absorption, and mechanical characteristics of normal- and high-strength mortar incorporating fine bottom ash aggregates. *Construction and Building Materials* **26**, 249–256 (2012).

157. Lynn, C.J., Ravindra, K., & Ghataora, G.S. Municipal incinerated bottom ash characteristics and potential for use as aggregate in concrete. *Construction and Building Materials* **127**, 504–517 (2016).

158. Saikia, N., Cornelis, G., Mertens, G., Elsen, J., van Balen, K., van Gerven, T. & Vandecasteele, C. Assessment of Pb-slag, MSWI bottom ash and boiler and fly ash for using as a fine aggregate in cement mortar. *Journal of Hazardous Materials* **154**, 766–777 (2008).

159. Aubert, J.E., Husson, B. & Vaquier, A. Metallic aluminum in MSWI fly ash: quantification and influence on the properties of cement-based products. *Waste Management* **24**, 589–596 (2004).

160. Aubert, J.E., Husson, B. & Sarramone, N. Utilization of municipal solid waste incineration (MSWI) fly ash in blended cement: Part 2. Mechanical strength of mortars and environmental impact. *Journal of Hazardous Materials* **146**, 12–19 (2007).

161. Yang, Z., Tian, S., Liu, L., Wang, X. & Zhang, Z. Recycling ground MSWI bottom ash in cement composites: Long-term environmental impacts. *Waste Management* **78**, 841–848 (2018).

162. An, J., Kim, J. & Nam, B.H. Investigation on Impacts of Municipal Solid Waste Incineration Bottom Ash on Cement Hydration. *ACI Materials Journal* **114**, (2017).

163. Pan, J.R., Huang, C., Kuo, J.-J. & Lin, S.-H. Recycling MSWI bottom and fly ash as raw materials for Portland cement. *Waste Management* **28**, 1113–1118 (2008).

164. Lawrence, P., Cyr, M. & Ringot, E. Mineral admixtures in mortars: Effect of inert materials on short-term hydration. *Cement and Concrete Research* **33**, 1939–1947 (2003).

165. Wei, Y., Shimaoka, T., Saffarzadeh, A. & Takahashi, F. Alteration of municipal solid waste incineration bottom ash focusing on the evolution of iron-rich constituents. *Waste Management* **31**, 1992–2000 (2011).

166. Johnson, C.A. & Furrer, G. Influence of Biodegradation Processes on the Duration of $CaCO_3$ as a pH Buffer in Municipal Solid Waste Incinerator Bottom Ash. *Environmental Science & Technology* **36**, 215–220 (2002).

167. Wilińska, I. & Pacewska, B. Influence of selected activating methods on hydration processes of mixtures containing high and very high amount of fly ash: A review. *Journal of Thermal Analysis and Calorimetry* **133**, 823–843 Preprint at https://doi.org/10.1007/s10973-017-6915-y (2018).

168. Patil, A.G. & Anandhan, S. Influence of planetary ball milling parameters on the mechano-chemical activation of fly ash. *Powder Technology* **281**, 151–158 (2015).

169. Sadique, M., Al-Nageim, H., Atherton, W., Seton, L. & Dempster, N. Mechano-chemical activation of high-Ca fly ash by cement free blending and gypsum aided grinding. *Construction and Building Materials* **43**, 480–489 (2013).

170. Vdovic, N., Jurina, I., Škapin, S.D. & Sondi, I. The surface properties of clay minerals modified by intensive dry milling - revisited. *Applied Clay Science* **48**, 575–580 (2010).

171. Al Saffar, D.M., Al Saad, A.J.K. & Tayeh, B.A. Effect of internal curing on behavior of high performance concrete: An overview. *Case Studies in Construction Materials* **10**, e00229 (2019).

172. Bentz, D.P., Garboczi, E.J., Haecker, C.J. & Jensen, O.M. Effects of cement particle size distribution on performance properties of Portland cement-based materials. *Cement and Concrete Research* **29**, 1663–1671 (1999).

173. Pelletier-Chaignat, L., Winnefeld, F., Lothenbach, B., Saout, G.L., Müller, C.J. & Famy, C. Influence of the calcium sulphate source on the hydration mechanism of Portland cement-calcium sulphoaluminate clinker-calcium sulphate binders. *Cement and Concrete Composites* **33**, 551–561 (2011).

174. Razavi-Tousi, S.S. & Szpunar, J.A. Effect of ball size on steady state of aluminum powder and efficiency of impacts during milling. *Powder Technology* **284**, 149–158 (2015).

175. Templeton, C.C. Solubility of Barium Sulfate in Sodium Chloride Solutions from 25° to 95°C. *Journal of Chemical and Engineering Data* **5**, 514–516 (1960).

176. Lin, W.Y., Heng, K.S., Sun, X. & Wang, J.Y. Influence of moisture content and temperature on degree of carbonation and the effect on Cu and Cr leaching from incineration bottom ash. *Waste Management* **43**, (2015).

177. Lenormand, T., Rozière, E., Loukili, A. & Staquet, S. Incorporation of treated municipal solid waste incineration electrostatic precipitator fly ash as partial replacement of Portland cement: Effect on early age behaviour and mechanical properties. *Construction and Building Materials* **96**, (2015).

178. van Eijk, R.J. Hydration of cement mixtures containing contaminants. PhD thesis, University of Twente (2001).

179. Caprai, V., Schollbach, K., Florea, M.V.A. & Brouwers, H.J.H. Evaluation of municipal solid waste incineration filter cake as supplementary cementitious material. *Construction and Building Materials* **250**, 118833 (2020).

180. van Zomeren, A. & Comans, R.N.J. Contribution of Natural Organic Matter to Copper Leaching from Municipal Solid Waste Incinerator Bottom Ash. *Environmental Science & Technology* **38**, 3927–3932 (2004).

181. Meima, J.A. & Comans, R.N.J. Overview of Geochemical Processes Controlling Leaching Characteristics of MSWI Bottom Ash. *Studies in Environmental Science* **71**, 447–457 (1997). doi:10.1016/S0166-1116(97)80228-2.

182. Rivard-Lentz, D., Sweeney, L. & Demars, K. Incinerator Bottom Ash as a Soil Substitute: Physical and Chemical Behavior. in *Testing Soil Mixed with Waste or Recycled Materials* 246-246–17 (ASTM International, 1997). doi:10.1520/STP15656S.

183. Bayuseno, A.P. & Schmahl, W.W. Understanding the chemical and mineralogical properties of the inorganic portion of MSWI bottom ash. *Waste Management* **30**, 1509–1520 (2010).

184. Arickx, S., Van Gerven, T., Knaepkens, T., Hindrix, K., Evens, R. & Vandecasteele, C. Influence of treatment techniques on Cu leaching and different organic fractions in MSWI bottom ash leachate. *Waste Management* **27**, 1422–1427 (2007).

185. Holm, O. & Simon, F.-G. Innovative treatment trains of bottom ash (BA) from municipal solid waste incineration (MSWI) in Germany. *Waste Management* **59**, 229–236 (2017).

186. Saikia, N., Mertens, G., van Balen, K., Elsen, J., van Gerven, T. & Vandecasteele, C. Pre-treatment of municipal solid waste incineration (MSWI) bottom ash for utilisation in cement mortar. *Construction and Building Materials* **96**, 76–85 (2015).

187. Wunsch, P., Greilinger, C., Bieniek, D. & Kettrup, A. Investigation of the binding of heavy metals in thermally treated residues from waste incineration. *Chemosphere* **32**, 2211–2218 (1996).

188. Arickx, S., van Gerven, T., Boydens, E., L'hoëst, P., Blanpain, B. & Vandecasteele, C. Speciation of Cu in MSWI bottom ash and its relation to Cu leaching. *Applied Geochemistry* **23**, 3642–3650 (2008).

189. Yang, S., Saffarzadeh, A., Shimaoka, T. & Kawano, T. Existence of Cl in municipal solid waste incineration bottom ash and dechlorination effect of thermal treatment. *Journal of Hazardous Materials* **267**, 214–220 (2014).

190. Ito, R., Dodbiba, G., Fujita, T. & Ahn, J.W. Removal of insoluble chloride from bottom ash for recycling. *Waste Management* **28**, 1317–1323 (2008).

191. Ramzi Hannan, N.I.R., Shahidan, S., Maarof, M.Z. & Ali, N. Physical and Chemical Properties of Coal Bottom Ash (CBA) from Tanjung Bin Power Plant. *IOP Conference Series: Materials Science and Engineering* **160**, 12056 (2016).

192. Forteza, R., Far, M., Segui, C. & Cerda, V. Characterization of bottom ash in municipal solid waste incinerators for its use in road base. *Waste Manag* **24**, 899–909 (2004).

193. Lynn, C.J., Ghataora, G.S. & Ravinda, K. Municipal Incinerated Bottom Ash (MIBA) Characteristics and Potential for Use in Road Pavements. *International Journal of Pavement Research and Technology* **10**, 185–201 (2016).

194. Alhassan, H.M., Musa, A., Alhassan, H.M. & Tanko, A.M. Characterization of Solid Waste Incinerator Bottom Ash and the Potential for its Use. *International Journal of Engineering Research and Applications* **2**, 516–522 (2012).

195. Dechaux, C., Nitschelm, L., Giard, L., Bioteau, T., Sessiecq, P. & Aissani, L. Development of the regionalised municipal solid waste incineration (RMWI) model and its application to France. *International Journal of Life Cycle Assessment* 1–29 (2017) doi:10.1007/s11367-017-1268-0.

196. Koehler, A., Peyer, F., Salzmann, C. & Saner, D. Probabilistic and technology-specific modeling of emissions from municipal solid-waste incineration. *Environmental Science and Technology* **45**, 3487–3495 (2011).

197. Chimenos, J.M., Fernández, A.I., Miralles, L., Segarra, M. & Espiell, F. Short-term natural weathering of MSWI bottom ash as a function of particle size. *Waste Management* **23**, 887–895 (2003).

198. Meima, J.A. & Comans, R.N.J. Geochemical modeling of weathering reactions in municipal solid waste incinerator bottom ash. *Environmental Science and Technology* **31**, 1269–1276 (1997).

199. Engelsen, C.J., van der Sloot, H.A. & Petkovic, G. Long-term leaching from recycled concrete aggregates applied as sub-base material in road construction. *Science of the Total Environment* **587–588**, (2017).

200. van der Sloot, H.A., Kosson, D.S. & van Zomeren, A. Leaching, geochemical modelling and field verification of a municipal solid waste and a predominantly non-degradable waste landfill. *Waste Management* Preprint at https://doi.org/10.1016/j.wasman.2016.07.032 (2016).

201. Park, J.Y. & Batchelor, B.A multi-component numerical leach model coupled with a general chemical speciation code. *Water Research* **36**, 156–166 (2002).

202. Dijkstra, J.J., van der Sloot, H.A. & Comans, R.N.J. Process identification and model development of contaminant transport in MSWI bottom ash. *Waste Management* **22**, 531–541 (2002).

203. Dijkstra, J.J., Meeussen, J.C.L., van der Sloot, H.A. & Comans, R.N.J. A consistent geochemical modelling approach for the leaching and reactive transport of major and trace elements in MSWI bottom ash. *Applied Geochemistry* **23**, 1544–1562 (2008).

204. Funari, V., Braga, R., Bokhari, S.N., Dinelli, E. & Meisel, T. Solid residues from Italian municipal solid waste incinerators: A source for “critical” raw materials. *Waste Manag* **45**, 206–216 (2015).

205. Meawad, A.S., Bojinova, D.Y. & Pelovski, Y.G. An overview of metals recovery from thermal power plant solid wastes. *Waste Management* **30**, 2548–2559 (2010).

206. Kraml, G. & Gritzner, G. Electrochemical measurements in the solvents hexamethylphosphoric triamide and hexamethylthiophosphoric triamide. *Journal of the Chemical Society, Faraday Transactions 1: Physical Chemistry in Condensed Phases* **81**, 2875–2888 (1985).

207. Zhang, H., He, P.J. & Shao, L.M. Fate of heavy metals during municipal solid waste incineration in Shanghai. *Journal of Hazardous Materials* **156**, 365–373 (2008).

208. Todorovic, J. & Ecke, H. Demobilisation of critical contaminants in four typical waste-to-energy ashes by carbonation. *Waste Management* **26**, 430–441 (2006).

Symbols and abbreviations

Acronyms

AAS	Atomic Absorption Spectrometry
APCr	Air Pollution Control residues
BA	Municipal Solid Waste Incineration Bottom Ash
BACF	Bottom Ash Coarse Fines
BET	Brunauer–Emmett–Teller
BF	Basic Fines, BA < 0.125 mm
CCFA	Coal-Combustion Fly Ash
EDTA	EthyleneDiamineTetraAcetate
EDX	Energy-Dispersive X-ray Spectroscopy
FA	Municipal Solid Waste Incineration Fly Ash
FTIR	Fourier-Transform Infrared Spectroscopy
IC	Ion chromatography
ICP–AES	Inductively Coupled Plasma Atomic Emission Spectrometry
L/S	Liquid to Solid ratio
LL	Legislation Limit
LOD	Limit Of Detection
LOI	Loss On Ignition
LOQ	Limit Of Quantification
MAC	Minor Additional Constituent
MCF	Milled Coarse Fines, BA 0.125 - 3 mm
MSW	Municipal Solid Waste
MSWI	Municipal Solid Waste Incineration
MSWI BA	Municipal Solid Waste Incineration Bottom Ash
MSWI FA	Municipal Solid Waste Incineration Fly Ash
Na-Gl	Sodium Gluconate
PC	Ordinary Portland Cement
PARC	PhAse Recognition and Characterization
PSD	Particle Size Distribution
PTE	Potentially Toxic Elements
RSD	Relative Standard Deviation
SEM	Scanning Electron Microscopy
SOF-42	Size Optimized Fines, MCF milled close to the size of CEM 42.5 N
SOF-52	Size Optimized Fines, MCF milled close to the size of CEM 52.5 R
SSA	Specific Surface Area

XRD	X-Ray Diffraction analysis
XRF	X-Ray Fluorescence spectroscopy

Formulas and idealized mineral formulas

Alite	C_3S	$3CaO{\cdot}SiO_2$
Aluminate	C_3A	$3CaO{\cdot}Al_2O_3$
Anhydrite	$CaSO_4$	
Apatite	$Ca_{10}(PO_4)_6(OH,F,Cl)_2$	
Barium sulfate	$BaSO_4$	
Bassanite	$2CaSO_4{\cdot}H_2O$	
Belite	C_2S	$2CaO{\cdot}SiO_2$
Brownmillerite	$Ca_2(Al,Fe)_2O_5$	
Calcite	$CaCO_3$	
Calcium hydroxide	CH	
Calcium silicate hydrate	$C_3S_2H_8$	
EDTA	$C_{10}H_{14}N_2Na_2O_8$	
Ettringite	$C_6A\hat{S}_3H_{32}$	
Feldspar	$KAlSi_3O_8 – NaAlSi_3O_8 – CaAl_2Si_2O_8$	
Gypsum	$C\hat{S}H_2$	$CaSO_4{\cdot}2H_2O$
Halite	NaCl	
Hematite	Fe_2O_3	
Hydrochloric acid	HCl	
Hydrofluoric acid	HF	
Ilmenite	$FeTiO_3$	
Limestone	$CaCO_3$	
Lithium bromide	LiBr	
Lithium metaborate	$LiBO_2$	
Lithium tetraborate	$Li_2B_4O_7$	
Magnesite	$MgCO_3$	
Melilite	$(Ca,Na)_2(Al,Mg,Fe^{2+})[(Al,Si)SiO_7]$	
Mg ferrite	$MgFe_2O_4$	
Mica	$AB_{2–3}(X, Si)_4O_{10}(O, F, OH)_2$	
Nitric acid	HNO_3	
Pyroxene	$XY(Si,Al)_2O_6$, X - Ca, Na, Fe, or Mg, rarely Zn, Mn, or Li; Y - Cr, Al, Mg, Co, Mn, Sc, Ti, V, or Fe	
Quartz	SiO_2	
Rutile	TiO_2	
Sitinakite	$KNa_2Ti_4(SiO_4)_2O_5(OH) \cdot 4H_2O$	
Sodium carbonate	Na_2CO_3	
Sodium gluconate	$NaC_6H_{11}O_7$	
Sphalerite	(Zn,Fe)S	
Spinel	$MgAl_2O_4$	
Sylvite	KCl	
Tricalcium aluminate	C_3A	
Tricalcium silicate	C_3S	
Willemite	Zn_2SiO_4	
Wustite	FeO	
Zeolite	$Na_2Al_2Si_3O_{10}{\cdot}2H_2O$	

APPENDIX: A

RSD values for total microelemental determination (BA fractions)

Table A.1 RSD values for total microelemental determination for 14 particle size fractions of BA (n = 3, P = 0.95); all values are multiplied by 10^3.

P. size\ Element		Al	Ba	Ca	Cd	Co	Cr	Cu	Fe	Mg	Mn	Na	Ni	Pb	Si	Sr	Sb	Sn	Ti	V	Zn	S	P
<63		130	96	24	220	110	110	71	10	72	15	49	150	66	68	62	120	10	100	120	18	32	89
63 - 90		120	150	45	41	15	130	73	18	88	38	30	88	19	57	91	190	42	110	140	43	22	100
90 - 125		100	110	81	170	75	150	61	19	110	45	26	57	47	18	140	190	57	100	110	110	180	86
125-180	**um**	130	79	29	81	12	160	83	16	76	38	33	66	14	75	77	150	54	92	100	42	11	83
180 - 250		130	100	60	190	74	150	68	15	79	25	41	48	29	37	76	190	110	100	110	43	100	120
250 - 355		110	120	28	120	30	92	52	56	57	23	71	160	14	70	73	250	200	100	120	25	50	88
355-710		140	220	13	13	190	150	51	47	60	71	66	160	28	92	37	170	28	81	120	100	270	93
0.71 - 1		160	100	53	15	28	84	60	49	85	130	71	110	74	41	74	190	19	120	140	12	82	40
1 - 2		61	48	17	290	110	71	130	39	47	53	45	100	54	27	64	18	400	64	30	49	130	44
2-2.8		46	60	41	17	150	54	29	35	13	26	84	31	12	15	77	39	22	11	38	98	23	20
2.8 - 4	**mm**	85	91	11	16	70	200	76	26	19	66	41	17	550	13	53	170	88	19	120	27	22	20
4 - 11.2		45	7	40	11	51	32	33	31	14	37	47	55	37	28	42	94	490	11	21	97	52	340
11.2 - 22.4		49	69	16	13	110	75	190	41	28	97	12	110	17	14	43	46	180	930	17	58	88	56
> 22.4		34	130	59	19	28	260	220	180	12	260	130	37	150	18	68	210	150	110	14	81	13	130

APPENDIX: B

Scheme of the study of the MSWI BA fines

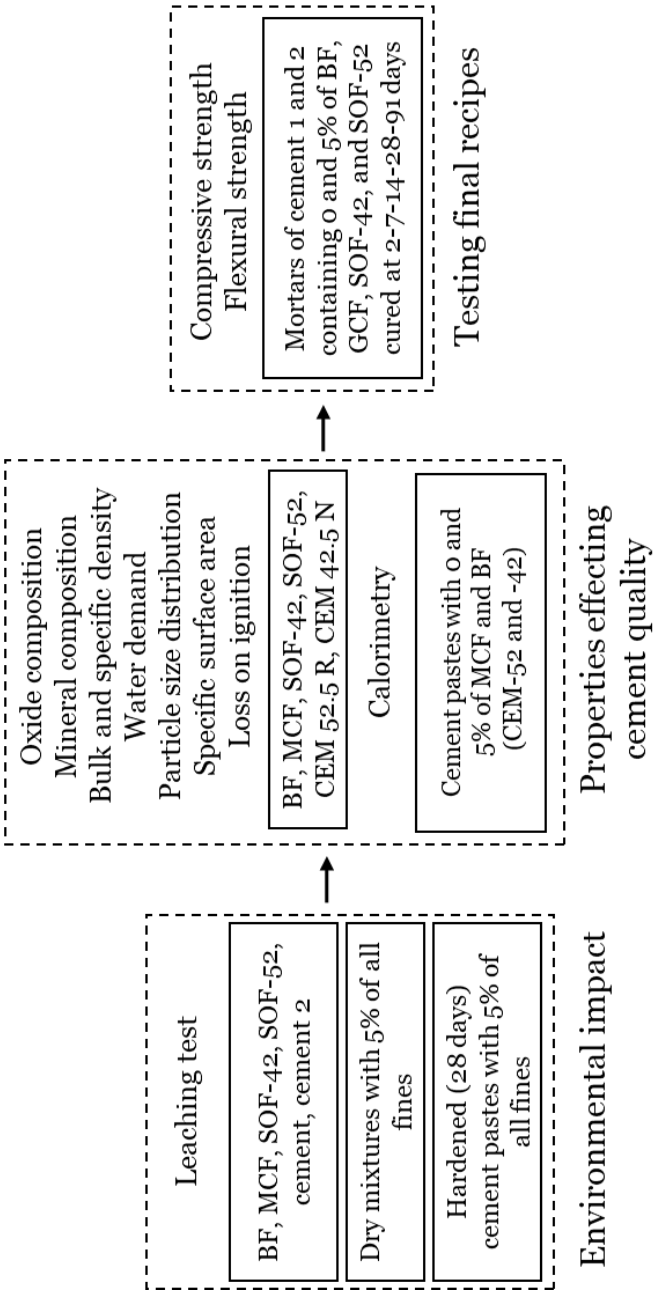

Figure B.1 Scheme of the study of MSWI BA fines.

APPENDIX: C

Relative standard deviation for each point of the leaching model for all elements (MSWI BA)

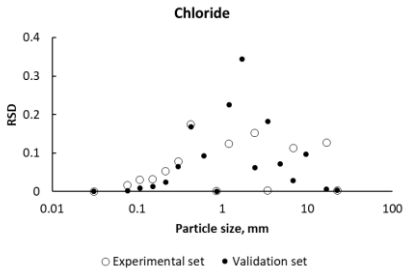
Chloride
RSD
Particle size, mm
Experimental set
Validation set

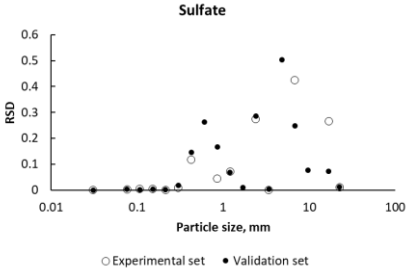
Sulfate
RSD
Particle size, mm
Experimental set
Validation set

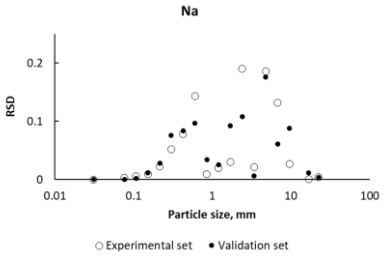
Na
RSD
Particle size, mm
Experimental set
Validation set

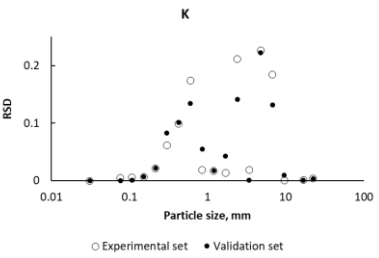
K
RSD
Particle size, mm
Experimental set
Validation set

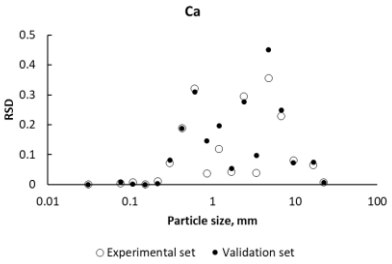
Ca
RSD
Particle size, mm
Experimental set
Validation set

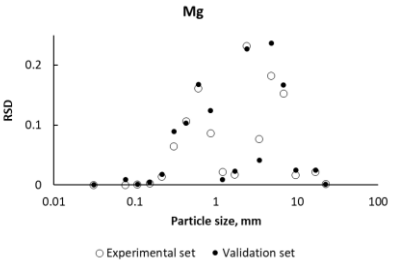
Mg
RSD
Particle size, mm
Experimental set
Validation set

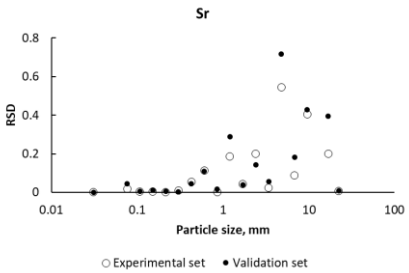
Sr
RSD
Particle size, mm
Experimental set
Validation set

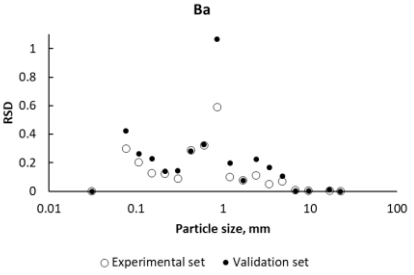
Ba
RSD
Particle size, mm
Experimental set
Validation set

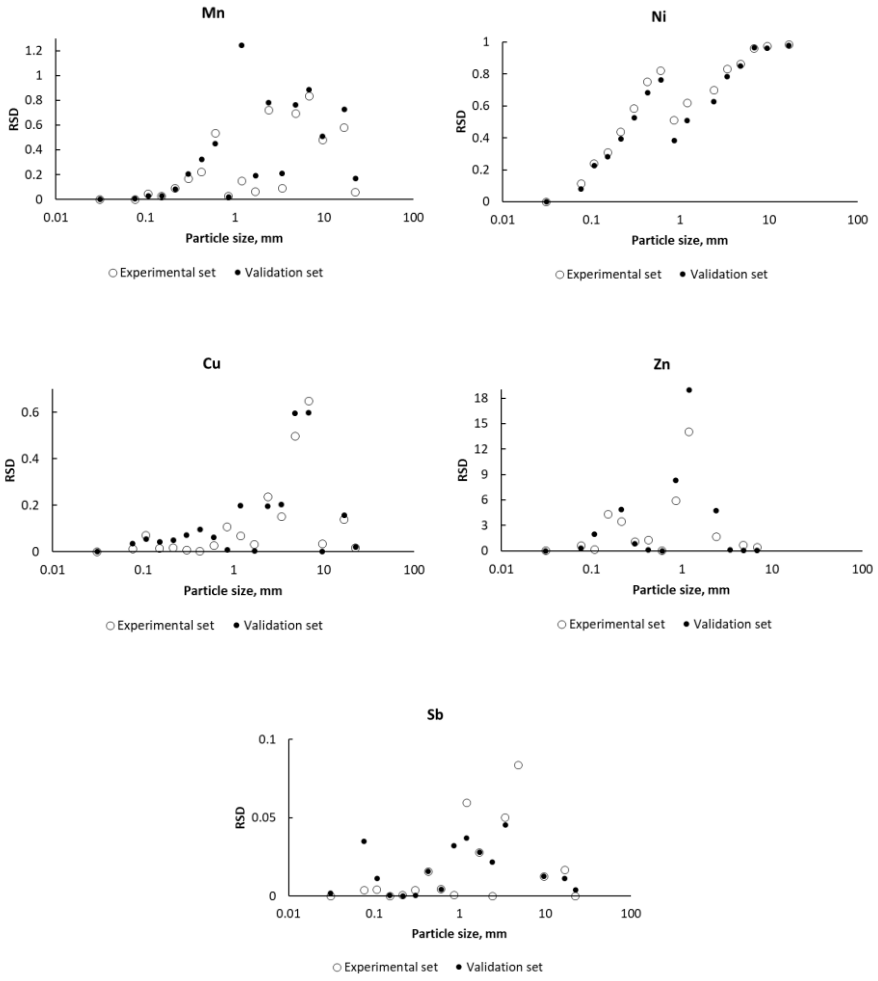

Figure C.1 RSDs for each data point of all elements for the leaching model (MSWI BA).

List of publications

Peer-Reviewed Journal Publications

1. **Loginova, E.**, Volkov, D. S., van de Wouw, P. M. F., Florea, M. V. A. & Brouwers, H. J. H., 2019. Detailed characterization of particle size fractions of municipal solid waste incineration bottom ash. Journal of Cleaner Production. 207, p. 866-874.

2. **Loginova, E.**, Proskurnin, M. & Brouwers, H. J. H., 2019. Municipal solid waste incineration (MSWI) fly ash composition analysis: a case study of combined chelatant-based washing treatment efficiency. Journal of Environmental Management. 235, p. 480-488.

3. van de Wouw, P. M. F., **Loginova, E.**, Florea, M. V. A. & Brouwers, H. J. H., 2020. Compositional modelling and crushing behaviour of MSWI bottom ash material classes. Waste Management. 101, p. 268-282.

4. **Loginova, E.**, Schollbach, K., Proskurnin, M. & Brouwers, H. J. H., 2021. Municipal Solid Waste Incineration Bottom Ash Fines: Transformation into a Minor Additional Constituent for Cements. Resources, Conservation and Recycling. 166, p. 105354.

5. **E. Loginova**, K. Schollbach, M. Proskurnin, H.J.H. Brouwers. Waste recycling in structural building components: Mechanical performance and microstructural properties of cement mortars containing BA as a minor additional constituent (submitted).

6. **E. Loginova**, K. Schollbach, M. Proskurnin, H.J.H. Brouwers. The connection between BA leaching and the quenching layer. Empirical leaching model (submitted).

Conference Proceedings

1. **Loginova, E.**, Florea, M. V. A. & Brouwers, H. J. H., 2017. Estimation of the environmental impact of MSWI bottom ash for reuse as a building material based on its composition, in: Proceedings of the 6th International Conference on Non-traditional Cement & Concrete. Brno, Czech Republic, pp. 217-225.

2. **E. Loginova**, P. Kalle, M.A. Proskurnin, H.J.H. Brouwers, 2017. Multicomponent identification and quantification of municipal solid waste

incineration bottom ash by FTIR, in 19th Euroanalysis Europe's Analytical Chemistry Meeting. Stockholm, Sweden.

3. **E. Loginova,** D.S. Volkov, M.V.A. Florea, H.J.H. Brouwers, 2018. Total metal composition analysis of MSWI bottom ash by ICP-AES for the estimation of its environmental impact, in: NAXOS 2018 6th International Conference on Sustainable Solid Waste Management, Naxos Island, Greece.

Curriculum Vitae

Ekaterina Loginova was born in 1991 in Penza-19, USSR (currently, Zarechny, Penza region, Russia). She obtained her specialization (equals to the Master of Science degree) in chemistry from the Lomonosov Moscow State University, Moscow, Russia in 2013. Her diploma work focused on the development of techniques for FTIR spectroscopic determination of the composition of copolymers of acrylic acid. Her diploma work resulted in creating of a patent «Method for IR-spectroscopic determination of the composition of acrylic acid copolymers». Afterward, for 1 year during the post-graduation study, she taught analytical chemistry at the Chemistry Department of the Lomonosov Moscow State University, Moscow, Russia. In 2016, she started a Ph.D. project in the Building Materials research group under the supervision of prof.dr.ir. H.J.H. Brouwers at the Eindhoven University of Technology, Eindhoven, the Netherlands, where she worked on the characterization, analysis, and treatments of Municipal Solid Waste Incineration residues to transform them into secondary building materials. The results of this work are presented in this dissertation.

Bouwstenen is een publicatiereeks
van de Faculteit Bouwkunde,
Technische Universiteit Eindhoven.
Zij presenteert resultaten van
onderzoek en andere activiteiten op
het vakgebied der Bouwkunde,
uitgevoerd in het kader van deze
Faculteit.

Bouwstenen en andere proefschriften van de
TU/e zijn online beschikbaar via:
https://research.tue.nl/

Reeds verschenen in de serie
Bouwstenen

nr 1
Elan: A Computer Model for Building Energy Design: Theory and Validation
Martin H. de Wit
H.H. Driessen
R.M.M. van der Velden

nr 2
Kwaliteit, Keuzevrijheid en Kosten: Evaluatie van Experiment Klarendal, Arnhem
J. Smeets
C. le Nobel
M. Broos
J. Frenken
A. v.d. Sanden

nr 3
Crooswijk: Van 'Bijzonder' naar 'Gewoon'
Vincent Smit
Kees Noort

nr 4
Staal in de Woningbouw
Edwin J.F. Delsing

nr 5
Mathematical Theory of Stressed Skin Action in Profiled Sheeting with Various Edge Conditions
Andre W.A.M.J. van den Bogaard

nr 6
Hoe Berekenbaar en Betrouwbaar is de Coëfficiënt k in x-ksigma en x-ks?
K.B. Lub
A.J. Bosch

nr 7
Het Typologisch Gereedschap: Een Verkennende Studie Omtrent Typologie en Omtrent de Aanpak van Typologisch Onderzoek
J.H. Luiten

nr 8
Informatievoorziening en Beheerprocessen
A. Nauta
Jos Smeets (red.)
Helga Fassbinder (projectleider)
Adrie Proveniers
J. v.d. Moosdijk

nr 9
Strukturering en Verwerking van Tijdgegevens voor de Uitvoering van Bouwwerken
ir. W.F. Schaefer
P.A. Erkelens

nr 10
Stedebouw en de Vorming van een Speciale Wetenschap
K. Doevendans

nr 11
Informatica en Ondersteuning van Ruimtelijke Besluitvorming
G.G. van der Meulen

nr 12
Staal in de Woningbouw, Korrosie-Bescherming van de Begane Grondvloer
Edwin J.F. Delsing

nr 13
Een Thermisch Model voor de Berekening van Staalplaatbetonvloeren onder Brandomstandigheden
A.F. Hamerlinck

nr 14
De Wijkgedachte in Nederland: Gemeenschapsstreven in een Stedebouwkundige Context
K. Doevendans
R. Stolzenburg

nr 15
Diaphragm Effect of Trapezoidally Profiled Steel Sheets: Experimental Research into the Influence of Force Application
Andre W.A.M.J. van den Bogaard

nr 16
Versterken met Spuit-Ferrocement: Het Mechanische Gedrag van met Spuit-Ferrocement Versterkte Gewapend Betonbalken
K.B. Lubir
M.C.G. van Wanroy

nr 17
De Tractaten van Jean Nicolas Louis Durand
G. van Zeyl

nr 18
Wonen onder een Plat Dak: Drie Opstellen over Enkele Vooronderstellingen van de Stedebouw
K. Doevendans

nr 19
Supporting Decision Making Processes: A Graphical and Interactive Analysis of Multivariate Data
W. Adams

nr 20
Self-Help Building Productivity: A Method for Improving House Building by Low-Income Groups Applied to Kenya 1990-2000
P. A. Erkelens

nr 21
De Verdeling van Woningen: Een Kwestie van Onderhandelen
Vincent Smit

nr 22
Flexibiliteit en Kosten in het Ontwerpproces: Een Besluitvormingondersteunend Model
M. Prins

nr 23
Spontane Nederzettingen Begeleid: Voorwaarden en Criteria in Sri Lanka
Po Hin Thung

nr 24
Fundamentals of the Design of Bamboo Structures
Oscar Arce-Villalobos

nr 25
Concepten van de Bouwkunde
M.F.Th. Bax (red.)
H.M.G.J. Trum (red.)

nr 26
Meaning of the Site
Xiaodong Li

nr 27
Het Woonmilieu op Begrip Gebracht: Een Speurtocht naar de Betekenis van het Begrip 'Woonmilieu'
Jaap Ketelaar

nr 28
Urban Environment in Developing Countries
editors: Peter A. Erkelens
George G. van der Meulen (red.)

nr 29
Stategische Plannen voor de Stad: Onderzoek en Planning in Drie Steden
prof.dr. H. Fassbinder (red.)
H. Rikhof (red.)

nr 30
Stedebouwkunde en Stadsbestuur
Piet Beekman

nr 31
De Architectuur van Djenné: Een Onderzoek naar de Historische Stad
P.C.M. Maas

nr 32
Conjoint Experiments and Retail Planning
Harmen Oppewal

nr 33
Strukturformen Indonesischer Bautechnik: Entwicklung Methodischer Grundlagen für eine 'Konstruktive Pattern Language' in Indonesien
Heinz Frick arch. SIA

nr 34
Styles of Architectural Designing: Empirical Research on Working Styles and Personality Dispositions
Anton P.M. van Bakel

nr 35
Conjoint Choice Models for Urban Tourism Planning and Marketing
Benedict Dellaert

nr 36
Stedelijke Planvorming als Co-Produktie
Helga Fassbinder (red.)

nr 37
Design Research in the Netherlands
editors: R.M. Oxman
M.F.Th. Bax
H.H. Achten

nr 38
Communication in the Building Industry
Bauke de Vries

nr 39
Optimaal Dimensioneren van Gelaste Plaatliggers
J.B.W. Stark
F. van Pelt
L.F.M. van Gorp
B.W.E.M. van Hove

nr 40
Huisvesting en Overwinning van Armoede
P.H. Thung
P. Beekman (red.)

nr 41
Urban Habitat: The Environment of Tomorrow
George G. van der Meulen
Peter A. Erkelens

nr 42
A Typology of Joints
John C.M. Olie

nr 43
Modeling Constraints-Based Choices for Leisure Mobility Planning
Marcus P. Stemerding

nr 44
Activity-Based Travel Demand Modeling
Dick Ettema

nr 45
Wind-Induced Pressure Fluctuations on Building Facades
Chris Geurts

nr 46
Generic Representations
Henri Achten

nr 47
Johann Santini Aichel: Architectuur en Ambiguiteit
Dirk De Meyer

nr 48
Concrete Behaviour in Multiaxial Compression
Erik van Geel

nr 49
Modelling Site Selection
Frank Witlox

nr 50
Ecolemma Model
Ferdinand Beetstra

nr 51
Conjoint Approaches to Developing Activity-Based Models
Donggen Wang

nr 52
On the Effectiveness of Ventilation
Ad Roos

nr 53
Conjoint Modeling Approaches for Residential Group preferences
Eric Molin

nr 54
Modelling Architectural Design Information by Features
Jos van Leeuwen

nr 55
A Spatial Decision Support System for the Planning of Retail and Service Facilities
Theo Arentze

nr 56
Integrated Lighting System Assistant
Ellie de Groot

nr 57
Ontwerpend Leren, Leren Ontwerpen
J.T. Boekholt

nr 58
Temporal Aspects of Theme Park Choice Behavior
Astrid Kemperman

nr 59
Ontwerp van een Geïndustrialiseerde Funderingswijze
Faas Moonen

nr 60
Merlin: A Decision Support System for Outdoor Leisure Planning
Manon van Middelkoop

nr 61
The Aura of Modernity
Jos Bosman

nr 62
Urban Form and Activity-Travel Patterns
Daniëlle Snellen

nr 63
Design Research in the Netherlands 2000
Henri Achten

nr 64
Computer Aided Dimensional Control in Building Construction
Rui Wu

nr 65
Beyond Sustainable Building
editors: Peter A. Erkelens
Sander de Jonge
August A.M. van Vliet
co-editor: Ruth J.G. Verhagen

nr 66
Das Globalrecyclingfähige Haus
Hans Löfflad

nr 67
Cool Schools for Hot Suburbs
René J. Dierkx

nr 68
A Bamboo Building Design Decision Support Tool
Fitri Mardjono

nr 69
Driving Rain on Building Envelopes
Fabien van Mook

nr 70
Heating Monumental Churches
Henk Schellen

nr 71
Van Woningverhuurder naar Aanbieder van Woongenot
Patrick Dogge

nr 72
Moisture Transfer Properties of Coated Gypsum
Emile Goossens

nr 73
Plybamboo Wall-Panels for Housing
Guillermo E. González-Beltrán

nr 74
The Future Site-Proceedings
Ger Maas
Frans van Gassel

nr 75
Radon transport in Autoclaved Aerated Concrete
Michel van der Pal

nr 76
The Reliability and Validity of Interactive Virtual Reality Computer Experiments
Amy Tan

nr 77
Measuring Housing Preferences Using Virtual Reality and Belief Networks
Maciej A. Orzechowski

nr 78
Computational Representations of Words and Associations in Architectural Design
Nicole Segers

nr 79
Measuring and Predicting Adaptation in Multidimensional Activity-Travel Patterns
Chang-Hyeon Joh

nr 80
Strategic Briefing
Fayez Al Hassan

nr 81
Well Being in Hospitals
Simona Di Cicco

nr 82
Solares Bauen: Implementierungs- und Umsetzungs-Aspekte in der Hochschulausbildung in Österreich
Gerhard Schuster

nr 83
Supporting Strategic Design of Workplace Environments with Case-Based Reasoning
Shauna Mallory-Hill

nr 84
ACCEL: A Tool for Supporting Concept Generation in the Early Design Phase
Maxim Ivashkov

nr 85
Brick-Mortar Interaction in Masonry under Compression
Ad Vermeltfoort

nr 86
Zelfredzaam Wonen
Guus van Vliet

nr 87
Een Ensemble met Grootstedelijke Allure
Jos Bosman
Hans Schippers

nr 88
On the Computation of Well-Structured Graphic Representations in Architectural Design
Henri Achten

nr 89
De Evolutie van een West-Afrikaanse Vernaculaire Architectuur
Wolf Schijns

nr 90
ROMBO Tactiek
Christoph Maria Ravesloot

nr 91
External Coupling between Building Energy Simulation and Computational Fluid Dynamics
Ery Djunaedy

nr 92
Design Research in the Netherlands 2005
editors: Henri Achten
Kees Dorst
Pieter Jan Stappers
Bauke de Vries

nr 93
Ein Modell zur Baulichen Transformation
Jalil H. Saber Zaimian

nr 94
Human Lighting Demands: Healthy Lighting in an Office Environment
Myriam Aries

nr 95
A Spatial Decision Support System for the Provision and Monitoring of Urban Greenspace
Claudia Pelizaro

nr 96
Leren Creëren
Adri Proveniers

nr 97
Simlandscape
Rob de Waard

nr 98
Design Team Communication
Ad den Otter

nr 99
Humaan-Ecologisch Georiënteerde Woningbouw
Juri Czabanowski

nr 100
Hambase
Martin de Wit

nr 101
Sound Transmission through Pipe Systems and into Building Structures
Susanne Bron-van der Jagt

nr 102
Het Bouwkundig Contrapunt
Jan Francis Boelen

nr 103
A Framework for a Multi-Agent Planning Support System
Dick Saarloos

nr 104
Bracing Steel Frames with Calcium Silicate Element Walls
Bright Mweene Ng'andu

nr 105
Naar een Nieuwe Houtskeletbouw
F.N.G. De Medts

nr 106 and 107
Niet gepubliceerd

nr 108
Geborgenheid
T.E.L. van Pinxteren

nr 109
Modelling Strategic Behaviour in Anticipation of Congestion
Qi Han

nr 110
Reflecties op het Woondomein
Fred Sanders

nr 111
On Assessment of Wind Comfort by Sand Erosion
Gábor Dezsö

nr 112
Bench Heating in Monumental Churches
Dionne Limpens-Neilen

nr 113
RE. Architecture
Ana Pereira Roders

nr 114
Toward Applicable Green Architecture
Usama El Fiky

nr 115
Knowledge Representation under Inherent Uncertainty in a Multi-Agent System for Land Use Planning
Liying Ma

nr 116
Integrated Heat Air and Moisture Modeling and Simulation
Jos van Schijndel

nr 117
Concrete Behaviour in Multiaxial Compression
J.P.W. Bongers

nr 118
The Image of the Urban Landscape
Ana Moya Pellitero

nr 119
The Self-Organizing City in Vietnam
Stephanie Geertman

nr 120
A Multi-Agent Planning Support System for Assessing Externalities of Urban Form Scenarios
Rachel Katoshevski-Cavari

nr 121
Den Schulbau Neu Denken, Fühlen und Wollen
Urs Christian Maurer-Dietrich

nr 122
Peter Eisenman Theories and Practices
Bernhard Kormoss

nr 123
User Simulation of Space Utilisation
Vincent Tabak

nr 125
In Search of a Complex System Model
Oswald Devisch

nr 126
Lighting at Work: Environmental Study of Direct Effects of Lighting Level and Spectrum on Psycho-Physiological Variables
Grazyna Górnicka

nr 127
Flanking Sound Transmission through Lightweight Framed Double Leaf Walls
Stefan Schoenwald

nr 128
Bounded Rationality and Spatio-Temporal Pedestrian Shopping Behavior
Wei Zhu

nr 129
Travel Information: Impact on Activity Travel Pattern
Zhongwei Sun

nr 130
Co-Simulation for Performance Prediction of Innovative Integrated Mechanical Energy Systems in Buildings
Marija Trčka

nr 131
Niet gepubliceerd

nr 132
Architectural Cue Model in Evacuation Simulation for Underground Space Design
Chengyu Sun

nr 133
Uncertainty and Sensitivity Analysis in Building Performance Simulation for Decision Support and Design Optimization
Christina Hopfe

nr 134
Facilitating Distributed Collaboration in the AEC/FM Sector Using Semantic Web Technologies
Jacob Beetz

nr 135
Circumferentially Adhesive Bonded Glass Panes for Bracing Steel Frame in Façades
Edwin Huveners

nr 136
Influence of Temperature on Concrete Beams Strengthened in Flexure with CFRP
Ernst-Lucas Klamer

nr 137
Sturen op Klantwaarde
Jos Smeets

nr 139
Lateral Behavior of Steel Frames with Discretely Connected Precast Concrete Infill Panels
Paul Teewen

nr 140
Integral Design Method in the Context of Sustainable Building Design
Perica Savanović

nr 141
Household Activity-Travel Behavior: Implementation of Within-Household Interactions
Renni Anggraini

nr 142
Design Research in the Netherlands 2010
Henri Achten

nr 143
Modelling Life Trajectories and Transport Mode Choice Using Bayesian Belief Networks
Marloes Verhoeven

nr 144
Assessing Construction Project Performance in Ghana
William Gyadu-Asiedu

nr 145
Empowering Seniors through Domotic Homes
Masi Mohammadi

nr 146
An Integral Design Concept for Ecological Self-Compacting Concrete
Martin Hunger

nr 147
Governing Multi-Actor Decision Processes in Dutch Industrial Area Redevelopment
Erik Blokhuis

nr 148
A Multifunctional Design Approach for Sustainable Concrete
Götz Hüsken

nr 149
Quality Monitoring in Infrastructural Design-Build Projects
Ruben Favié

nr 150
Assessment Matrix for Conservation of Valuable Timber Structures
Michael Abels

nr 151
Co-simulation of Building Energy Simulation and Computational Fluid Dynamics for Whole-Building Heat, Air and Moisture Engineering
Mohammad Mirsadeghi

nr 152
External Coupling of Building Energy Simulation and Building Element Heat, Air and Moisture Simulation
Daniel Cóstola

nr 153
Adaptive Decision Making In Multi-Stakeholder Retail Planning
Ingrid Janssen

nr 154
Landscape Generator
Kymo Slager

nr 155
Constraint Specification in Architecture
Remco Niemeijer

nr 156
A Need-Based Approach to Dynamic Activity Generation
Linda Nijland

nr 157
Modeling Office Firm Dynamics in an Agent-Based Micro Simulation Framework
Gustavo Garcia Manzato

nr 158
Lightweight Floor System for Vibration Comfort
Sander Zegers

nr 159
Aanpasbaarheid van de Draagstructuur
Roel Gijsbers

nr 160
'Village in the City' in Guangzhou, China
Yanliu Lin

nr 161
Climate Risk Assessment in Museums
Marco Martens

nr 162
Social Activity-Travel Patterns
Pauline van den Berg

nr 163
Sound Concentration Caused by Curved Surfaces
Martijn Vercammen

nr 164
Design of Environmentally Friendly Calcium Sulfate-Based Building Materials: Towards an Improved Indoor Air Quality
Qingliang Yu

nr 165
Beyond Uniform Thermal Comfort on the Effects of Non-Uniformity and Individual Physiology
Lisje Schellen

nr 166
Sustainable Residential Districts
Gaby Abdalla

nr 167
Towards a Performance Assessment Methodology using Computational Simulation for Air Distribution System Designs in Operating Rooms
Mônica do Amaral Melhado

nr 168
Strategic Decision Modeling in Brownfield Redevelopment
Brano Glumac

nr 169
Pamela: A Parking Analysis Model for Predicting Effects in Local Areas
Peter van der Waerden

nr 170
A Vision Driven Wayfinding Simulation-System Based on the Architectural Features Perceived in the Office Environment
Qunli Chen

nr 171
Measuring Mental Representations Underlying Activity-Travel Choices
Oliver Horeni

nr 172
Modelling the Effects of Social Networks on Activity and Travel Behaviour
Nicole Ronald

nr 173
Uncertainty Propagation and Sensitivity Analysis Techniques in Building Performance Simulation to Support Conceptual Building and System Design
Christian Struck

nr 174
Numerical Modeling of Micro-Scale Wind-Induced Pollutant Dispersion in the Built Environment
Pierre Gousseau

nr 175
Modeling Recreation Choices over the Family Lifecycle
Anna Beatriz Grigolon

nr 176
Experimental and Numerical Analysis of Mixing Ventilation at Laminar, Transitional and Turbulent Slot Reynolds Numbers
Twan van Hooff

nr 177
Collaborative Design Support: Workshops to Stimulate Interaction and Knowledge Exchange Between Practitioners
Emile M.C.J. Quanjel

nr 178
Future-Proof Platforms for Aging-in-Place
Michiel Brink

nr 179
Motivate: A Context-Aware Mobile Application for Physical Activity Promotion
Yuzhong Lin

nr 180
Experience the City: Analysis of Space-Time Behaviour and Spatial Learning
Anastasia Moiseeva

nr 181
Unbonded Post-Tensioned Shear Walls of Calcium Silicate Element Masonry
Lex van der Meer

nr 182
Construction and Demolition Waste Recycling into Innovative Building Materials for Sustainable Construction in Tanzania
Mwita M. Sabai

nr 183
Durability of Concrete with Emphasis on Chloride Migration
Przemysław Spiesz

nr 184
Computational Modeling of Urban Wind Flow and Natural Ventilation Potential of Buildings
Rubina Ramponi

nr 185
A Distributed Dynamic Simulation Mechanism for Buildings Automation and Control Systems
Azzedine Yahiaoui

nr 186
Modeling Cognitive Learning of Urban Networks in Daily Activity-Travel Behavior
Şehnaz Cenani Durmazoğlu

nr 187
Functionality and Adaptability of Design Solutions for Public Apartment Buildings in Ghana
Stephen Agyefi-Mensah

nr 188
A Construction Waste Generation Model for Developing Countries
Lilliana Abarca-Guerrero

nr 189
Synchronizing Networks: The Modeling of Supernetworks for Activity-Travel Behavior
Feixiong Liao

nr 190
Time and Money Allocation Decisions in Out-of-Home Leisure Activity Choices
Gamze Zeynep Dane

nr 191
How to Measure Added Value of CRE and Building Design
Rianne Appel-Meulenbroek

nr 192
Secondary Materials in Cement-Based Products: Treatment, Modeling and Environmental Interaction
Miruna Florea

nr 193
Concepts for the Robustness Improvement of Self-Compacting Concrete: Effects of Admixtures and Mixture Components on the Rheology and Early Hydration at Varying Temperatures
Wolfram Schmidt

nr 194
Modelling and Simulation of Virtual Natural Lighting Solutions in Buildings
Rizki A. Mangkuto

nr 195
Nano-Silica Production at Low Temperatures from the Dissolution of Olivine - Synthesis, Tailoring and Modelling
Alberto Lazaro Garcia

nr 196
Building Energy Simulation Based Assessment of Industrial Halls for Design Support
Bruno Lee

nr 197
Computational Performance Prediction of the Potential of Hybrid Adaptable Thermal Storage Concepts for Lightweight Low-Energy Houses
Pieter-Jan Hoes

nr 198
Application of Nano-Silica in Concrete
George Quercia Bianchi

nr 199
Dynamics of Social Networks and Activity Travel Behaviour
Fariya Sharmeen

nr 200
Building Structural Design Generation and Optimisation including Spatial Modification
Juan Manuel Davila Delgado

nr 201
Hydration and Thermal Decomposition of Cement/Calcium-Sulphate Based Materials
Ariën de Korte

nr 202
Republiek van Beelden:
De Politieke Werkingen van het Ontwerp in Regionale Planvorming
Bart de Zwart

nr 203
Effects of Energy Price Increases on Individual Activity-Travel Repertoires and Energy Consumption
Dujuan Yang

nr 204
Geometry and Ventilation:
Evaluation of the Leeward Sawtooth Roof Potential in the Natural Ventilation of Buildings
Jorge Isaac Perén Montero

nr 205
Computational Modelling of Evaporative Cooling as a Climate Change Adaptation Measure at the Spatial Scale of Buildings and Streets
Hamid Montazeri

nr 206
Local Buckling of Aluminium Beams in Fire Conditions
Ronald van der Meulen

nr 207
Historic Urban Landscapes:
Framing the Integration of Urban and Heritage Planning in Multilevel Governance
Loes Veldpaus

nr 208
Sustainable Transformation of the Cities:
Urban Design Pragmatics to Achieve a Sustainable City
Ernesto Antonio Zumelzu Scheel

nr 209
Development of Sustainable Protective Ultra-High Performance Fibre Reinforced Concrete (UHPFRC):
Design, Assessment and Modeling
Rui Yu

nr 210
Uncertainty in Modeling Activity-Travel Demand in Complex Uban Systems
Soora Rasouli

nr 211
Simulation-based Performance Assessment of Climate Adaptive Greenhouse Shells
Chul-sung Lee

nr 212
Green Cities:
Modelling the Spatial Transformation of the Urban Environment using Renewable Energy Technologies
Saleh Mohammadi

nr 213
A Bounded Rationality Model of Short and Long-Term Dynamics of Activity-Travel Behavior
Ifigeneia Psarra

nr 214
Effects of Pricing Strategies on Dynamic Repertoires of Activity-Travel Behaviour
Elaheh Khademi

nr 215
Handstorm Principles for Creative and Collaborative Working
Frans van Gassel

nr 216
Light Conditions in Nursing Homes: Visual Comfort and Visual Functioning of Residents
Marianne M. Sinoo

nr 217
Woonsporen: De Sociale en Ruimtelijke Biografie van een Stedelijk Bouwblok in de Amsterdamse Transvaalbuurt
Hüseyin Hüsnü Yegenoglu

nr 218
Studies on User Control in Ambient Intelligent Systems
Berent Willem Meerbeek

nr 219
Daily Livings in a Smart Home: Users' Living Preference Modeling of Smart Homes
Erfaneh Allameh

nr 220
Smart Home Design: Spatial Preference Modeling of Smart Homes
Mohammadali Heidari Jozam

nr 221
Wonen: Discoursen, Praktijken, Perspectieven
Jos Smeets

nr 222
Personal Control over Indoor Climate in Offices: Impact on Comfort, Health and Productivity
Atze Christiaan Boerstra

nr 223
Personalized Route Finding in Multimodal Transportation Networks
Jianwe Zhang

nr 224
The Design of an Adaptive Healing Room for Stroke Patients
Elke Daemen

nr 225
Experimental and Numerical Analysis of Climate Change Induced Risks to Historic Buildings and Collections
Zara Huijbregts

nr 226
Wind Flow Modeling in Urban Areas Through Experimental and Numerical Techniques
Alessio Ricci

nr 227
Clever Climate Control for Culture: Energy Efficient Indoor Climate Control Strategies for Museums Respecting Collection Preservation and Thermal Comfort of Visitors
Rick Kramer

nr 228
Fatigue Life Estimation of Metal Structures Based on Damage Modeling
Sarmediran Silitonga

nr 229
A multi-agents and occupancy based strategy for energy management and process control on the room-level
Timilehin Moses Labeodan

nr 230
Environmental assessment of Building Integrated Photovoltaics: Numerical and Experimental Carrying Capacity Based Approach
Michiel Ritzen

nr 231
Performance of Admixture and Secondary Minerals in Alkali Activated Concrete: Sustaining a Concrete Future
Arno Keulen

nr 232
World Heritage Cities and Sustainable Urban Development: Bridging Global and Local Levels in Monitoring the Sustainable Urban Development of World Heritage Cities
Paloma C. Guzman Molina

nr 233
Stage Acoustics and Sound Exposure in Performance and Rehearsal Spaces for Orchestras: Methods for Physical Measurements
Remy Wenmaekers

nr 234
Municipal Solid Waste Incineration (MSWI) Bottom Ash: From Waste to Value Characterization, Treatments and Application
Pei Tang

nr 235
Large Eddy Simulations Applied to Wind Loading and Pollutant Dispersion
Mattia Ricci

nr 236
Alkali Activated Slag-Fly Ash Binders: Design, Modeling and Application
Xu Gao

nr 237
Sodium Carbonate Activated Slag: Reaction Analysis, Microstructural Modification & Engineering Application
Bo Yuan

nr 238
Shopping Behavior in Malls
Widiyani

nr 239
Smart Grid-Building Energy Interactions: Demand Side Power Flexibility in Office Buildings
Kennedy Otieno Aduda

nr 240
Modeling Taxis Dynamic Behavior in Uncertain Urban Environments
Zheng Zhong

nr 241
Gap-Theoretical Analyses of Residential Satisfaction and Intention to Move
Wen Jiang

nr 242
Travel Satisfaction and Subjective Well-Being: A Behavioral Modeling Perspective
Yanan Gao

nr 243
Building Energy Modelling to Support the Commissioning of Holistic Data Centre Operation
Vojtech Zavrel

nr 244
Regret-Based Travel Behavior Modeling: An Extended Framework
Sunghoon Jang

nr 245
Towards Robust Low-Energy Houses: A Computational Approach for Performance Robustness Assessment using Scenario Analysis
Rajesh Reddy Kotireddy

nr 246
Development of sustainable and functionalized inorganic binder-biofiber composites
Guillaume Doudart de la Grée

nr 247
A Multiscale Analysis of the Urban Heat Island Effect: From City Averaged Temperatures to the Energy Demand of Individual Buildings
Yasin Toparlar

nr 248
Design Method for Adaptive Daylight Systems for buildings covered by large (span) roofs
Florian Heinzelmann

nr 249
Hardening, high-temperature resistance and acid resistance of one-part geopolymers
Patrick Sturm

nr 250
Effects of the built environment on dynamic repertoires of activity-travel behaviour
Aida Pontes de Aquino

nr 251
Modeling for auralization of urban environments: Incorporation of directivity in sound propagation and analysis of a framework for auralizing a car pass-by
Fotis Georgiou

nr 252
Wind Loads on Heliostats and Photovoltaic Trackers
Andreas Pfahl

nr 253
Approaches for computational performance optimization of innovative adaptive façade concepts
Roel Loonen

nr 254
Multi-scale FEM-DEM Model for Granular Materials: Micro-scale boundary conditions, Statics, and Dynamics
Jiadun Liu

nr 255
Bending Moment - Shear Force Interaction of Rolled I-Shaped Steel Sections
Rianne Willie Adriana Dekker

nr 256
Paralympic tandem cycling and handcycling: Computational and wind tunnel analysis of aerodynamic performance
Paul Fionn Mannion

nr 257
Experimental characterization and numerical modelling of 3D printed concrete: Controlling structural behaviour in the fresh and hardened state
Robert Johannes Maria Wolfs

nr 258
Requirement checking in the building industry: Enabling modularized and extensible requirement checking systems based on semantic web technologies
Chi Zhang

nr 259
A Sustainable Industrial Site Redevelopment Planning Support System
Tong Wang

nr 260
Efficient storage and retrieval of detailed building models: Multi-disciplinary and long-term use of geometric and semantic construction information
Thomas Ferdinand Krijnen

nr 261
The users' value of business center concepts for knowledge sharing and networking behavior within and between organizations
Minou Weijs-Perrée

nr 262
Characterization and improvement of aerodynamic performance of vertical axis wind turbines using computational fluid dynamics (CFD)
Abdolrahim Rezaeiha

nr 263
In-situ characterization of the acoustic impedance of vegetated roofs
Chang Liu

nr 264
Occupancy-based lighting control: Developing an energy saving strategy that ensures office workers' comfort
Christel de Bakker

nr 265
Stakeholders-Oriented Spatial Decision Support System
Cahyono Susetyo

nr 266
Climate-induced damage in oak museum objects
Rianne Aleida Luimes

nr 267
Towards individual thermal comfort: Model predictive personalized control of heating systems
Katarina Katic

nr 268
Modelling and Measuring Quality of Urban Life: Housing, Neighborhood, Transport and Job
Lida Aminian

nr 269
Optimization of an aquifer thermal energy storage system through integrated modelling of aquifer, HVAC systems and building
Basar Bozkaya

nr 270
Numerical modeling for urban sound propagation: developments in wave-based and energy-based methods
Raúl Pagán Muñoz

nr 271
Lighting in multi-user office environments: improving employee wellbeing through personal control
Sanae van der Vleuten-Chraibi

nr 272
A strategy for fit-for-purpose occupant behavior modelling in building energy and comfort performance simulation
Isabella I. Gaetani dell'Aquila d'Aragona

nr 273
Een architectuurhistorische waardestelling van naoorlogse woonwijken in Nederland: Het voorbeeld van de Westelijke Tuinsteden in Amsterdam
Eleonore Henriette Marie Mens

nr 274
Job-Housing Co-Dependent Mobility Decisions in Life Trajectories
Jia Guo

nr 275
A user-oriented focus to create healthcare facilities: decision making on strategic values
Emilia Rosalia Catharina Maria Huisman

nr 276
Dynamics of plane impinging jets at moderate Reynolds numbers – with applications to air curtains
Adelya Khayrullina

nr 277
Valorization of Municipal Solid Waste Incineration Bottom Ash - Chemical Nature, Leachability and Treatments of Hazardous Elements
Qadeer Alam

nr 278
Treatments and valorization of MSWI bottom ash - application in cement-based materials
Veronica Caprai

nr 279
Personal lighting conditions of office workers - input for intelligent systems to optimize subjective alertness
Juliëtte van Duijnhoven

nr 280
Social influence effects in tourism travel: air trip itinerary and destination choices
Xiaofeng Pan

nr 281
Advancing Post-War Housing: Integrating Heritage Impact, Environmental Impact, Hygrothermal Risk and Costs in Renovation Design Decisions
Lisanne Claartje Havinga

nr 282
Impact resistant ultra-high performance fibre reinforced concrete: materials, components and properties
Peipeng Li

nr 283
Demand-driven Science Parks: The Perceived Benefits and Trade-offs of Tenant Firms with regard to Science Park Attributes
Wei Keat Benny Ng

nr 284
Raise the lantern; how light can help to maintain a healthy and safe hospital environment focusing on nurses
Maria Petronella Johanna Aarts

nr 285
Modelling Learning and Dynamic Route and Parking Choice Behaviour under Uncertainty
Elaine Cristina Schneider de Carvalho

nr 286
Identifying indoor local microclimates for safekeeping of cultural heritage
Karin Kompatscher

nr 287
Probabilistic modeling of fatigue resistance for welded and riveted bridge details. Resistance models and estimation of uncertainty.
Davide Leonetti

nr 288
Performance of Layered UHPFRC under Static and Dynamic Loads: Effects of steel fibers, coarse aggregates and layered structures
Yangyueye Cao

nr 289
Photocatalytic abatement of the nitrogen oxide pollution: synthesis, application and long-term evaluation of titania-silica composites
Yuri Hendrix

nr 290
Assessing knowledge adoption in post-disaster reconstruction: Understanding the impact of hazard-resistant construction knowledge on reconstruction processes of self-recovering communities in Nepal and the Philippines
Eefje Hendriks

nr 291
Locating electric vehicle charging stations: A multi-agent based dynamic simulation
Seheon Kim

nr 292
De invloed van Lean Management op de beheersing van het bouwproces
Wim van den Bouwhuijsen

nr 293
Neighborhood Environment and Physical Activity of Older Adults
Zhengying Liu

nr 294
Practical and continuous luminance distribution measurements for lighting quality
Thijs Willem Kruisselbrink

nr 295
Auditory Distraction in Open-Plan Study Environments in Higher Education
Pieternella Elizabeth Braat-Eggen

nr 296
Exploring the effect of the sound environment on nurses' task performance: an applied approach focusing on prospective memory
Jikke Reinten

nr 297
Design and performance of water resistant cementitious materials– Mechanisms, evaluation and applications
Zhengyao Qu

nr 298
Design Optimization of Seasonal Thermal Energy Storage Integrated District Heating and Cooling System: A Modeling and Simulation Approach
Luyi Xu

nr 299
Land use and transport: Integrated approaches for planning and management
Zhongqi Wang

nr 300
Multi-disciplinary optimization of building spatial designs: co-evolutionary design process simulations, evolutionary algorithms, hybrid approaches
Sjonnie Boonstra

nr 301
Modeling the spatial and temporal relation between urban land use, temperature, and energy demand
Hung-Chu Chen

nr 302
Seismic retrofitting of masonry walls with flexible deep mounted CFRP strips
Ömer Serhat Türkmen

nr 303
Coupled Aerostructural Shape and Topology Optimization of Horizontal-Axis Wind Turbine Rotor Blades
Zhijun Wang

nr 304
Valorization of Recycled Waste Glass and Converter Steel Slag as Ingredients for Building Materials: Hydration and Carbonation Studies
Gang Liu

nr 305
Low-Carbon City Development based on Land Use Planning
Gengzhe Wang

nr 306
Sustainable energy transition scenario analysis for buildings and neighborhoods - Data driven optimization
Shalika Saubhagya Wickramarachchi Walker

nr 307
In-between living and manufactured: an exploratory study on biobuilding components for building design
Berrak Kirbas Akyurek

nr 308
Development of alternative cementitious binders and functionalized materials: design, performance and durability
Anna Monika Kaja

nr 309
Development a morphological approach for interactive kinetic façade design: Improving multiple occupants' visual comfort
Seyed Morteza Hosseini

nr 310
PV in urban context: modeling and simulation strategies for analyzing the performance of shaded PV systems
Ádám Bognár

nr 311
Life Trajectory, Household Car Ownership Dynamics and Home Renewable Energy Equipment Adoption
Gaofeng Gu

nr 312
Impact of Street-Scale Built Environment on Walking/Cycling around Metro Stations
Yanan Liu

nr 313
Advances in Urban Traffic Network Equilibrium Models and Algorithms
Dong Wang

nr 314
Development of an uncertainty analysis framework for model-based consequential life cycle assessment: application to activity-based modelling and life cycle assessment of multimodal mobility
Paul Martin Baustert

nr 315
Variable stiffness and damping structural joints for semi-active vibration control
Qinyu Wang

nr 316
Understanding Carsharing-Facilitating Neighborhood Preferences
Juan Wang

nr 317
Dynamic alignment of Corporate Real Estate to business strategies: An empirical analysis using historical data and in-depth modelling of decision making
Howard Cooke

nr 318
Local People Matter: Towards participatory governance of cultural heritage in China
Ji Li

nr 319
Walkability and Walkable Healthy Neighborhoods
Bojing Liao

nr 320
Light directionality in design of healthy offices: exploration of two methods
Parisa Khademagha

nr 321
Room acoustic modeling with the time-domain discontinuous Galerkin method
Huiqing Wang

nr 322
Sustainable insulating lightweight materials for enhancing indoor building performance: miscanthus, aerogel and nano-silica
Yuxuan Chen

nr 323
Computational analysis of the impact of façade geometrical details on wind flow and pollutant dispersion
Xing Zheng

nr 324
Analysis of urban wind energy potential around high-rise buildings in close proximity using computational fluid dynamics
Yu-Hsuan Jang

nr 325
A new approach to automated energy performance and fault detection and diagnosis of HVAC systems: Development of the 4S3F method
Arie Taal

nr 326
Innovative Admixtures for Modifying Viscosity and Volume Change of Cement Composites
Hossein Karimi

nr 327
Towards houses with low grid dependency: A simulation-based design optimization approach
Zahra Mohammadi

nr 328
Activation of demand flexibility for heating systems in buildings: Real-life demonstration of optimal control for power-to-heat and thermal energy storage
Christian Finck

nr 329
A computational framework for analysis and optimisation of automated solar shading systems
Samuel B. de Vries

nr 330
Challenges and potential solutions for cultural heritage adaptive reuse: a comparative study employing the Historic Urban Landscape approach
Nadia Pintossi

nr 331
Shared control in office lighting systems
Tatiana Aleksandrovna Lashina

nr 332
Comfort in Urban Public Spaces
You Peng

nr 333
Numerical modelling of metal soap formation in historical oil paintings
Gerardus Johannes Anna Maria Eumelen

nr 334
A transdisciplinary decision-making approach to food-water-energy nexus: A guide towards sustainable development
Maryam Ghodsvali

nr 335
Numerical modelling of transient low-frequency sound propagation and vibration in buildings
Indra Sihar

nr 336
Characterization of impact sound from lightweight joist floors
Yi Qin

nr 337
Cities for Children: Supporting Children and Caregivers in Participatory Urban Planning
Özlemnur Ataol

nr 338
Engaging the unengaged: Exploring citizen participation in nature-based solutions in China
Li Dai

The amount of domestic waste produced in the world grows annually. To avoid harmful effects on the environment from handling it through Municipal Solid Waste Incineration (MSWI), it is necessary to develop solutions for the by-products such as bottom ash and fly ash to be suitable for recycling. Because those residues contain serious amounts of contaminants, they cannot be reused or landfilled directly. Therefore, it is necessary to develop treatments and applications that provide a way to overcome the disadvantages of these materials.
Having a potential to be used as secondary building materials, these by-products could also be instrumental in developing eco-concretes: concretes, where part of the natural components is substituted with an alternative. This would allow not only economizing natural recourses but also reducing the environmental impact that comes with cement production. This thesis aims to investigate the broad spectrum of properties of MSWI bottom ash and fly ash. An elaborate overview of these materials and their qualities is provided, to create tailored treatments. This maximizes the share of these by-products that can be successfully utilized in various cement and concrete applications.

DEPARTMENT OF THE BUILT ENVIRONMENT

TU/e EINDHOVEN UNIVERSITY OF TECHNOLOGY